SEISMIC DESIGN AND PERFORMANCE OF

YIELDING SHEAR PANEL DEVICE

Mrinmoy Nath

A Thesis in
The Department of
Building, Civil and Environmental Engineering

Presented in Partial Fulfillment of the Requirements
for the Degree of Master of Applied Science (Civil Engineering)
at Concordia University, Montreal, Quebec, Canada

November 2016

CONCORDIA UNIVERSITY

School of Graduate Studies

This is to certify that the thesis prepared

By: Mrinmoy Nath

Entitled: Seismic design and performance of Yielding Shear Panel Device

and submitted in partial fulfillment of the requirements for the degree of

MASc Civil Engineering

complies with the regulations of the University and meets the accepted standards with respect to originality and quality.

Signed by the final examining committee:

Dr. Adel M. Hanna Chair

Dr. Sivakumar Narayanswami Examiner

Dr. Ashutosh Bagchi Examiner

Dr. Anjan Bhowmick Supervisor

Approved by

_____

Chair of Department or Graduate Program Director

_____

Dean of Faculty

Date _____

ABSTRACT

SEISMIC DESIGN AND PERFORMANCE OF

YIELDING SHEAR PANEL DEVICE

Mrinmoy Nath

Yielding shear panel device (YSPD) is a metal yielding passive energy dissipation device that utilizes the inelastic shear deformation capability of a steel plate. The device is made of a steel plate welded inside a square hollow section (SHS) to absorb seismic energy. It showed stable hysteresis response in the previous experiments. It is inexpensive and also simple to manufacture and install in a seismic force resisting system. Research on yielding shear panel device is still in the initial stage and a significant amount of research is needed before it can be adopted by the engineering society. The objective of this research is twofold: first, to study the behavior of yielding shear panel as a device and then, to evaluate the performance of lateral load resisting system equipped with YSPD. A nonlinear finite element model which includes both material and geometric nonlinearities is used for this study. The finite element model of the YSPD device is validated by comparing the results from an experimental program. Excellent correlation between the test results and the finite element analysis results is observed. With the validated finite element model, detailed parametric study has been done to study the behavior of the YSPD devices of different configurations. The model is further validated for a frame equipped with YSPD using the results from a mathematical model published in the literature. This study also evaluates the performance of a 4-story building frame equipped with YSPD when the device is used for retrofitting. Seismic design of a 2-story lateral load resisting frame with YSPD has been done by direct displacement based design method. The seismic performance of the designed building has

been verified under spectrum compatible seismic records for Vancouver. Nonlinear seismic analysis shows that YSPDs, in a high seismic region, behave in a stable and ductile manner. It has also been observed that the device absorbs the seismic energy and deforms in shear and effectively reduces the deformation of the structure, which confirms the intended design philosophy of YSPD device. An analytical approach has been developed to estimate fundamental period of the frames with YSPD. A series of frames with YSPD devices of different geometry are designed and analysed to estimate the fundamental period. It has been observed that the fundamental period obtained from finite element analysis can be well predicted by the proposed analytical model.

ACKNOWLEDGEMENTS

I would like to express my deep gratitude and sincere appreciation to Dr. Anjan Bhowmick for his guidance and encouragement throughout the course of my graduate studies.

Funding for this research project is provided by the Faculty of Engineering and Computer Science, Concordia University, Montreal, Canada and the Fonds de recherche du Québec – Nature et technologies (FRQNT). Their support is gratefully acknowledged.

Thanks to all my colleagues and friends, especially Amit Chandra, Sandip Dey, Mona Raissi, Kallol Barua, Md. Imran Kabir and Moon Moon Dhar for making my graduate studies so memorable. Wish you all the best in your future endeavors. Hope to stay in touch with you all and derive help as always.

I would also like to thank my family for their support and encouragement during my studies.

TABLE OF CONTENTS

LISTOF FIGURES

LIST OF TABLES

NOTATIONS

A_b	Cross sectional area of one bolt
d	Size of diaphragm plate
D	SHS Size
E_D	Dissipated hysteretic energy by EDD
E_I	Earthquake input energy
E_K	Kinetic energy
E_S	Elastic strain energy
E_V	Viscous Damping Energy
E	Modulus of elasticity
E_t	Tangent modulus
E_{SHS}	Modulus of elasticity of SHS plate
E_b	Modulus of elasticity of bolt material
f_y	Yield strength
$f_{y,SHS}$	Yield strength of SHS plate
$f_{y,dia}$	Yield strength of diaphragm plate
F_y	Yield force
F	Restoring force
F_e	Elastic component of the restoring force
F_h	Hysteretic component of the restoring force
G	Shear modulus
k_{YSPD}	Stiffness of YSPD
k_{dia}	Stiffness of the diaphragm

k_{SHS}	Stiffness of the SHS
k_{eff}	Effective stiffness
k_t	Tangential stiffness
N_b	Number of nodes per bolt hole
P_{ls}	Limit state annual exceeding probability
r	Radius of the bolt hole
S_n	Nodal spacing in the SHS plate
S_a	Spectral acceleration
t	Diaphragm Thickness
T	SHS Thickness
T_1	Fundamental period of structure
λ	Reduction factor (Chapter 3)
ζ_{eq}	Equivalent damping ratio
δ_y	Yield displacement
τ_y	Shear yielding stress

ABBREVIATIONS

ASCE	American Society of Civil Engineers
CSA	Canadian Standards Association
DI	Damage index
ECCS	European Convention for Constructional Steelwork
EDD	Energy dissipating device
EDS	Energy dissipation system
FE	Finite element
FEMA	Federal Emergency Management Agency
FR	Force ratio
LVDT	Linear variable differential transducer
MDOF	Multi-degree-of-freedom
MRF	Moment resisting frame
NBCC	National Building Code Of Canada
NDP	Nonlinear dynamic procedure
NEHRP	National Earthquake Hazards Reduction Program
NLTHA	Non-Linear Time History Analysis
NSP	Nonlinear static procedure
PBSD	Performance Based Design
PGA	Peak ground acceleration
PEER	Pacific Earthquake Engineering Research Center
PsD	Pseudo-dynamic
SDOF	Single-degree-of-freedom

SEAONC	Structural Engineers Association of Northern California
SFRF	Seismic force resisting frame
SFRS	Seismic force resisting system
SHS	Square hollow section
SPD	Shear panel devices
SR	Stiffness ratio
SSWP	Steel shear wall panel
YSPD	Yielding Shear Panel Device

CHAPTER 1: INTRODUCTION

1.1. General

Earthquake is one of the major catastrophic events for destroying cities and its inhabitants. The last few decades' have seen a large number of sustainable solution to diminish the effects caused by earthquakes. This process led to the innovation of various control devices for dissipating seismic energy.

Steel has inherent strength and ductile property to sustain a large amount of deformation without rupture. This can prove advantageous if the steel members are arranged and detailed properly. The arrangement of the steel members plays a vital role in connection to the ductility of the structure. Also, detailing requirements ensure robustness and the deformability of dissipative zones. This allows cyclic deformation of the frame and a portion of the seismic input energy is dissipated here.

The damage control concept has a remarkable importance in the seismic codes. Under the action of moderate earthquakes, the structure should withstand the generated force with a minimum structural damage. In case of strong seismic events the structure is allowed to be damaged, but without the structural collapse. The passive control devices are used to enhance the strength and/ or stiffness of the building frames.

Friction sliding, fluid orificing, the yielding of metals, deformation of a viscoelastic solid or fluid are some of the examples of mechanisms used in energy dissipation. Yielding of metals is another popular mechanism that is deployed for the dissipation of input seismic energy. Stable hysteretic behavior, long term reliability, good fatigue performance, and relative insensitivity to

environmental effects such as temperature are some of the desirable features of such a mechanism (Habibi, 2013).

Yielding shear panel device (YSPD) is an energy dissipating device that utilizes yielding of metals. The in-plane shear deformation of a steel plate is exploited to dissipate seismic energy (Chan, 2008). YSPD is inexpensive and it is also simple to manufacture and install in a seismic force resisting system. This device can be fabricated using mild steel standard structural sections and can easily be installed on the inverted V braces of structural frames.

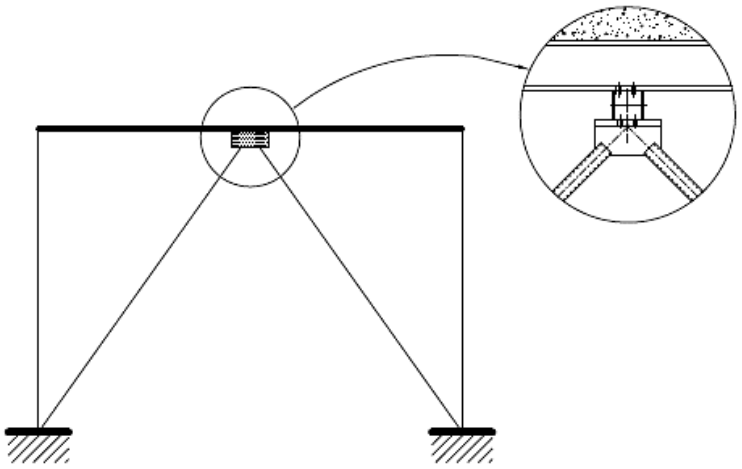

Figure 1.1 Yielding shear panel device assembly (Chan, 2008)

Very limited research has been conducted on YSPD. Seismic design of a lateral load resisting system equipped with this energy dissipation system for a new construction has not been studied. Also, the performance of a designed frame under real earthquake records needs to be explored. Therefore, more work is required to ensure the viability of this new device and make it more acceptable to design engineers.

Passive energy dissipation devices need to be designed properly to maximize dissipated hysteretic energy. As the seismic performance of the structure is much dependent on the resulting deformation rather than forces, displacement-based approach can be used for design of these devices (Priestley et al., 1997). In this design method, target displacement and yield displacement are assumed at the beginning. The ductility factor is calculated based on this assumption. Finally, after going through an iteration process, the lateral load resisting system is designed. This simple displacement based approach can be implemented to design a steel lateral load resisting system equipped with YSPD.

When the YSPD is installed into a parent frame, the dynamic properties such as fundamental period changes for the whole frame. Current practice is to develop a FE model of the frame equipped with YSPD and then conduct a frequency analysis to determine the fundamental period. While frequency analysis of a detailed FE model can provide a good estimate of period of YSPD system, it is very time consuming. A simple analytical model is thus required to estimate period of steel frame with YSPD

1.2. Objectives of the thesis

The main objectives of this research are as follows:

1. To study the behavior of yielding shear panel device (isolated from the structure) under monotonic and cyclic loads. A nonlinear finite element (FE) model is developed to achieve this objective. The finite element model is validated against available experimental program. A detailed parametric study is carried out to investigate a number of different parameters that affect behavior of YSPD.

2. To study the seismic performance of steel lateral load resisting frame equipped with YSPD. It is done by conducting nonlinear seismic analysis of a 4-story braced frame for an office building.

3. To compare the seismic design methods in connection to a lateral load resisting frame with YSPD as passive energy dissipation devices. Further, suitable design method is suggested and presented in detail. For this reason, one 2-story frame equipped with YSPD has been designed according to direct displacement based approach and its performance is evaluated through seismic analysis.

4. To develop a simple analytical procedure to determine the fundamental period of the frame equipped with yielding shear panel device.

1.3. Thesis outline

Chapter 2 presents a literature review and background of this thesis. Passive energy dissipation mechanism is discussed elaborately and an overview of some recently developed passive control devices is given. The development of the yielding shear panel device (YSPD) and the study on YSPD by other researchers including experimental evaluation are also presented.

Chapter 3 presents the numerical modelling of the yielding shear panel device using finite element methods. Material modelling and modeling of boundary conditions are included in the finite element models. Finite element simulation results are compared against the available experimental results. The validated finite element model is also used for conducting detailed parametric study of the device.

Chapter 4 presents the numerical modelling of a lateral load resisting frame equipped with yielding shear panel device. The model is validated against available mathematical modelling of

YSPD. The seismic performance of a 4-story moment resisting frame retrofitted with YSPD has been done. The effectiveness of the device as a passive energy dissipater has been verified.

Chapter 5 presents the seismic design of a 2-story lateral load resisting frame having YSPD as a passive energy dissipation device, for an office building located in Vancouver, BC. The frame is designed according to direct displacement based seismic design of buildings. Non-linear dynamic analysis of the frame has been conducted to study the performance of the designed frame. The results from analysis are used to evaluate the efficiency of YSPD as a device in new construction.

Chapter 6 presents an analytical procedure to determine the fundamental frequency of frames with YSPD. The device-brace-frame mechanism is discussed in detail and considering the contribution of all the elements, lateral stiffness and fundamental frequency of the frame are calculated. Different combinations of buildings are studied and calculated frequencies from the analytical model are compared with the frequencies derived from the numerical model, developed in this study.

Finally, **Chapter 7** provides a summary of the research conducted. Conclusions, future scopes and recommendations for further research are also presented in this chapter.

CHAPTER 2: LITERATURE REVIEW OF YIELDING SHEAR PANEL DEVICE (YSPD)

2.1. Introduction

Earthquake causes severe damage to the structure, and thus it has significant impact on the service life of the structure. For regaining the normal functionality, rehabilitation of the damaged components is necessary. But, most of the times, rehabilitation is a complex process and also, it is costly. This is the reason behind the development of the control mechanisms, to control the damage of structures. These control mechanisms are of different types: active, semi-active and passive. These mechanisms help in reducing the energy dissipation demand of the major structural elements.

In recent times, Passive Energy Dissipation (PED) technique is more used than the other methods. Different types of PEDs are designed to perform efficiently in case of seismic excitation. This chapter states the functionality of passive energy dissipation devices. Structural control mechanism is also briefly explained. Further, a detailed review of metal yielding devices is presented and a recently developed metal device, Yielding Shear Panel Device (YSPD) is described.

2.2. Structural response control

Structural response control systems are designed by researchers and engineers to reduce the displacement, velocity, and acceleration experienced by a structure during an earthquake event. These control systems can be classified into two broad categories - Active control system and Passive control system. The classification of structural control system is shown in Figure 2.1

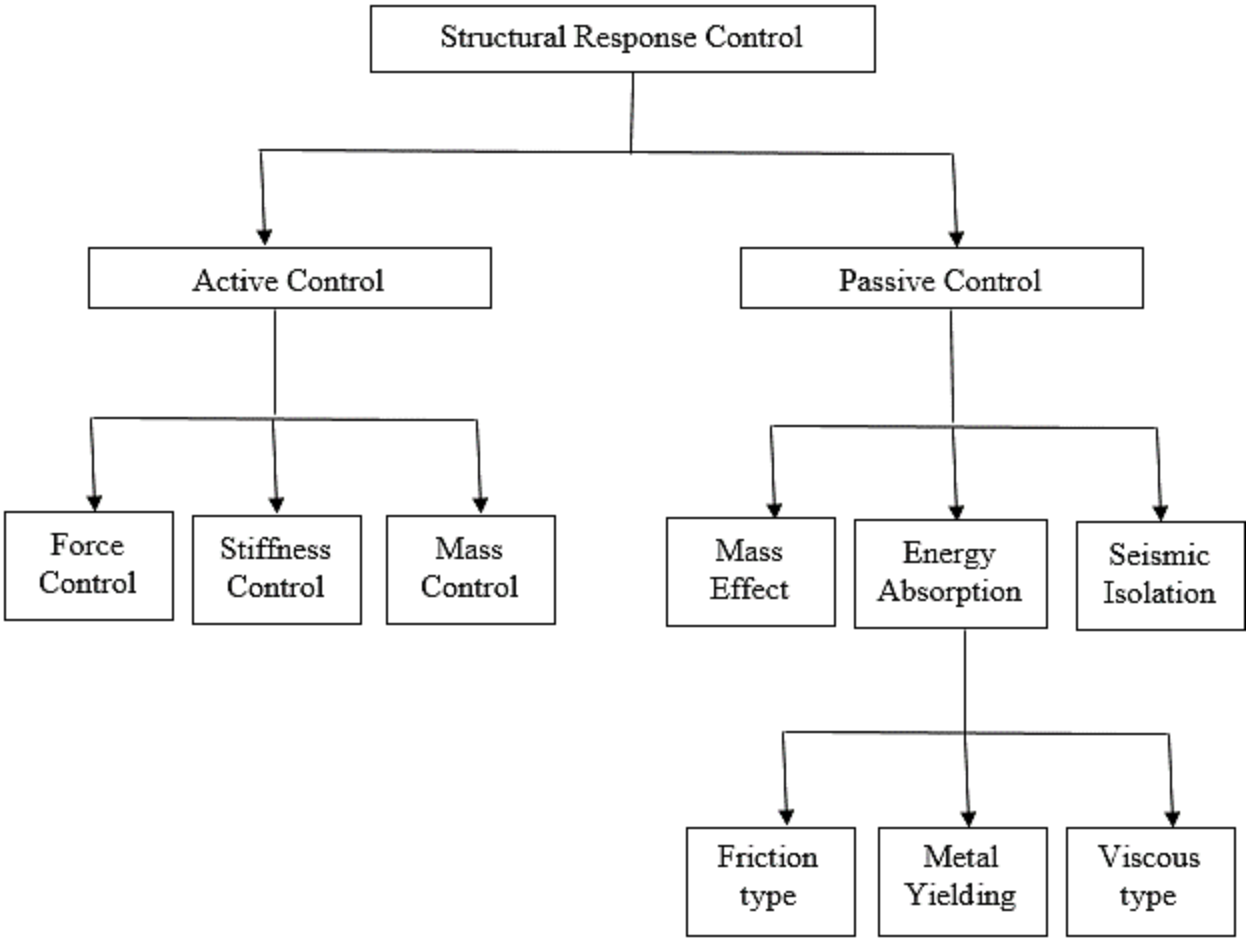

Figure 2.1 Structural response control systems (Chan, 2008)

Active control system identifies the ground excitation through sensors. In case of seismic event, a computer based monitoring system readily activates the control mechanism. This control system is dependent on the data collected through real time recording instrumentation. Hence, disruption of power supply may be an issue of smooth functioning.

Passive control devices, are designed and positioned to absorb seismic energy without external power. Unlike active control systems the passive control device functioning do not require active data collection. Additionally, these devices are simple to manufacture and relatively inexpensive. They can be replaced in case of post-earthquake damage with minimal time and cost. Depending

upon their applications, different types of passive control systems are available such as visco-elastic dampers, metal yielding dampers, viscous dampers, friction dampers, tuned mass dampers, tuned liquid dampers, tuned liquid column dampers, super-elastic dampers, base isolators etc. Present study focusses on the use of metal yielding devices for passive energy dissipation and are discussed in following sections.

2.3. Passive Energy Dissipation Using Metal Yielding Devices

Catastrophic event like earthquake imposes massive lateral force on structures. The elastic design of structure to resist this force is therefore uneconomical. For this, usually the structures are proportioned to respond inelastically during a design earthquake. This inelastic response results in the energy dissipation through its plastic deformation. Therefore, it is imperative to rehabilitate the permanently damaged structure post an earthquake event. To minimize the complex and costly retrofitting of the main structure, energy dissipating devices (EDDs) are installed within the structure. EDDs have been proven to be effective in localizing the damage and thereby reducing the overall cost and extent of retrofitting (Aguirre, 1997). Some of the EDDs utilizes metal yielding. The metal yielding dissipates considerable amount of energy by deforming inelastically in seismic excitation. The deformation in these devices may be of different types i.e. axial, flexural, shear or torsional. This proves to be effective as it reduces the deformation of the parent frame and minimize the rehabilitation cost.

The mechanism of passive energy dissipation using metal yielding EDDs is illustrated considering a single degree of freedom system (SDOF) (Soong and Dargush, 1997).

Figure 2.2(a) shows a typical SDOF system with an EDD represented by the symbol Γ. In the figure m, k and c denote mass, stiffness and damping coefficient of the parent structure

respectively. The force acting on the EDD is a function of lateral displacement u. Figure 2.2(b) shows the force-displacement relationship of an elastic, perfectly-plastic EDD. It shows a linear stable hysteretic loop. Here, F_y denotes the yield force and $\bar{k}$ denotes the stiffness of the EDD.

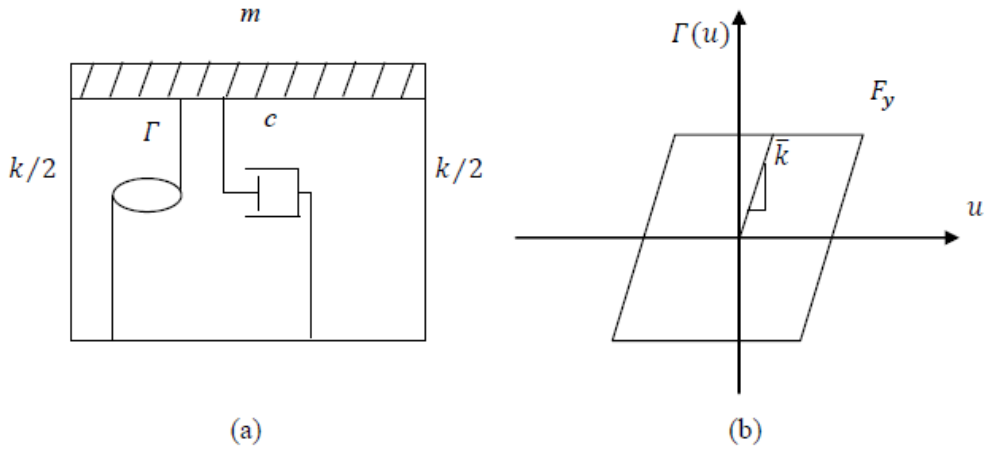

Figure 2.2 (a) Dissipative SDOF system, (b) Force-displacement relationship of the EDD

(Soong and Dargush, 1997)

The equation of motion for an SDOF system subjected to ground acceleration $\ddot{u}_g$ can be expressed as,

[2.1] $m\ddot{u} + c\dot{u} + ku + \Gamma(u) = -(m + m_d)\ddot{u}_g$

where, m_d is the mass of the EDD, which can be neglected. Hence, the equation of motion becomes

[2.2] $m\ddot{u} + c\dot{u} + ku + \Gamma(u) = -m\ddot{u}_g$

The energy balance equation for the SDOF system can be written as,

[2.3] $E_I = E_K + E_S + E_V + E_D$

Where, E_I denotes Earthquake input energy, E_K denotes Kinetic energy, E_S denotes Elastic strain energy, E_V denotes Viscous Damping Energy and E_D denotes Dissipated hysteretic energy.

$$E_I = -\int_0^u m\ddot{u}_g\, du = -\int_0^t m\ddot{u}_g\, \dot{u} dt$$

$$E_K = \int_0^u m\ddot{u}du = \frac{m\dot{u}^2}{2E_k} = \int_0^u m\ddot{u}du = \frac{m\dot{u}^2}{2}$$

$$E_S = \int_0^u kudu = \frac{ku^2}{2E_S} = \int_0^u kudu = \frac{ku^2}{2}$$

$$E_V = \int_0^u c\dot{u}du = \int_0^t c\dot{u}^2 dt$$

$$E_D = \int_0^u \Gamma(u)du$$

The energy balance equation shows that EDDs installed within a structure can absorb a part of input energy thereby decreasing the energy dissipation demand of the parent structure. The inelastic energy dissipation of structural elements gets reduced. Clearly, early yielding of EDD increases the amount of dissipated energy. Moreover, the added stiffness provided by EDDs results in reduction of the maximum deflection of the structure (Hossain, 2013)

2.4. Metal Yielding Devices for Passive Energy Dissipation

Kelly and Skinner (1974) designed sacrificial elements in the structure that could dissipate a large portion of the input energy. They developed a number of passive energy dissipation devices for seismic risk mitigation in bridge and building structures. Some of their developed metallic EDDs were Torsional Beam, Flexural Beam, and U-Strip devices etc. The metal yielding devices for passive energy dissipation make use of the stable hysteretic force-displacement behavior of metals

to dissipate energy (Aiken et al., 1993; Williams et al., 2003). They absorb energy through axial yielding, flexural yielding, shear yielding or torsional yielding based on the design. A brief review of some popular and recently developed EDDs is given in the following section.

2.4.1. Added Damping And Stiffness (ADAS):

The steel-plate Added Damping And Stiffness (ADAS) device is an assembly of steel plates. By yielding a large volume of steel, the ADAS device can dissipate substantial energy during an earthquake (Xia and Hanson, 1992). Its force-displacement relationship shows a stable hysteresis response. The Wells Fargo Bank building, San Francisco was retrofitted using ADAS after it was damaged due to Loma Prieta earthquake in 1989 (Perry et al. 1993).

It is composed of a number (typically four to seven) of X-shaped mild-steel plates bolted together (on both sides), as shown in Fig. 2.3. These are installed between the inverted V-brace and the beam soffit. In case of seismic excitation, the device's plates deform in a double curvature. The X-shape of the element produces a close-to-uniform stress distribution over its height (as *M/EI* is approximately constant). Hence, the energy dissipation of the section is utilized. This shape is also effective in avoiding concentration of stress across the section and thus delays premature failure from low-cycle fatigue (Aiken et al., 1993).

Extensive research on ADAS elements were conducted at the Earthquake Engineering Research Centre (EERC) of the University of California at Berkeley during the period of 1986 to 1991 (Whittaker et al. 1991, Aiken et al. 1993). They used ADAS devices made from ASTM Grade A-36 steel and were having four, six or seven plates.

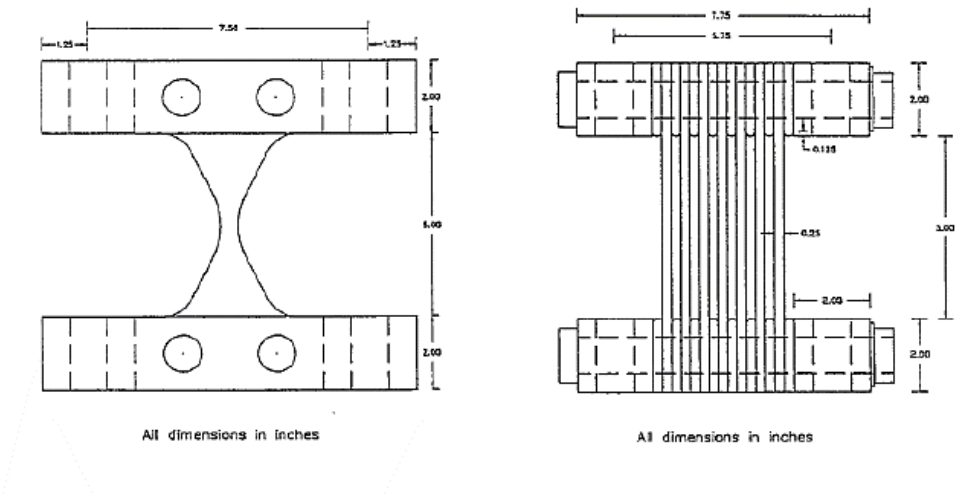

Figure 2.3 Added Damping and Stiffness (ADAS) Element (Aiken et al., 1993)

Figure 2.4 shows the force-displacement plot of an ADAS element consisting of seven plates. It shows a stable hysteresis response for more than 100 cycles at an amplitude of three times the yield deformation and can be safely designed for ten times yield deformation (Aiken et al. 1993).

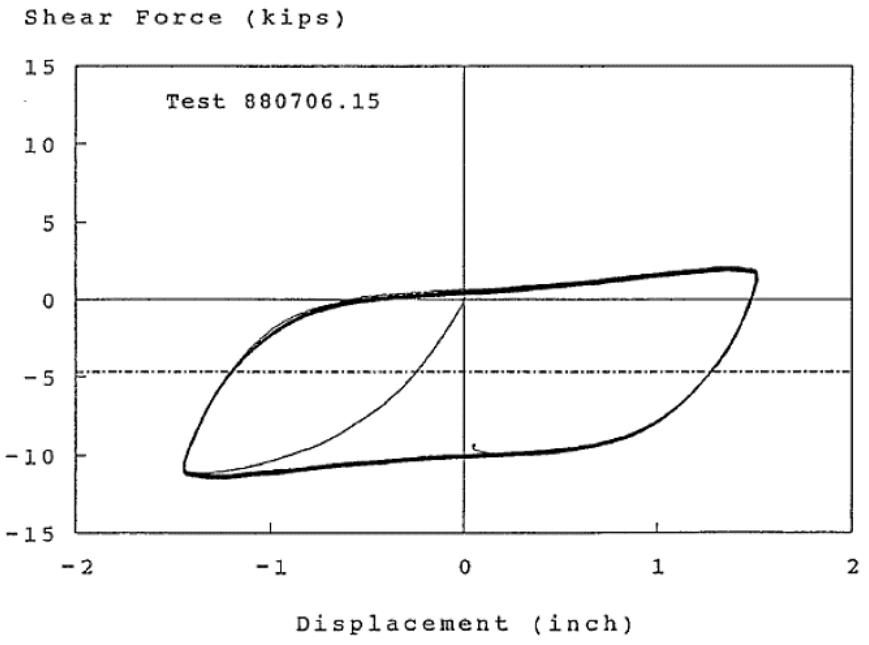

Figure 2.4 Seven Plate ADAS Element Hysteretic Behavior (Whittaker et al., 1991)

Xia and Hanson (1992) reported that the effect of brace stiffness to device stiffness ratio is negligible for building under nonlinear response. A parametric study using ADAS device for a 10-story frame structure was used for their study. Dynamic analysis for a 4-story fame, upgraded with ADAS elements, was done by Tehranizadeh (2001). The experiment was done on a half-scale model, which shows a significant reduction in the acceleration response spectrum in implementing ADAS device to the parent structure.

Whittaker et al. (1991) derived load–deformation response of the ADAS device using an equivalent X-triangular-shaped geometry of the ADAS device. Tenacolunga (1997) developed mathematical modelling assuming an hourglass shape of the ADAS device, which is approximated by an exponential function. Design procedure for tall buildings implementing ADAS device was suggested by Martinez-Romero (1995).

Perry et al. (1993), Martinez-Romero (1993) and Soong and Spencer (2002) mentioned several successful applications of ADAS devices in North America. The Wells Fargo Bank building was retrofitted in San Francisco using seven ADAS devices (Perry et al. 1993). The building was built on 1967 but got damaged due to the Loma Prieta earthquake in 1989.

2.4.2. Triangular Added Damping And Stiffness (TADAS):

Tsai and Hong (1992) and Tsai et al. (1993) presented a special type of ADAS with triangular steel plates (Figure 2.5). The main intention was to reduce the sensitivity of end restraint on the stiffness. Instead of fixed ends at both sides, Tsai et al (1993) implemented one end fixed and the other end pin supported. As the transverse point load at the tip produces uniform bending curvature, no stress concentration occurs in this arrangement. TADAS makes utilization of the hysteretic flexural deformation for energy dissipation like ADAS, that eliminates the possibility of buckling.

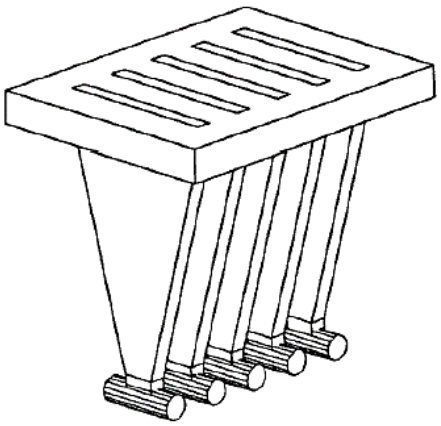

Figure 2.5 TADAS Device (Tsai et al., 1993)

Tsai et al. (1993) presented a simple analytical force-displacement relationship for the device,

$$P = \left(\frac{NEw_0h^3}{6L^3}\right)\Delta$$

where N is the number of triangular plates in the device, w_0 is the base width of the plate, L is the length of the plate, and h is the thickness of the plate.

Tsai and Hong (1992) conducted cyclic tests on a steel TADAS device. Test results showed a stable hysteretic response. Also, good agreement was found with the analytical model to derive elastic stiffness. The stiffness of the TADAS increased due to significant strain hardening at relatively large displacements. Yeh et al. (2001) conducted a full scale forced vibration test on a 5-story steel frame. The result showed a significant increase in the stiffness of the frame with TADAS device. Hwang (2003) reported an application of TADAS device in Taipei Living Mall Shopping Centre in Taiwan.

2.4.3. Buckling restrained brace (BRB)

Buckling restrained brace (BRB) was developed to overcome the problem associated to buckling of slender braces under compression which results in limited ductility of the frames. It is also identified as Unbonded Brace (Wada et al., 2000, Clark et al., 1999) and Buckling Inhibited Brace (Chen and Lu, 1990). BRB consists of two elements, one is the load carrying element and the other is the lateral support element (Figure 2.6). The load carrying element deforms inelastically due to the diagonal tension and compression in case of lateral movement of the frame, whereas the lateral support system protects the central load carrying element from buckling. An un-bonding material layer is generally coated between the elements to ensure free extension and contraction of the central core without buckling.

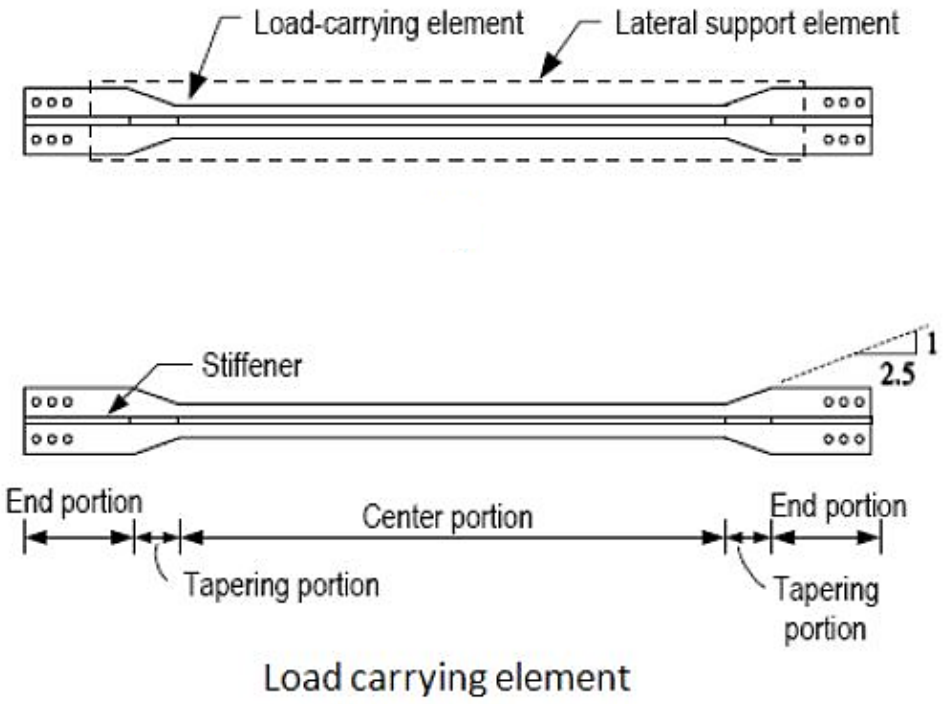

Figure 2.6 Elements of BRB (Chen, 2002)

Black et al. (2004), identified three distinct modes of stability failure or BRBs: (1) global flexural buckling of the entire brace, (2) buckling of the inner core in higher modes and (3) plastic torsional buckling of the portion of the steel core which extends outside the confining tube.

BRB devices were tested at University of California, Barkley during 1999 to 2000. Plastic torsional buckling load was the critical buckling load for these mild steel specimens. It showed a stable hysteretic response. Chen (2002) used Low Yield Steel (LYS) for BRB device and conducted tests on Concentrated Braced Frames (CBF) incorporating BRB. The BRB elements showed stable hysteretic behavior in the test and were found very effective in dissipating energy. Clark et al. (1999) reported that the frames with BRB can be designed for the same force as in eccentrically braced frames.

Clark et al. (1999) reported the first application of BRB device in the USA in a three story building at University of California, Davis. Nine tall building projects were designed in Japan during 1995-1998 using steel core BRB (Wada et al. 2000). The Wallales F Bennett Federal Building, Utah, USA was retrofitted successfully by making use of 344 BRB (Brown et al. 2001).

2.5. Yielding Shear Panel Device (YSPD)

YSPD is another recently developed energy dissipating device (Williams and Albermani, 2003; Chan et al. 2008, Hossain et al. 2011) which consists of a short segment of a Square Hollow Section (SHS) with a diaphragm plate welded inside it. A frame with YSPD has been shown in figure 2.7. YSPD utilizes shear yielding developed in the post-buckling regime to dissipate energy of earthquake. In other words, YSPD relies on “in-plane shear deformation” of steel plate to dissipate energy. Thin plate buckles under low levels of stress, and thick plate usually deforms under “pure shear” action (Chan, 2008). Now, if the thin plate can be adequately supported along its

boundaries, under the tension field action, thin steel plates can offer reasonably higher degrees of strength and ductility.

The SHS provides a boundary to the installed diaphragm plate, so that shear force acts in the plate. Secondly, it offers a suitable connection to the parent structural frame and finally, it helps in anchoring the tension field during the post-buckling of the diaphragm plate.

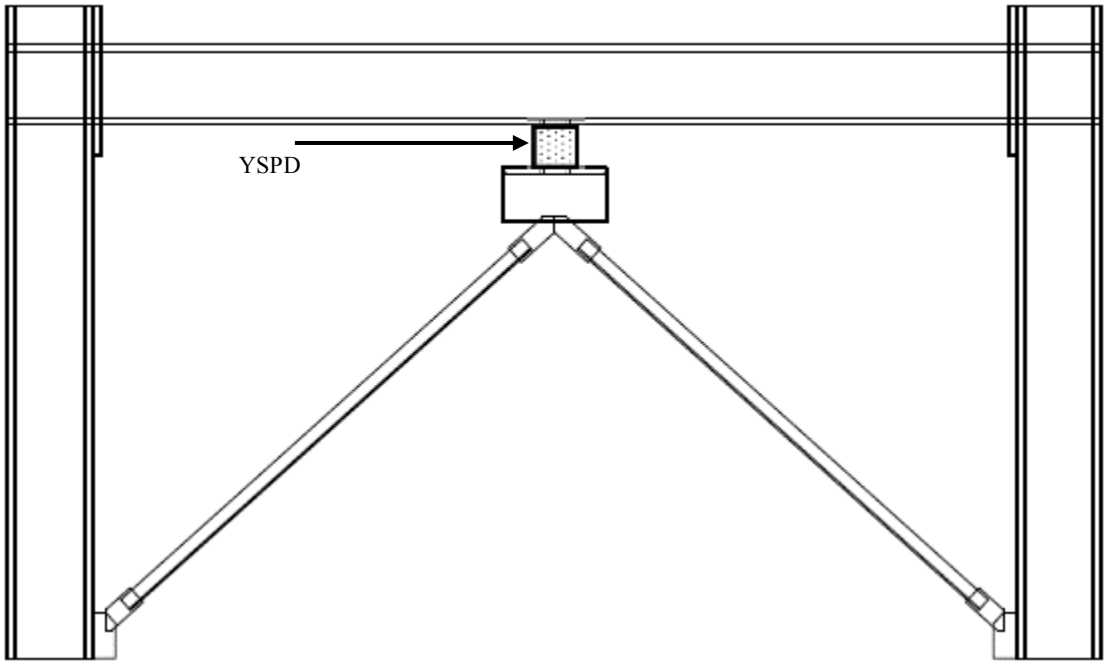

Figure 2.7 YSPD-brace assembly in a frame

2.5.1. Previous research on YSPD

The YSPD device was introduced and designed by Professor Dorka of the University of Kassel in Germany (Pradlwarter et al 1998, Williams et al 2003 and Schmidt et al 2004). A series of studies involving the experimental set-ups of Shear Panel Devices (SPD) (Schmidt et al. 2004) was commissioned by the European Commission Joint Research Centre. These SPDs were essentially identical to the YSPD, only differentiating between boundary. The boundary of these SPDs were

made up of 2 channel sections. The researchers carried out ramped-cyclic and pseudo-dynamic tests on a 3-story, 2-bay moment-resistant frame with a SPD fitted on inverted V-braces.

A response spectrum compatible (Eurocode 8) synthetic time history was applied. The damping was considered as 2% for stiff solids and the time history was scaled to a peak ground acceleration (PGA) of 0.30 g. In addition, the Kocaeli earthquake time history (scaled to 0.30 g) was also applied. Schmidt et al. (2004) reported that stable hysteresis was achieved in the ramped cyclic tests and approximately 85% of the input energy was dissipated by the device in the pseudo-dynamic tests. The parent structure remained elastic.

In the study conducted by Schmidt et al. 2004 only one SPD geometry was used for experiment (fabricated by welding two 5-mm thick channel sections and a 3-mm diaphragm plate). Therefore, the effects of diaphragm plate slenderness and flange thickness were not evaluated. In addition, the maximum displacement amplitude input to the device was limited to 10 mm.

Nakashima et al. (1994, 1995a, 1995b) tested shear panel specimens made of a special low-yield steel having 0.2% offset yield stress of 120 MPa. Both, stiffened and unstiffened specimens of various plate slenderness ratios were tested. They showed that the pinching of hysteresis could be eliminated by the proper arrangement of stiffeners. The strain hardening was significant and it added to the post-yield strength of the specimens.

Williams and Albermani (2003) performed quasi-static tests on a half-scale moment resisting frame equipped with an YSPD (Fig. 2.8). 1.5-m-high steel Moment Resisting Frame (MRF) was designed to the AS41000 Australian steelwork code. YSPD specimens were fabricated by welding a steel plate inside of a Square Hollow Section (SHS). YSPDs of various plate thicknesses (2 mm,

3 mm and 4 mm single and double plate) were positioned between an inverted V-brace and the portal beam. Total 24 monotonic and cyclic loading tests were conducted.

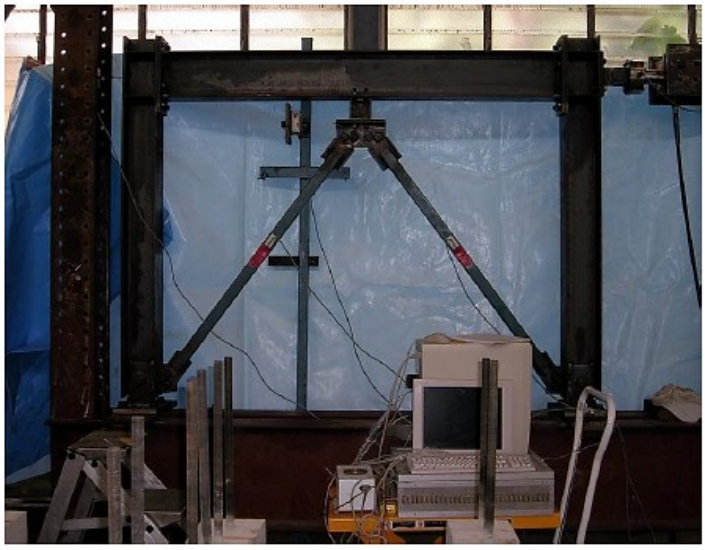

Figure 2.8 Assembly of YSPD in the frame (Williams and Albermani, 2003)

The devices yielded at low deformations. Still, YSPD devices were able to sustain a large degree of ductility (between 11.4 and 24.2). This implied that such devices begin to dissipate energy early in an earthquake and continue to do so on increasing the displacement. The devices showed stable hysteretic stress-strain behavior in most of the cases and thus proved effective in energy dissipation during earthquake. The study proves that the YSPD is an effective and viable solution as well as an inexpensive passive device.

Chan et al. (2008) studied the performance of the YSPD alone (tested as an isolated from the main frame). A series of sub-assemblage tests were done on half-scaled YSPD specimens. A total of 27 such tests were conducted (Figure 2.9). The parameters were plate slenderness and device configurations.

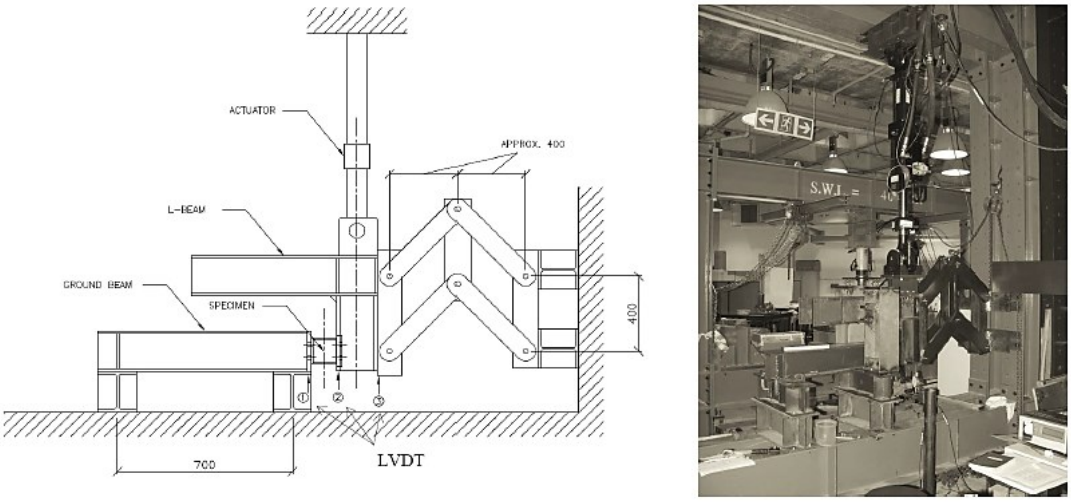

Figure 2.9 Experimental Set-up of Yielding Shear Panel Device (Chan, 2008)

Two different sizes of YSPD, 100mm x 100mm and 120mm x 120mm, with three different thicknesses of 2 mm, 3 mm and 4 mm for the diaphragm plate were tested. 4 Nos. M16 bolts on each side of the square hollow section (SHS) were used to install the test specimen between the ground beam and the L-beam as shown in Figure 2.10. Bolt spacing of 50 mm was used.

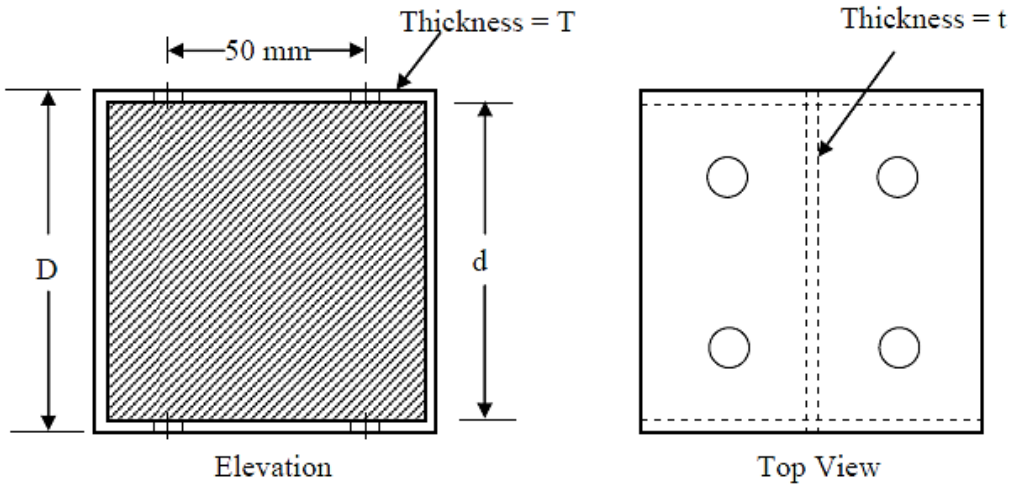

Figure 2.10 Schematic diagram showing the geometric parameters of YSPD (Chan, 2008)

Table 2-1: Geometric details and material properties of YSPD test specimens (Chan et al., 2009)

YSPD designation (DxTxt)	SHS size, D (mm)	SHS thickness, T (mm)	Diaphragm thickness, t (mm)	Tensile yield strength of SHS (MPa)	Tensile yield strength of diaphragm plate (MPa)
100x4x2	100	3.76	1.86	414.9	211.3
100x4x3	100	3.76	2.83	414.9	321.3
100x4x4	100	3.76	3.78	414.9	351.2
120x5x2	120	4.91	1.86	333.3	211.3
120x5x3	120	4.91	2.83	333.3	321.3
120x5x4	120	4.91	3.78	333.3	351.2

Both monotonic and cyclic tests on YSPD were carried out. The specimens were tested under quasi-static conditions with a displacement rate of 0.2 mm/sec. In monotonic tests, a displacement controlled force was applied to the specimen. The maximum actuator displacement was set to be 20 mm. For cyclic tests, a quasi-static loading history comprising three repeated cycles at amplitudes of 0.5, 1.0, 3.0, 5.0, 10 and 20 mm (a total of 18 cycles) was applied.

Elastic shear buckling in thin steel plates under low levels of shear stress was observed as the plate was adequately supported along its boundaries. In presence of tension field action, plates offered substantially higher degrees of strength and ductility. The observed load-deformation behavior of YSPD 100x4x4 under monotonic and cyclic loading are shown in Figure 2.11 and 2.12 respectively.

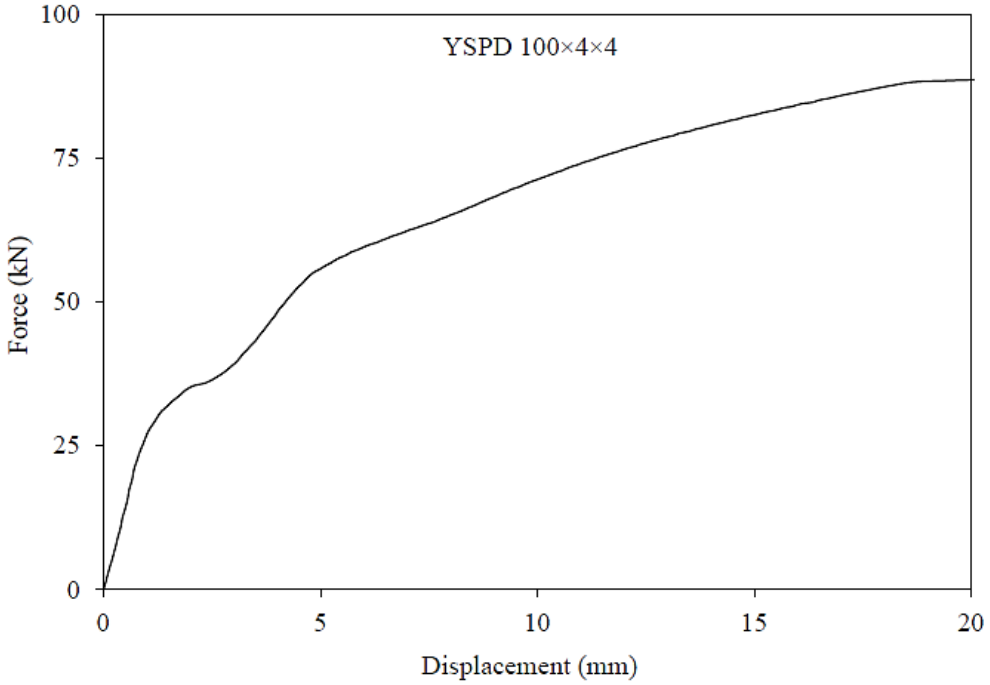

Figure 2.11 Test results of YSPD 100x4x4 under monotonic loading Chan et al. (2008, 2009)

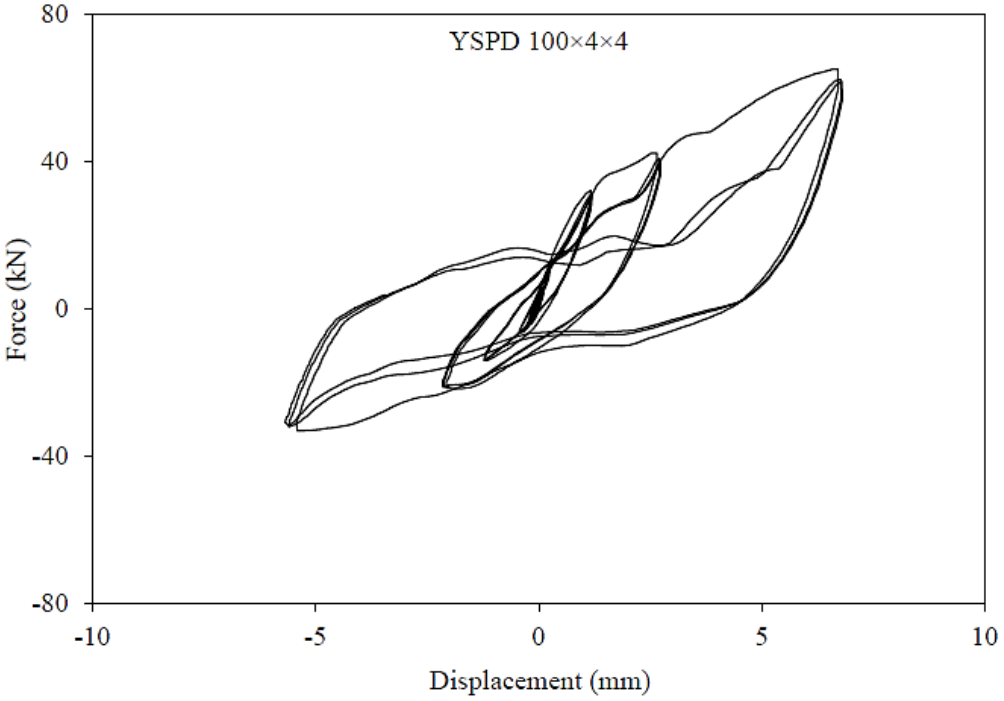

Figure 2.12 Test results of YSPD 100x4x4 under cyclic loading Chan et al. (2008, 2009)

Hossain et al. (2011) numerically modelled the device (isolated from the parent frame) with special emphasis on modelling appropriate support conditions, initial geometric imperfections and residual stresses. Spring elements were used for simulating the effect of the bolted connection between the device and the parent structure as shown in Figure 2.13. The developed finite element models were studied under the action of monotonic and cyclic loading. The analysis results showed good agreement with the test results, done by Chan et al. (2008). Hossain et al (2011) proposed a "Bilinear analytical model" as shown in Figure 2.14 to predict the initial stiffness of YSPD. The effect of material properties on the energy dissipation characteristics was also studied and it was reported that Lean duplex stainless steel show a superior performance when compared with mild steel.

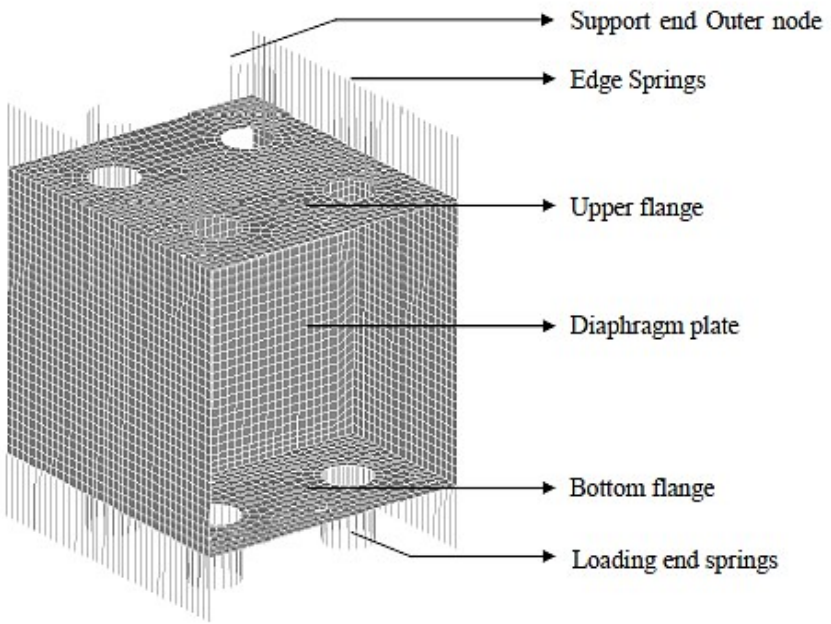

Figure 2.13 Spring elements used to model appropriate boundary conditions for YSPD

(Hossain, 2011)

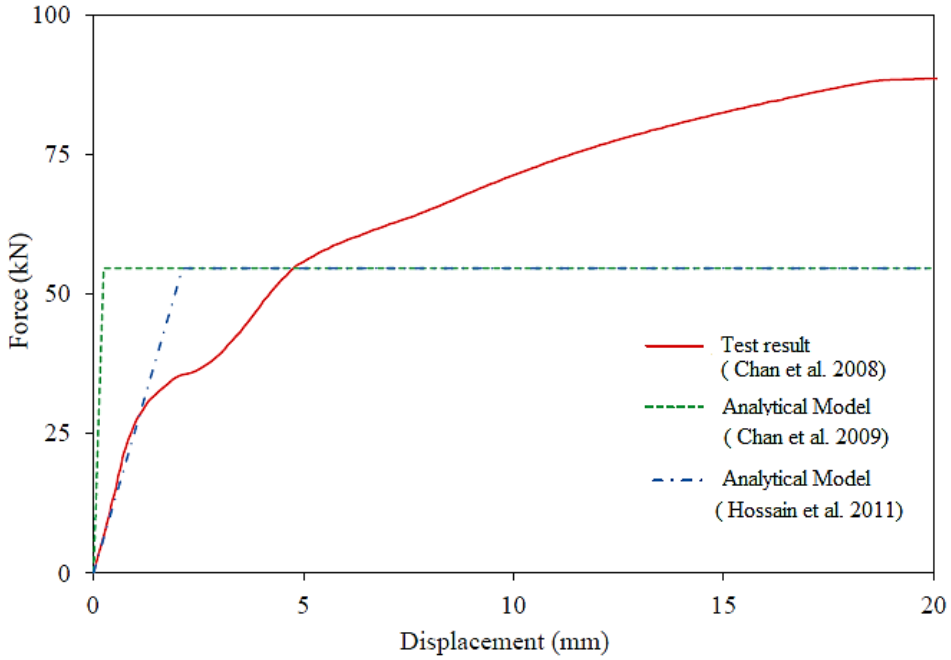

Figure 2.14 Analytical model of YSPD (Hossain, 2011)

Three different models, i.e., Informational, Mathematical and Hybrid informational models of YSPD were proposed to represent the force displacement behavior of the device. Trained neural networks were developed in the informational model from the force displacement data of YSPD and the model showed the ability to replicate the response. The Bouc-Wen-Baber-Noori (BWBN) model (Wen, 1976, Baber and Noori, 1986) was used in the mathematical modelling for the simulation of the hysteretic response of YSPD (Figure 2.15) to include the pinching characteristics. The model parameters were derived using the results obtained from numerical modelling. The hybrid modelling combined a mathematical model to represent the complex pinching hysteretic response and an informational model to relate the design variables with the model parameters. The mathematical model showed better accuracy compared with the hybrid informational model when validated against test results and not limited to a single YSPD compared to the informational model.

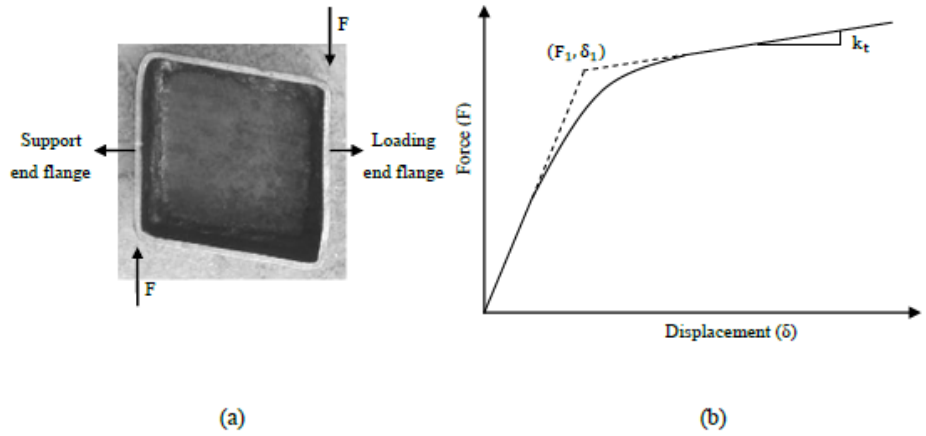

Figure 2.15 (a) Deformed shape of YSPD (b) Nonlinear force displacement (F-δ) relationship of YSPD as implemented in BWBN model (Hossain, 2013)

Seismic performance evaluation of YSPD was carried out by "Limit state probabilistic analysis" on SAC (Phase II Steel Project) Building (FEMA, 2000a, Ohtori and Spencer Jr, 2004). A Finite Element model was developed with modified BWBN model and included in the OpenSees platform to simulate the behavior of YSPD. Six different YSPD configurations including three different YSPD sizes were studied. The results from the nonlinear dynamic analyses were used for to study seismic fragility and limit state probability analysis. The fragility analysis provides the probability of exceeding various levels of damage in terms of inter story drift, whilst the limit state probability analysis demonstrates the annual probabilities of damage state exceedance at a given site. Figure 2.13 and 2.14 show the seismic fragility and annual performance limit state exceeding probability (P_{LS}) for the level of damage "Life safety". The YSPD showed better damage state risk reduction in the high-seismic zone compared with moderate-seismic zones in terms of retrofitted buildings in different hazard conditions. This method was suggested as a risk based decision making tool to evaluate seismic response of structures with installed YSPDs.

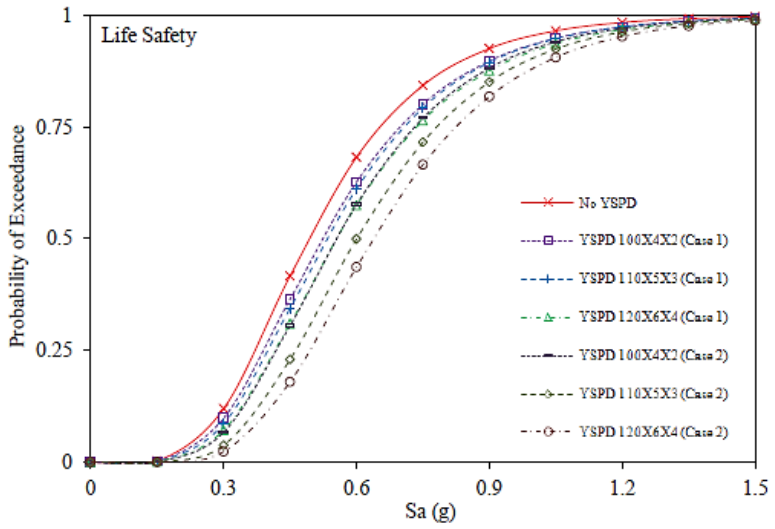

Figure 2.16 Fragility curves for the North-South lateral load-bearing frame of the SAC three storied LA building with and without YSPDs (Hossain, 2013)

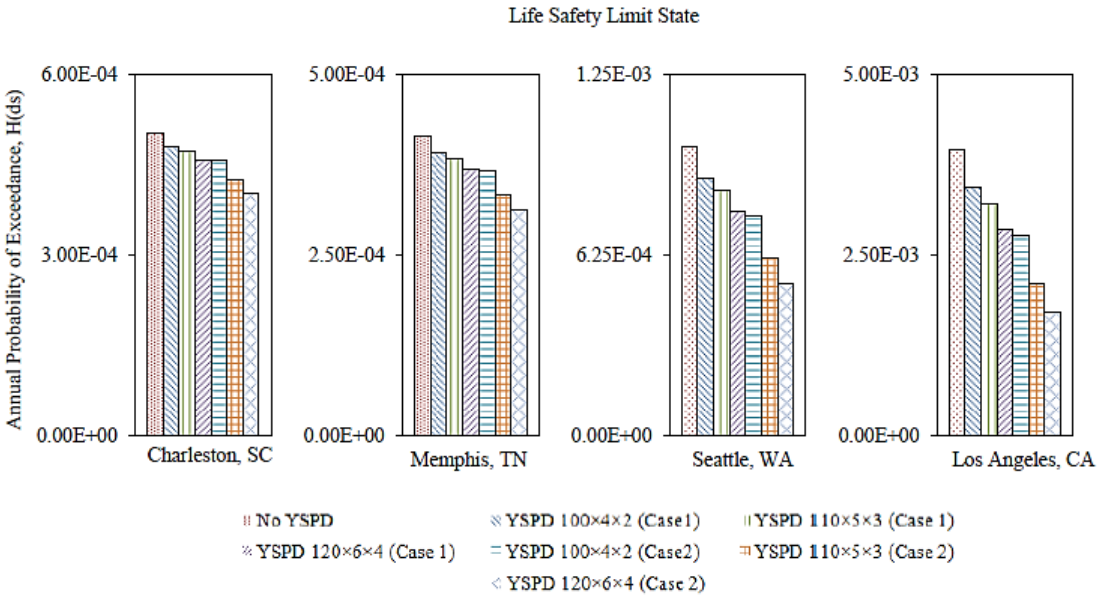

Figure 2.17 Annual performance limit state exceeding probability (P_{LS}) for regions of moderate seismicity and high seismicity (Hossain, 2013)

The traditional YSPDs were found damaged in SHS near bolt holes in Chan's (2008) experiment. The reason can be associated to a high in-plane stiffness of the plate imposing a large demand on the supporting SHS. Also, a significant pinching of the hysteresis response was noticed in the experiment. Low F_y along with bolt slippage and nut loosening were the reasons as reported.

To resolve this, a modified YSPD (M-YSPD) was introduced and tested by Yung (2010) as shown in Figure 2.18. M-YSPD consists of two thick base plates and these plates are welded to the YSPD. The bolted connections are located outside the SHS on the base plates. The hysteresis response of the device improved significantly and 99% of theoretical value of F_y was achieved as reported.

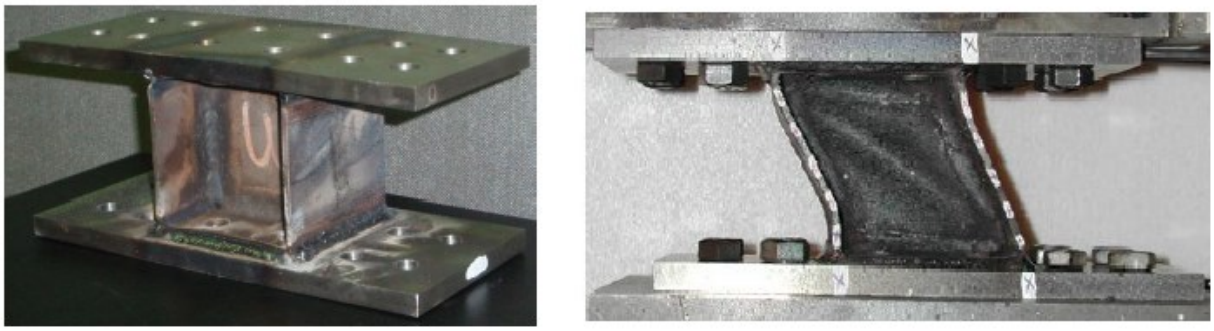

Figure 2.18 M-YSPD (Un-deformed and deformed by shear) (Yung, 2010)

Ali Habibi et al. (2013) proposed a stepwise multi-mode energy-based design method for seismic retrofitting with passive energy dissipation systems. The modal pushover analysis method was utilized to calculate the modal yield force and ductility factor of an equivalent single-degree-of-freedom (ESDOF) system. Only two modes, with highest participation factor, was considered. The energy contribution for two modes was calculated using energy spectra. The required amount of energy dissipation was estimated. A method to distribute the energy along the height of the

structure was proposed. The modified yielding shear panel device (M-YSPD) was used for retrofitting three moment resisting frames (SAC Phase II Steel Project, Los Angeles, California region) of 3-story, 9-story and 20-story. The story drift and absorbed energy for nonlinear time history analysis (NTHA) were evaluated by the proposed design method. The modified yielding shear panel device (M-YSPD) was used to retrofit existing structures. It was reported that M-YSPD is not a good passive energy dissipation device choice to retrofitting the building for strong ground motions, as it leads to using too many parallel thin plates in each device, which results in affecting the performance of the device. The M-YSPD device was suggested for moderate and low ground motions.

2.5.2. Summary

The previous studies show that the experimental test of the device has been done successfully and numerical model can be developed to get the similar characteristics of the device. The numerical model can be used to explore various configurations of the device. This is discussed in chapter 3 in this study. The calibration of mathematical modelling (Hossain, 2013) has been done from the numerical modelling of the device. Hence, this mathematical model can be used to compare the device force-displacement response when it the device is attached to a frame. This frame with device can be modelled numerically, which is done in chapter 4 in this study. Also, the researchers implemented the device for retrofitting purpose only and designed the device according to an energy based design method. A simple design method may be followed for this purpose and can be implemented in a new construction, which is done in chapter 5 in this study. Hence, these areas are explored and discussed in details leading to a better understanding of the system.

CHAPTER 3: NUMERICAL MODELLING OF YSPD

3.1. Introduction

YSPD is a relatively new passive energy dissipation device, which is designed to use the shear deformation capacity of a metallic plate to absorb seismic energy. In order to study behavior of this new energy dissipation device an appropriate Finite Element (FE) model is required to be developed. The current chapter presents the development of FE models for YSPD using a general purpose finite element software ABAQUS 6.11. The modelling is based on the test carried out at the University of Queensland and City University of Hong Kong (Chan 2008, Chan et al. 2009). Results obtained from this FE analysis are compared against those obtained from test results for both monotonic and cyclic loadings.

3.2. Mechanism of YSPD

When subjected to the loading, the YSPD has to resist two equal and opposite forces acting through the bolted connections. The diaphragm plate and the square hollow section (SHS) deform simultaneously as shown in Figure 3.1. When displacement occurs, the plate yields and deforms plastically. As a result, the input energy is dissipated. Also, the flexural deformation of the SHS is expected to build.

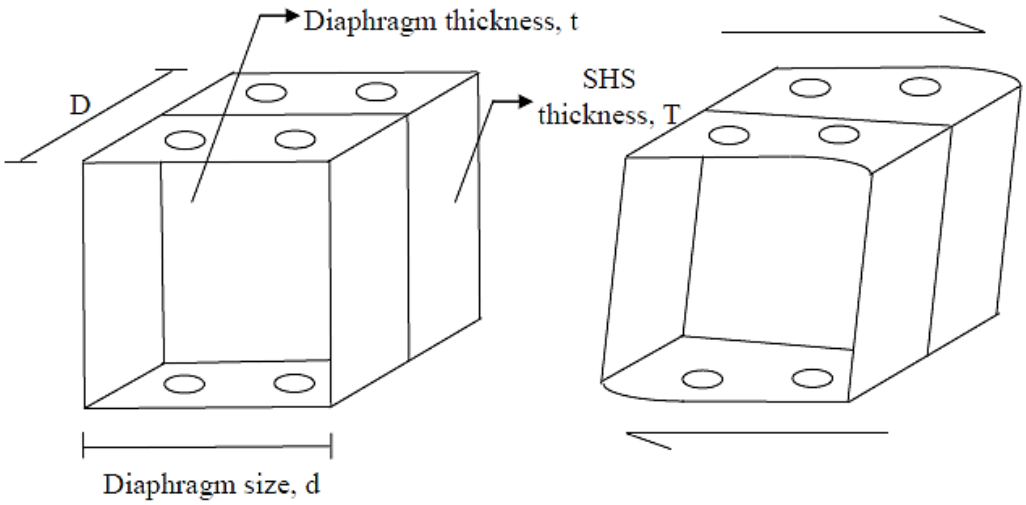

Figure 3.1 Un-deformed and deformed shapes of YSPD (Hossain et al. 2011)

Considering the development of 45-degree tension field, the square section is more effective than a rectangular section (Chan, 2008). The length and width of the diaphragm plate inside YSPD are equal and it is denoted by 'd'. The relative horizontal displacement between the flanges of the YSPD is denoted by δ (Fig. 3.2). It causes the diaphragm plate to deform in shear with a shear strain $\gamma = \delta/d$.

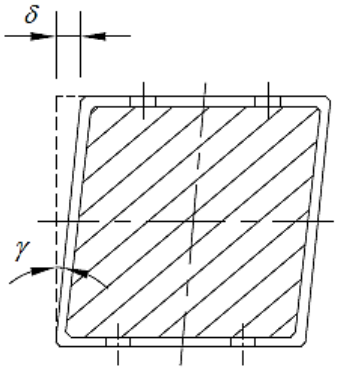

Figure 3.2 Deformation shape of the diaphragm plate (Chan, 2008)

The theoretical elastic in-plane lateral stiffness of the device K_d, by neglecting SHS due to a minor contribution, as proposed by Chan (2008) is,

$$[3.1]\ K_d = \frac{Gtd}{d} = Gt$$

where G and t are shear modulus of steel and the thickness of the diaphragm plate, respectively. The yield force in shear for a compact diaphragm plate (F_y) is defined as:

$$[3.2]\ F_y = \frac{f_y}{\sqrt{3}}\ td$$

where f_y is tensile yield stress of the diaphragm plate and d is the width of it. Therefore, the yield displacement, u_y, of the device can be found by the equation below,

$$[3.3]\ u_y = \frac{F_y}{k_d} = \frac{f_y d}{\sqrt{3}G}$$

For a device with slender diaphragm plate, elastic shear buckling is likely to occur. For a simply supported plate, the critical shear stress is calculated with the equation below,

$$[3.4]\ \tau_{cr} = k_s \frac{\pi^2 E}{12(1-\upsilon^2)}\left(\frac{t}{d}\right)^2$$

k_s equals to 9.34 for square plate depending on the aspect ratio of the plate. E is Young's modulus and ν is Poisson's ratio. Considering E = 200 GPa and ν = 0.3, the slenderness ratio of the plate at which buckling happens is (Chan, 2008)

$$[3.5]\ \frac{d}{t} = \frac{1710}{\sqrt{f_y}}$$

where f_y is the tensile yield stress of the diaphragm plate (MPa).

YSPD with slender diaphragm plates are prone to out-of-plane shear buckling. In the other hand, a device with compact diaphragm plate eliminates buckling but the very high in-plane stiffness of the plate may cause undesirable damage in SHS near the bolt holes (Chan, 2008).

3.3. Numerical modelling of YSPD

3.3.1. Material modelling

Williams and Albermani (2003) and Chan et al. (2009) used ordinary carbon steel plates and steel SHS sections to manufacture the tested YSPD specimens. For this numerical modelling in ABAQUS, isotropic hardening with bilinear idealization (elastic- plastic) is used for monotonic test. Kinematic hardening is used for the modelling of YSPD in cyclic test. The hardening rule describes how the yield surface changes (size, center, and shape) as the result of plastic deformation. The hardening rule determines when the material will yield again if the loading is continued or reversed. For isotropic hardening, the yield surface expands uniformly in all directions with plastic flow. For kinematic hardening, the yield surface remains constant in size and translates in the direction of yielding. The tangent modulus after yielding is assumed as 1% of the Young's modulus of elasticity for taking care of strain hardening. This has the reference of the coupon test results conducted by Chan et al. (2009) as shown in the Fig. 3.3. In sequence with the test description (Chan et al. 2009), the value of Elastic Modulus (E) and Poisson ratio (ν) are taken as 205 GPa and 0.3 respectively. Also, the tensile yield stress of SHS and plate sections are used as found the test report.

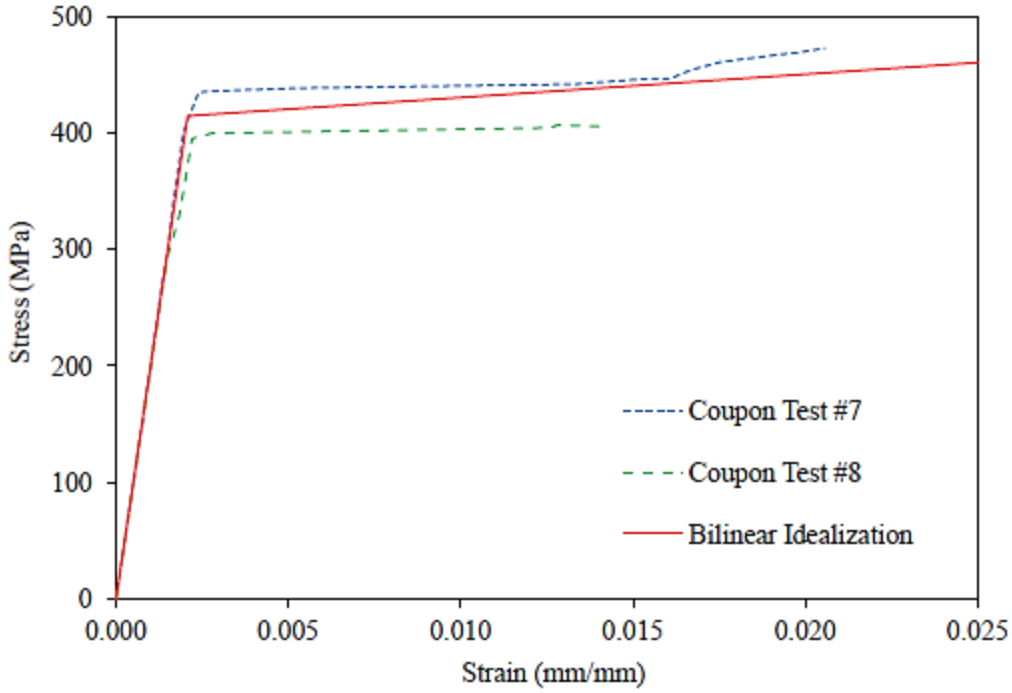

Figure 3.3 Material properties of the steel plate of YSPD 100x100x4 (Chan, 2008)

3.3.2. Element type

Shell elements are widely used by the researchers to model thin walled metallic structures. Four-node quadrilateral shell element S4R available in ABAQUS is used for this numerical modelling. S4R is a general purpose conventional shell element, which is able to model either thin or thick shell behavior. In general, shell elements may be utilized when the in-plane dimensions of the elements are much higher than its thickness. The shell elements are advantageous because they reduce the computational demands significantly. S4R element has 6 degrees of freedom (DOF) at each node. These are 3 translations and 3 rotations, defined in a global coordinate system. This element accounts for finite membrane strains and arbitrarily large rotations; therefore, they are suitable for large-strain analysis.

3.3.3. Support conditions

The YSPD is connected to the bottom flange of the beam of the braced frame using bolts to ensure easy installation and replacement. The modelling of the support conditions has to be done properly to achieve the similar behavior of YSPD as found in the experiment. The following sections carry the details of the support conditions, implemented in experiment and FE modelling.

3.3.4. Boundary conditions considered in Experimental Setup

In the experiment, Chan et al. (2009) installed the test specimens between a ground beam and an L-beam, securely fastened by four M16 bolts (snug tight) on each side. The load was applied by using an actuator quasi-statically to the specimen via the L-beam. Displacement measurements obtained from the LVDTs indicated some initial in-plane rotation of the L-beam (Figure 3.4a). Considerable deformations were also observed in YSPD specimens. The upper flange of the YSPD (support end flange) moved towards right, whilst the lower flange (loading flange) moved in the opposite direction due to this in-plane rotation. These movements caused the support end flange and the loading end flange to experience bending in upper and lower portions respectively. The upper two bolts at the support end and the lower two bolts at the loading end experienced minor deformations due to this bending. Opposite movements and deformations were observed when the actuator was moved upwards. Figure 3.4(b) shows the deformed shape for YSPD 100x4x3 after it was subjected to monotonic test. Noticeable bending deformations observed at the flanges are highlighted by circles in Figure 3.4 (b).

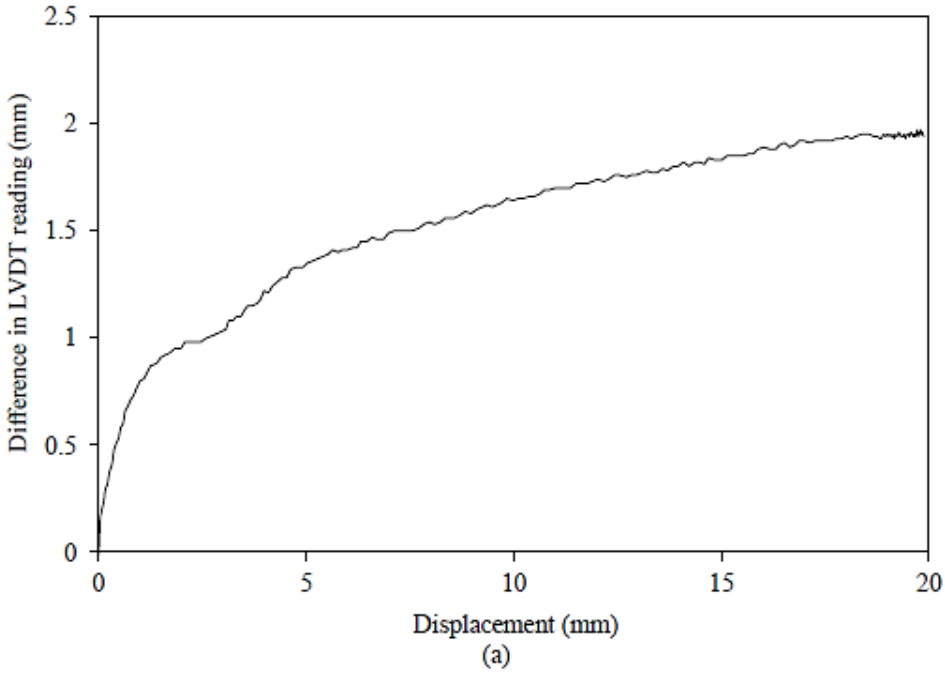

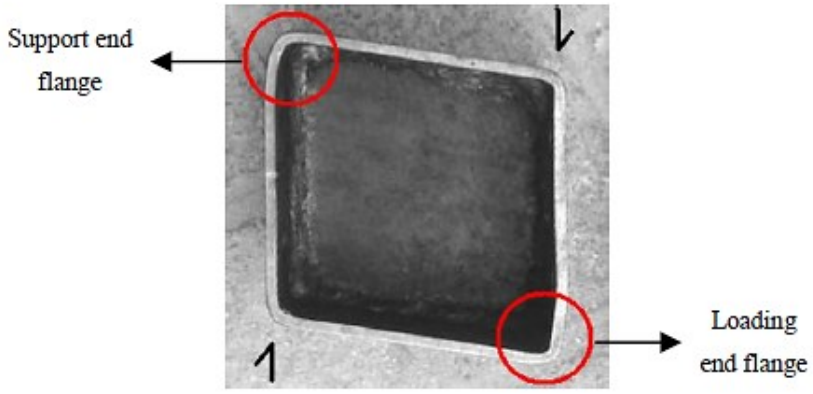

(b)

Figure 3.4 (a) Observed difference in LVDT readings placed at the bottom of the L-beam of YSPD 100×4×3 under monotonic loading (b) Deformed shape of YSPD 100×4×3 under monotonic loading (Chan, 2008)

3.3.5. Boundary conditions implemented in numerical modelling

For numerical modelling of the boundary conditions, similar steps are followed as done by Hossain et al. (2011). The upper flange of YSPD is connected to the bottom of beam section and the bottom flange is connected to the V-brace. Both the connections are bolted. When the force is applied, the V- braces try to move the bottom flange of YSPD. This is simulated in the numerical model by applying horizontal displacements to the nodes around the bolt holes of the lower flange of YSPD.

All the nodes along edges of the device are modelled as springs in FE simulation. These edge springs are subjected to tension and compression on the application of the load. Hence, the springs act as tension-compression elements. The tension stiffness of the spring is considered to be a small value, 0.0001 to eliminate the numerical singularity. The compression stiffness is considered to be same as the stiffness of the SHS flange. On the loading side, the stiffness of the springs are reduced by multiplying a factor λ where λ accounts the in-plane rotation.

Table 3.1 Magnitudes of spring stiffness used for modelling the boundary conditions of YSPD

Spring	Stiffness
Tensile stiffness of the edge springs, K_{et}	0.0001
Compressive stiffness of the edge springs, K_{ec}	$T \times S_n \times E_{SHS}$
Stiffness of the springs at bolt holes, K_b	$A_b \times E_b / N_b$

T = Thickness of the SHS plate

S_n = Nodal spacing in the SHS plate

E_{SHS} = Modulus of elasticity of SHS section

A_b = Cross-sectional area of one bolt

E_b = Modulus of elasticity of bolt material

N_b = Number of nodes per bolt hole

The bolted connections are also modelled using springs. The bolt holes are divided into 2 categories. The inner nodes are simulated as fully restrained and the outer nodes are restrained against in-plane translations only (Fig. 3.5). For the bolts also, the stiffness of the node springs are reduced by multiplying with the factor λ to account for in-plane rotation, similar to the edge springs. Hossain et al. (2011) conducted a parametric study to define the parameter λ. They considered a value of 0.00002 based on the parametric study for the numerical modelling. For this study, same λ value has been used as suggested.

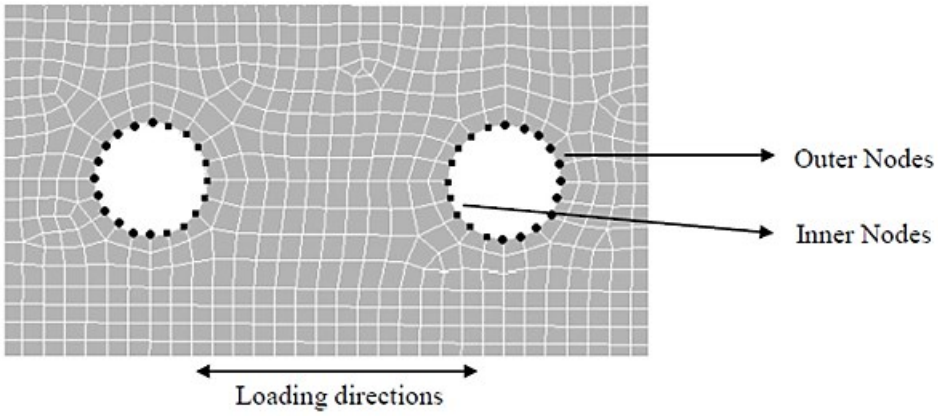

Figure 3.5 Modelling of inner and outer nodes around the bolt hole (Hossain, 2011)

3.3.6. Residual Stress

The diaphragm plate is welded inside the SHS section to build the YSPD. This welding process induces residual stress both in the diaphragm plate and SHS. As the distribution of residual stress is complex in nature, simplified distribution is generally adopted by the researchers to study its effect. Here, a simplified rectangular stress distribution is assumed and magnitudes are taken from ECCS specification (Fig. 3.6). Tensile residual stress is developed in the nearby region of welding and compressive stress is developed in the remaining region of the cross-section. The value of tensile residual stress is set to the yield stress and compressive stress is taken as 25 percent of yield strength of the material. The effect of residual stress is, overall, negligible and it marginally reduces the initial slope of the force-deformation response in some cases.

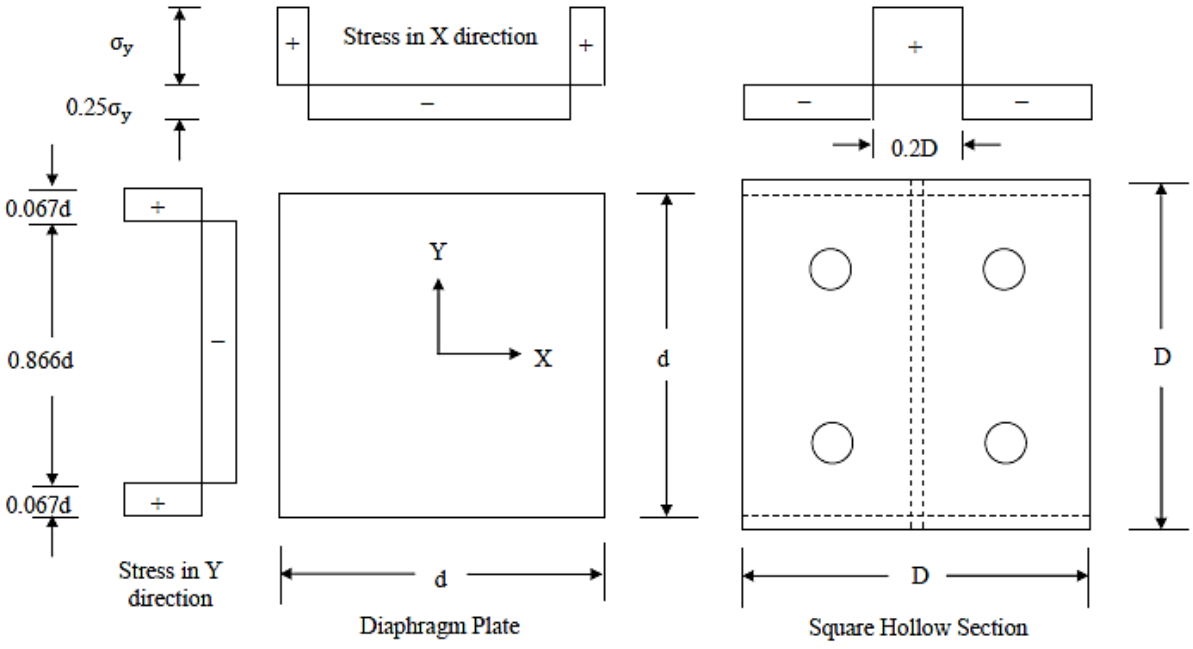

Figure 3.6 Residual stress Distribution in YSPD (Hossain, 2011)

3.3.7. Finite Element Analysis of YSPD

The selection of appropriate mesh is very important in the FE analysis. Three different mesh sizes are considered for the simulation as shown in Figure 3.7. The element size in the finer mesh (total number of elements is 7293) is half of the element size used in medium mesh (total number of elements is 1738) and one-sixth of that considered in the coarse mesh (total number of elements is 392). The results from the analysis show both the finer mesh and the medium mesh provide good agreement with test result. However, the finer mesh has been chosen in the finite element models to ensure accuracy of the analysis.

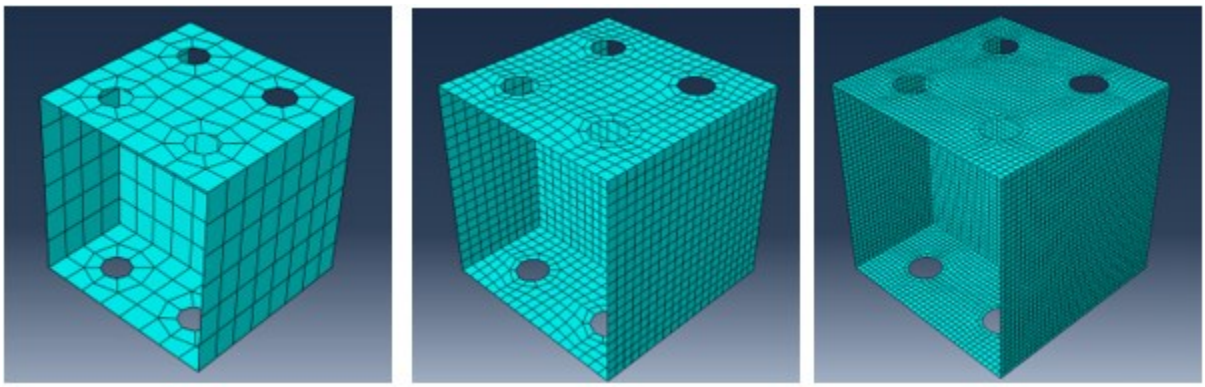

Figure 3.7 FE models of different mesh sizes

As for the thin plates, the non-linearity is expected to happen, non-linear geometry is considered by selecting the NLGEOM option available in ABAQUS. The monotonic analysis is performed by using smooth step function in amplitude section. The displacement is the input in the FE analysis. For the cyclic analysis, displacement is applied in the cycles similar to the experiment (Fig. 3.8). This cyclic displacement can be simulated in a time-amplitude table in ABAQUS. For both the cases, static general method is considered to run the analysis.

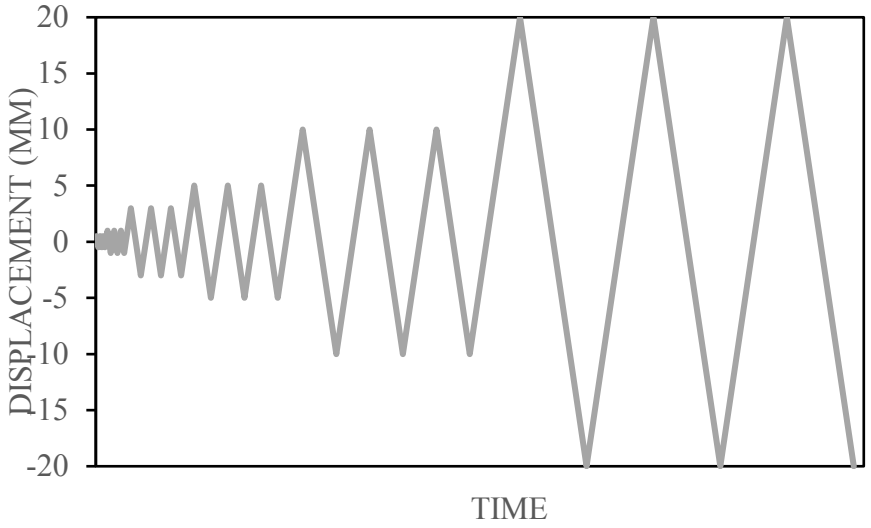

Figure 3.8 Displacement history for cyclic analysis (Chan, 2008)

3.3.8. FE Analysis Results

3.3.8.1. Monotonic loading

The force-displacement response for different YSPDs under monotonic loading are presented in the figure 3.9. The results from the analysis have shown good agreement with the test results. For the YSPD 120x5x4 and YSPD 120x5x3, finite element analysis over-predicts the initial stiffness in comparison to the test results. This may be happened due to the initial slippage of the bolted connections during the test.

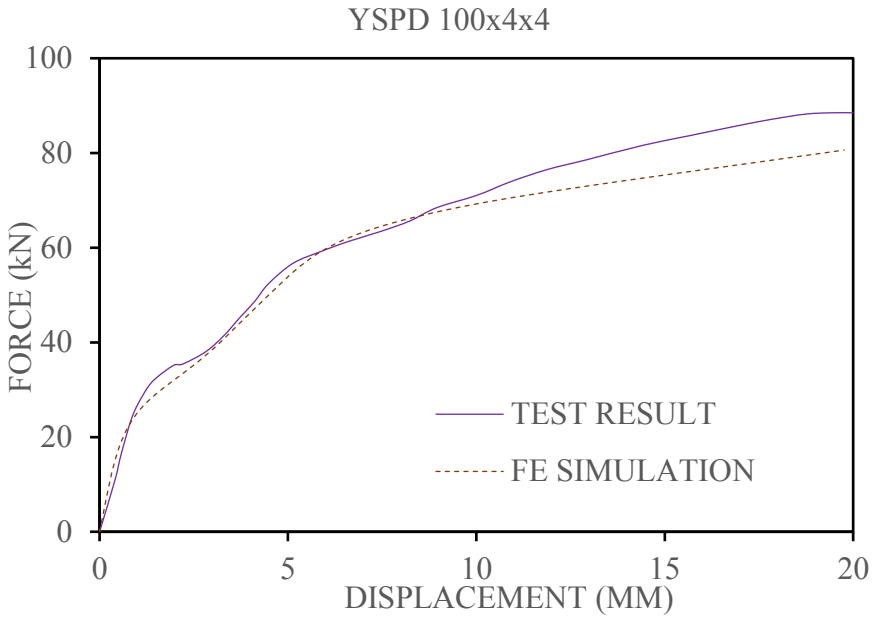

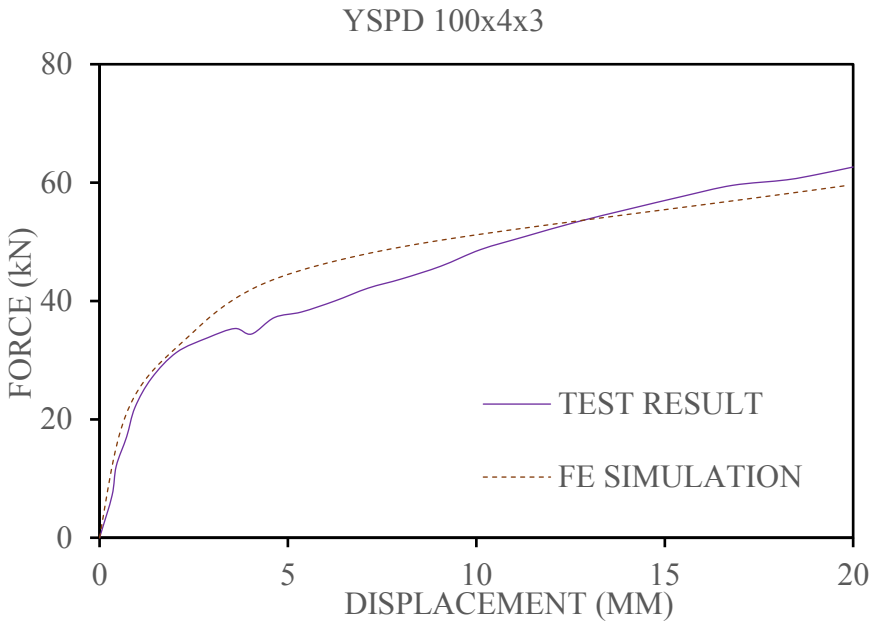

Figure 3.9 Force-displacement response of YSPDs under monotonic loading

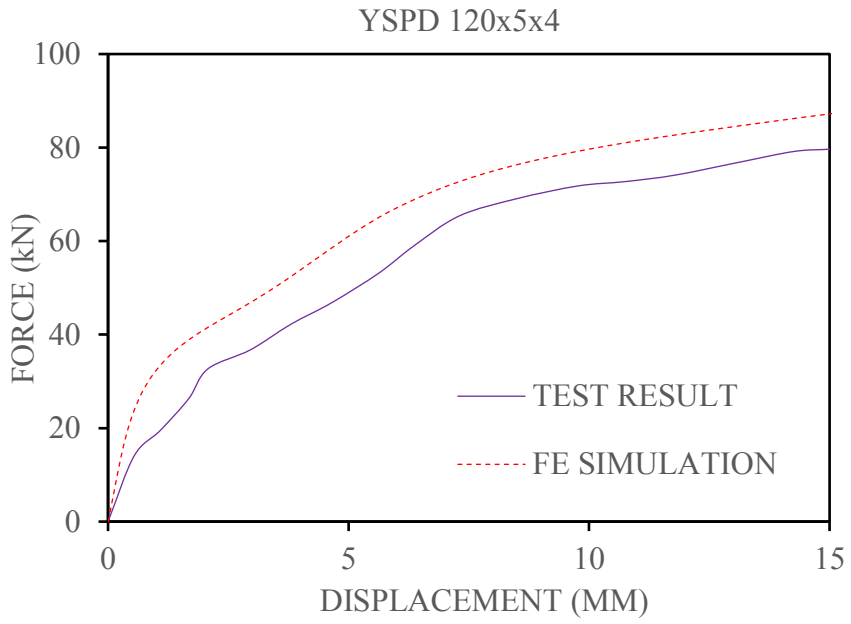

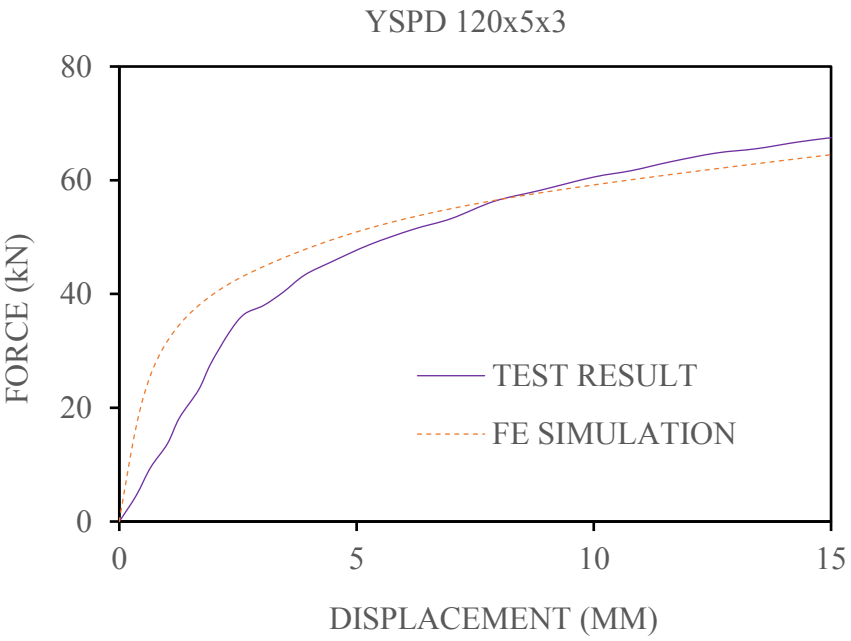

Figure 3.9 (contd.) Force-displacement response of YSPDs under monotonic loading

3.3.8.2 Cyclic loading

The developed FE models are further subjected to a cyclic deformation history. Displacement-control analysis is executed in ABAQUS. The deformation history is defined in the "Amplitude" module. The horizontal displacements are applied (say, in the x-direction) at the bolt hole nodes located at the loading flange i.e. bottom flange of YSPD. Reaction force (in the x-direction) at the bolt hole nodes located at the support flange i.e. top flange of YSPD are the output from the analysis. These reaction forces are added to calculate the total force resisted by YSPD. Force-displacement responses for the specimens subjected to displacement controlled cyclic loading are shown in Fig. 3.10.

The stiffness of the loading and unloading path was close to the experimental values. For all cases, considerable portions of plates have been yielded. In some cases, yielding has also been observed in SHS flanges, especially in the area near the bolt holes. It may be because of localized distortion, as reported by Chan et al. (2009). The FE model generally overestimates the transition strength between the elastic and inelastic regimes, and the peak strength values. Overall, the FE models have shown reasonable agreement with the test results.

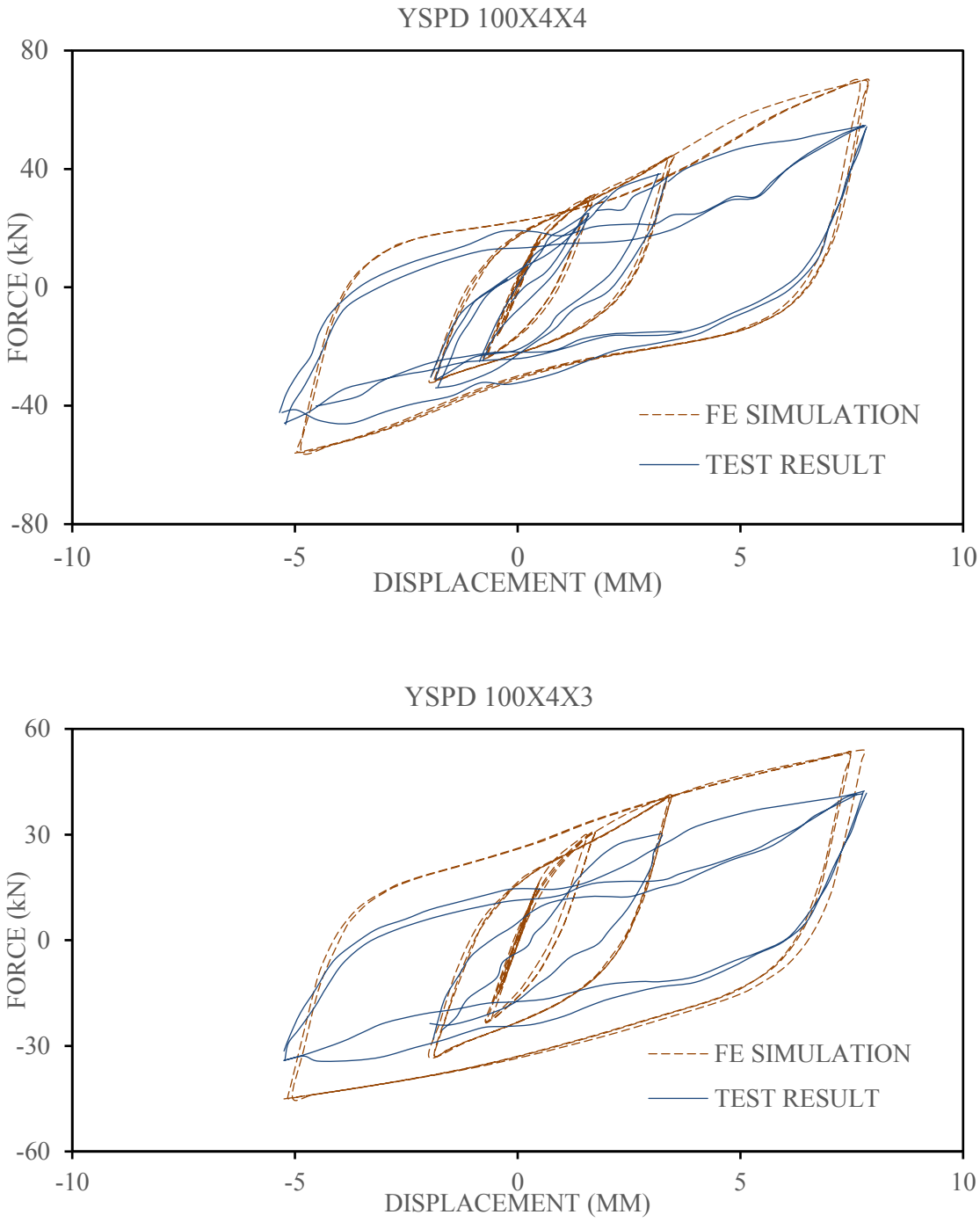

Figure 3.10 Force-displacement response of YSPDs under cyclic loading

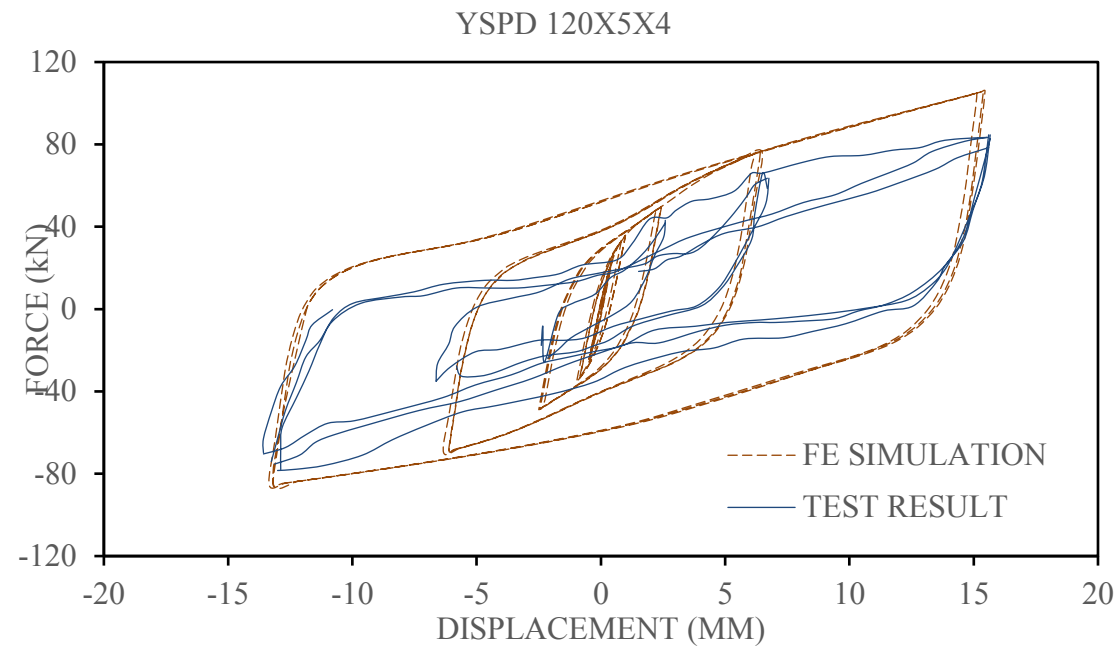

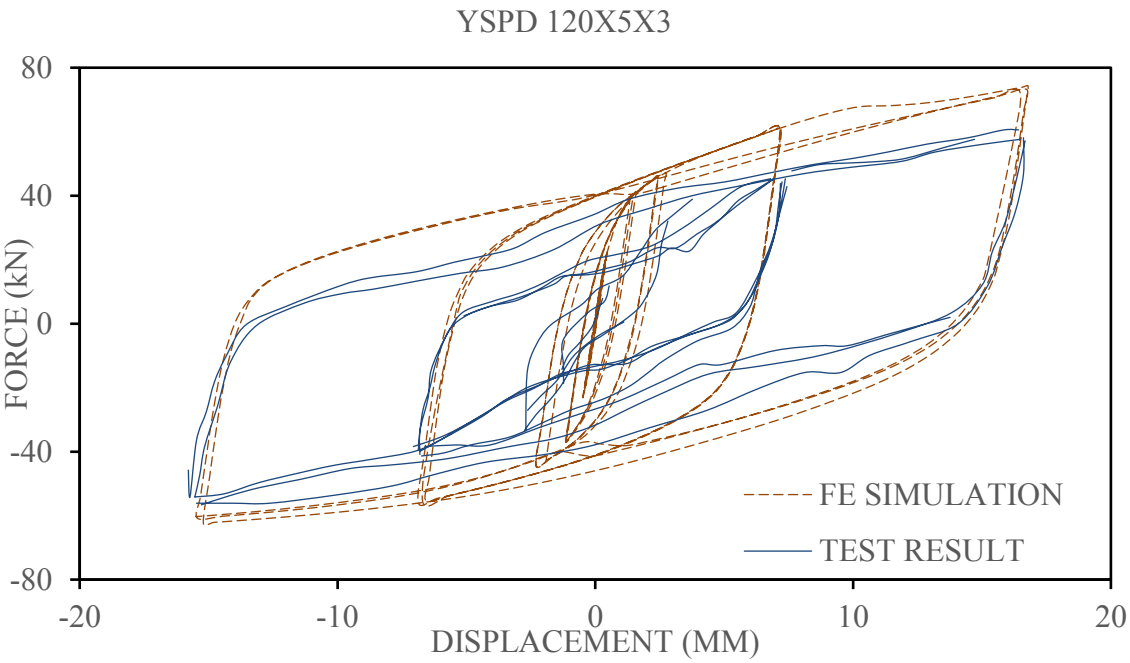

Figure 3.10 (contd.) Force-displacement response of YSPDs under cyclic loading

3.4. Compact and slender diaphragm plates

Elastic shear buckling depends on the slenderness ratio of the diaphragm plate. Slender plates show elastic shear buckling whereas compact plates don't show buckling before shear yielding.

The compact diaphragm plate within YSPD, deforms in shear without buckling (Chan, 2008). The SHS within YSPD deforms in flexure (Fig. 3.11)

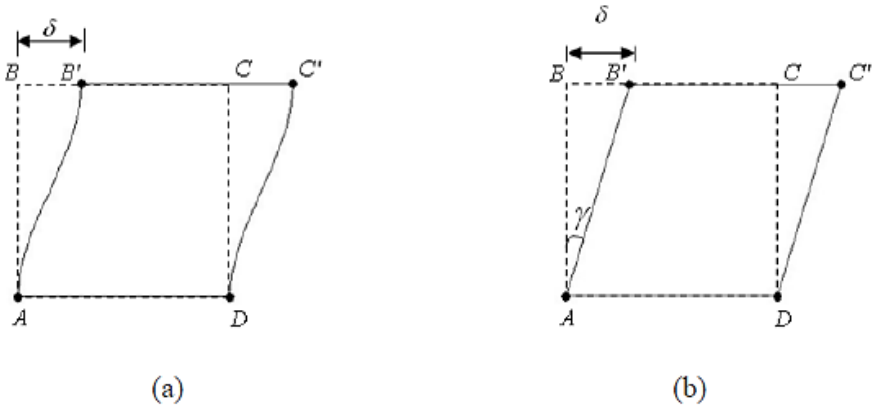

Figure 3.11 (a) Deformed shape of SHS, (b) Deformed shape of diaphragm plate (Chan, 2008)

The theoretical elastic in-plane lateral stiffness of the device K_d, assuming a minor contribution from SHS, as proposed by Chan et al. (2009) is (recalling equation 3.1)

$$K_d = \frac{Gtd}{d} = Gt$$

where G and t are shear modulus of steel and the thickness of the diaphragm plate, respectively.

Now, considering the contribution from SHS section, Chan (2008) proposed the following equation of calculating the total elastic in-plane lateral stiffness of the device.

$$[3.7] K_d = K_{SHS} + K_{dia} = \frac{2ET^3}{D^2} + Gt$$

T is the thickness of the SHS and D is the size of the YSPD section.

Recalling equation [3.3], the yield displacement of the device is

$$u_y = \frac{f_y d}{\sqrt{3}G}$$

where f_y is tensile yield stress of the steel plate and d is the width of the plate. The yield strength (F_y) can be rewritten as,

$$[3.8] F_y = K_d \; x \; u_y$$

For slender plates, after the development of critical shear stress, a tension field is developed at angle θ from the horizontal throughout the plate (Fig. 3.12). Here, σ_{ty} represents the tension field stress at which yielding occurs.

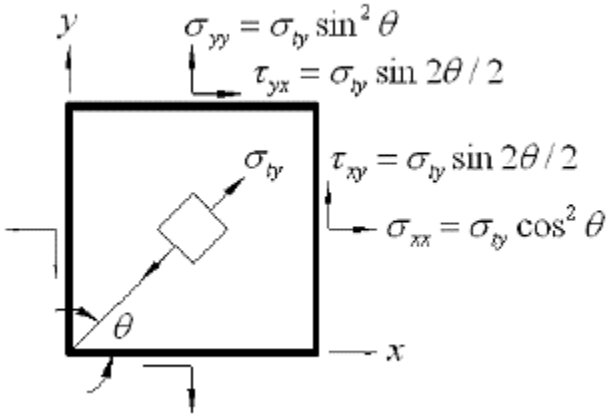

Figure 3.12 Tension field development in the thin diaphragm plates (Chan, 2008)

The shear strength of the slender plate can be written as,

$$[3.9] F_u = \tau_{xy} dt = \left(\tau_{cr} + 0.5\sigma_{ty} \sin 2\theta\right) dt$$

The tension field inclination angle θ has been proposed in a range of 35-55° (Timler et al. 1983, Lubell 1997). Moreover, when the diaphragm plate is very thin (i.e., $\tau_{cr} \approx 0$), the tension field action dominates the behavior (Chan, 2008).

3.4.1. Elastic shear buckling verification

Now, elastic shear buckling in the slender plates can be verified by using a numerical model. Six different plate thickness have been chosen (Table 3-2). The width of the plate remains same (100 mm) to allow change in stiffness. All the sections are assumed to have a yield strength of 200MPa. The numerical model, used for the experimental validation work, is utilized to study the shear yielding and shear buckling phenomenon in these YSPD sections. All the other properties including SHS width and thickness remain unaltered.

Table 3-2: Comparison of the yield strength of YSPD from analytical and numerical models

YSPD specification (DxTxt)	d/t ratio	Elastic shear buckling
100x4x4	23	No
100x4x3	30.67	No
100x4x2	46	No
100x4x1	92	No
100x4x0.8	115	Yes
100x4x0.5	184	Yes

The limiting value of d/t for a diaphragm plate having tensile yield stress (f_y) of 200 MPa can be found from the equation [3.4]. Hence, limiting d/t value is 122. The YSPD section 100x4x0.5 is therefore consists of a slender plate (d/t = 184). Elastic shear buckling is likely to happen in this section.

From the numerical analysis, it has been found that the YSPD sections 100x4x0.8 and 100x4x0.5 have showed elastic shear buckling although the first section is not slender according to equation [3.5]. But, the d/t is very close of limit for 100x4x0.8 section. Hence, the results from numerical analysis is well agreed with the analytical model. Inelastic buckling has been identified in the relatively thicker sections, which is expected to build.

3.5. Parametric study

Parametric studies allow to identify the influencing parameters that can affect behavior of structures. A parametric study is conducted to explore the mechanics of the YSPDs. Effect of different parameters such as panel thickness, SHS Plate thickness ratio, and shear panel aspect ratio are considered in this research.

3.5.1. Diaphragm plate thickness

The diaphragm plate thickness is varied for this case and all the other parameters like material properties, boundary conditions, geometric features and mesh densities remain the same. The panel thickness changes the slenderness ratio (d/t) for the YSPDs. For this study, slenderness ratio varies from 20 to 200. The results show that the yield strength is increased with increase in plate thickness or decrease in plate slenderness (Fig. 3.13). The initial stiffness is not greatly influenced for thicker plates, but yield strength and post-yield strength are significantly changed. FE 100x4x5 (slenderness 20) has the greatest strength among all the selected models. But, local distortion of

the SHS plates near the bolt holes are observed more in thicker plates. This signifies that for thicker diaphragm plates, the SHS sections are more distorted and the plate may not be utilized fully for energy dissipation. For 0.5 mm and 1 mm plate, plates are buckled significantly, whereas in thicker plates, no buckling is observed in plates (Fig. 3.14).

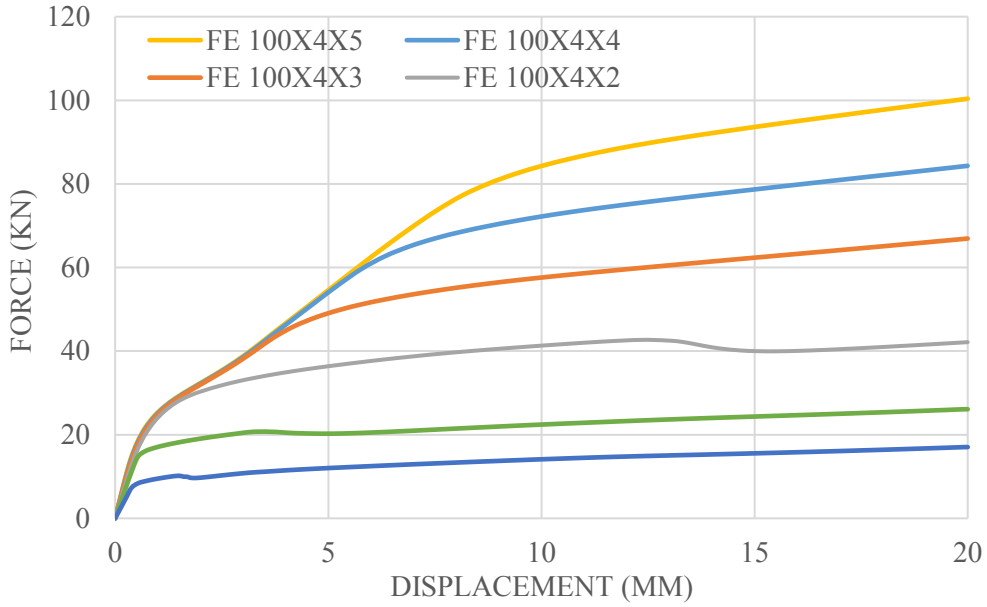

Figure 3.13 Force- displacement response for different plate thickness

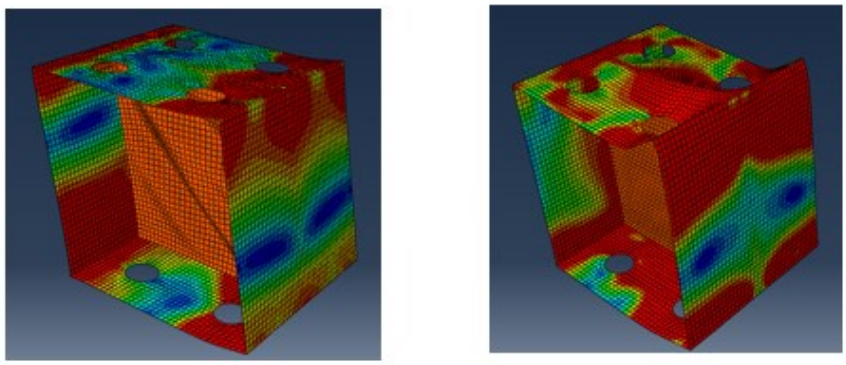

Figure 3.14 Deformed shape for 100x4x0.5 and FE 100x4x5 under monotonic loading

3.5.2. SHS section width

The parameter here is SHS section width and all the other parameters are kept constant. As expected, FE analysis shows that with an increase in d/t ratio, the yield strength and post-yield strength increased significantly (Fig. 3.15). FE 100, FE 120, FE 152 and FE 203 sections are studied for this purpose. It is evident that larger SHS sections like 203x5x4 can carry more force.

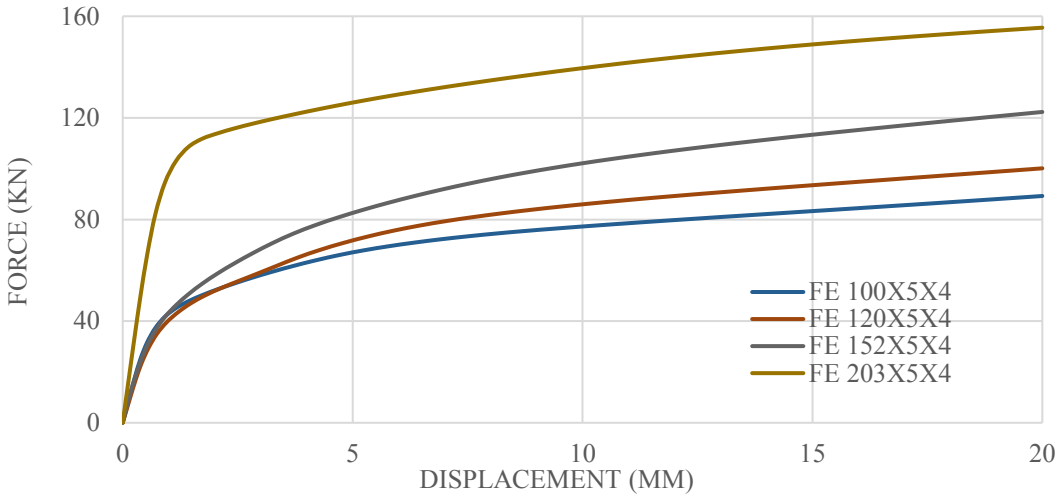

Figure 3.15 Force- displacement response for different SHS sections

3.5.3. SHS thickness ratio

In this section, effect of SHS section thickness is studied. Like the previous studies, all the other parameters are kept constant. Figure 3.16 shows that for an increase of T/t ratio (T = SHS section thickness, t = diaphragm plate thickness), the yield strength and post-yield strength are increased significantly. FE models of SHS 100 sections are studied for this purpose. For the responses, the thickness of plate is 2 mm and 4 mm. It is evident that thicker SHS sections can be used to fully utilise the energy dissipation capacity of the diaphragm plate.

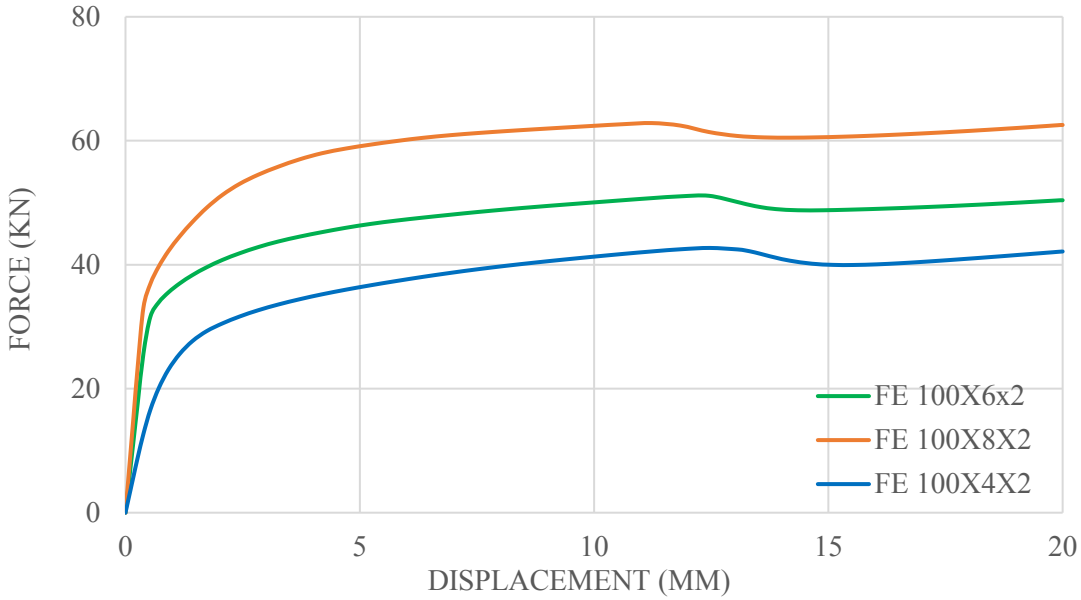

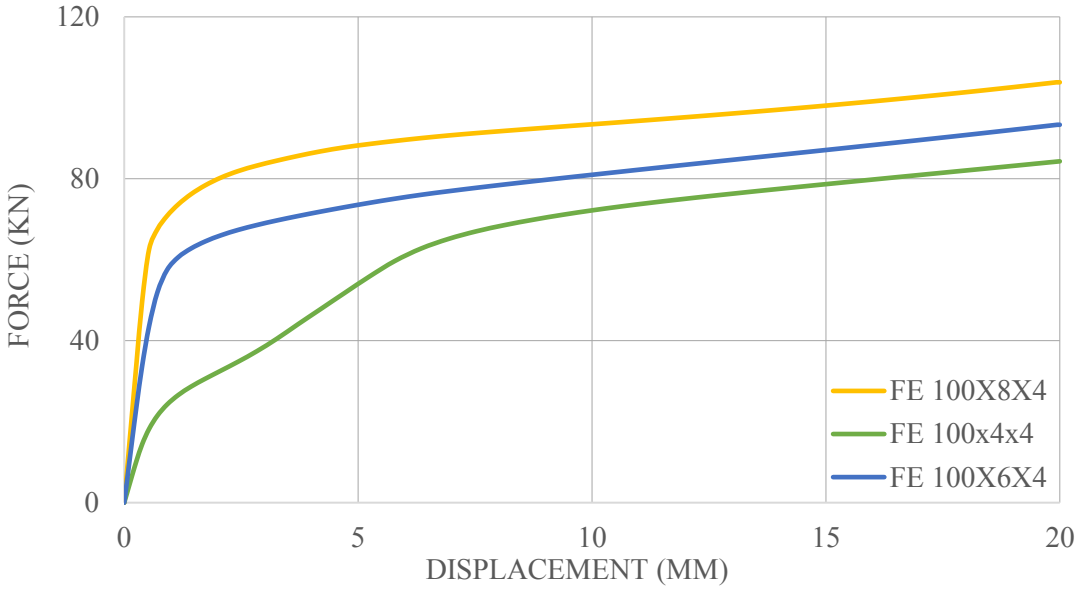

Figure 3.16 Force- displacement response for different SHS thickness

To demonstrate the actual effect of SHS thickness on the behavior of the YSPD, the load and displacement of the sections are normalized to the diaphragm plate yield strength (F_y) and shear strain ($\gamma = \delta/D$), respectively. The results are shown in Fig. 3.17. Among the studied sections, FE100x8x2 (T/t = 4, d/t = 50) has the highest level of stiffness and normalized strength. The maximum normalized strength for this section approaches 1.6 as shown in the figure. This implies a stiff boundary (SHS section) and a slender diaphragm plate make the most efficient YSPD. The thick SHS reduces development of any stress concentration and it allows the tensile strips in the diaphragm plate to be anchored effectively after formation of the tension field.

On the other hand, FE 100x4x4 (T/t = 1, d/t = 25) possesses the lowest level of stiffness and normalized strength. The flexibility of the SHS is the reason behind the low performance of this YSPD. It can be noted that the normalized strength is below 1.0 for FE 100x4x4 prior to a 10 percent shear strain. This demonstrates an ineffective use of the plate material.

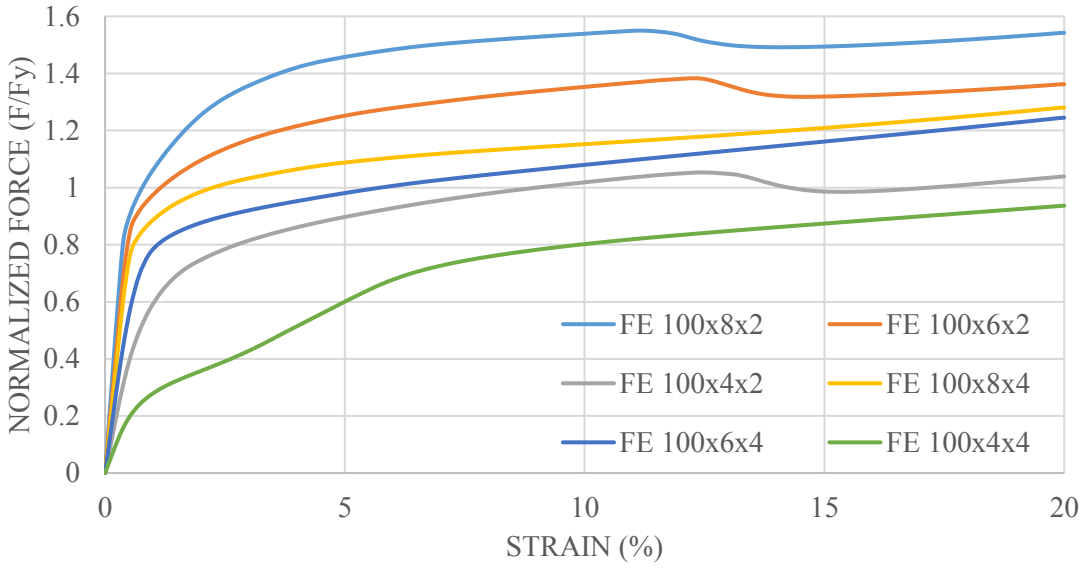

Figure 3.17 Force- displacement response for different SHS thickness

3.6. Study on larger SHS sections

Further, the larger SHS sections are studied to investigate the overall behavior of YSPD. In the experiments, Chan et al. (2009) used 100 and 120 mm SHS specimens with different plate thicknesses. For this study, FE models are developed for 203x203x8 SHS sections in the similar procedure as FE 100 YSPDs. For the 203 SHS section, 8 bolts are used in each side (Fig. 3.19). The target strain in monotonic loading is set to be 20 percent in panel for the sections. The parametric studies are carried out for panel thickness and they show similar conclusion. The thick plates are capable of dissipating more energy and thicker plate shows no buckling of the diaphragm plate. The force displacement curves under monotonic loading are shown in Fig. 3.18 for various thickness of plate (2, 4, and 6 mm). Thus, the slenderness ratio varies from 34 to 101. Also, the initial stiffness for the FE 203 sections are more than that of FE 100 sections.

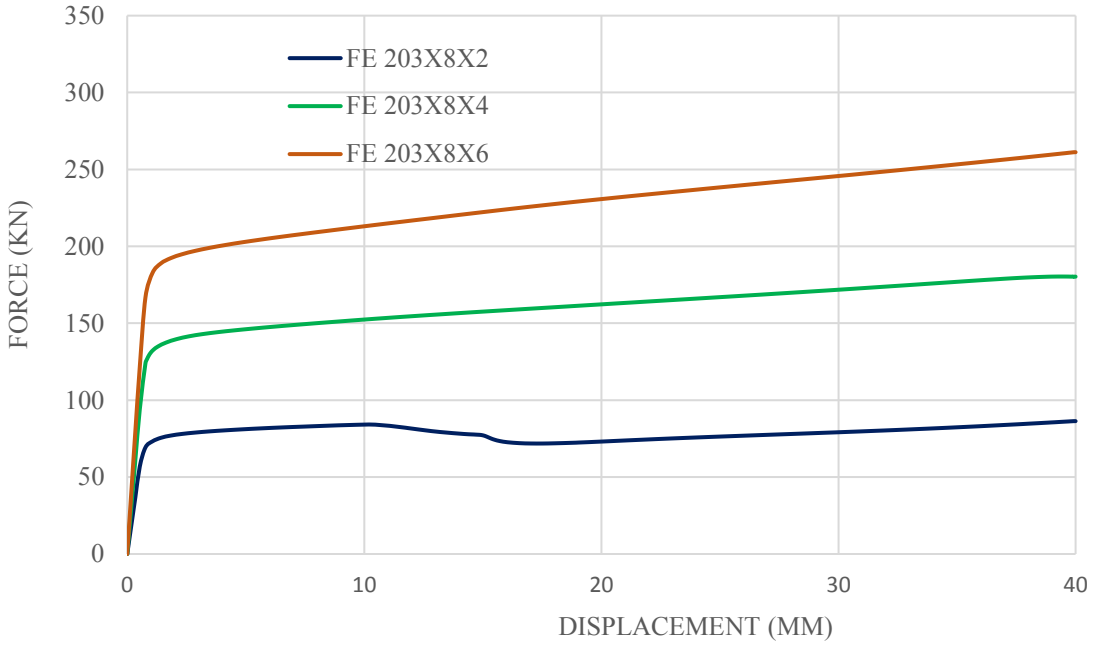

Figure 3.18 Force- displacement response for different plate thickness for FE 203 sections

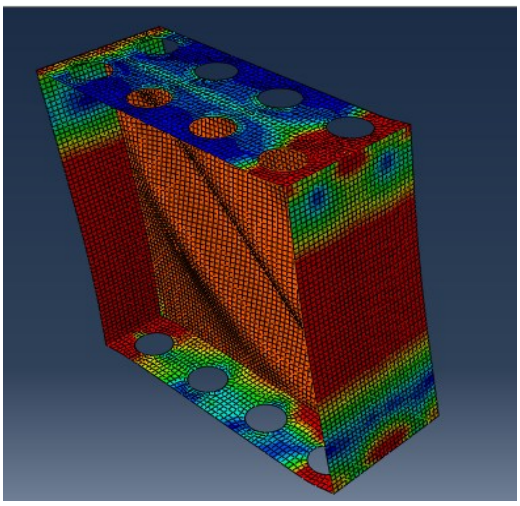

Figure 3.19 Deformation of plate under monotonic loading in FE 203x8x2 section

3.7. Discussion

A FE model is developed to study the behavior of Yielding shear panel device (YSPD). FE models for different sections showed good correlation with the available test results under monotonic and cyclic loading. Compact and slender plates within YSPD are studied and elastic shear buckling is verified by a numerical model. Further, parametric studies are carried out and the results suggest that a stiff SHS section which works as a boundary and a slender plate make an effective YSPD. This allows effective use of the plastic strength for the diaphragm plate and local distortion of SHS section near the bolt holes can also be avoided. Tension field is anchored effectively by the SHS for this device. Hence, the numerical model can be used instead of conducting costly and time consuming experiments. In the next chapter, this device is installed in a building frame and the performance of the frame is studied under real ground motion data.

CHAPTER 4: SESIMIC PERFORMANCE OF FRAME EQUIPPED WITH YIELDING SHEAR PANEL DEVICE

4.1. Introduction

A finite element model of YSPD (isolated from the parent structure) has been developed in the previous chapter to study the behavior. The finite element model has also been validated with the available experiment data. This chapter presents the finite element modelling of the lateral load bearing frame with YSPD and validated with the available mathematical model. This validated FE model is further used for seismic performance of a 4-story building frame with YSPD when the device is used for retrofitting purpose. Nonlinear dynamic analysis is carried out and the results from analysis are being used to evaluate the efficiency of YSPD as a device in retrofitting. This chapter also demonstrates the methodology that is used to select the ground motions for the nonlinear time-history analysis.

4.2. Numerical modelling of a frame equipped with YSPD

YSPDs may be installed in the lateral load-bearing frame to dissipate seismic energy in the event of an earthquake. Also, YSPDs have been proposed by the researchers to use for retrofitting of the existing buildings with moment resisting frames. Hossain et al. (2013) reported the load-displacement relationship of different YSPDs under the cyclic load. They studied the effectiveness of YSPD's by installing in the north-south lateral load-bearing frame of the three story Los Angeles SAC structure for improving its seismic performance (Fig. 4.1). They used mathematical model based on BWBN parameters to model the YSPD. The proposed numerical model in this chapter is validated with the mentioned mathematical model of YSPD.

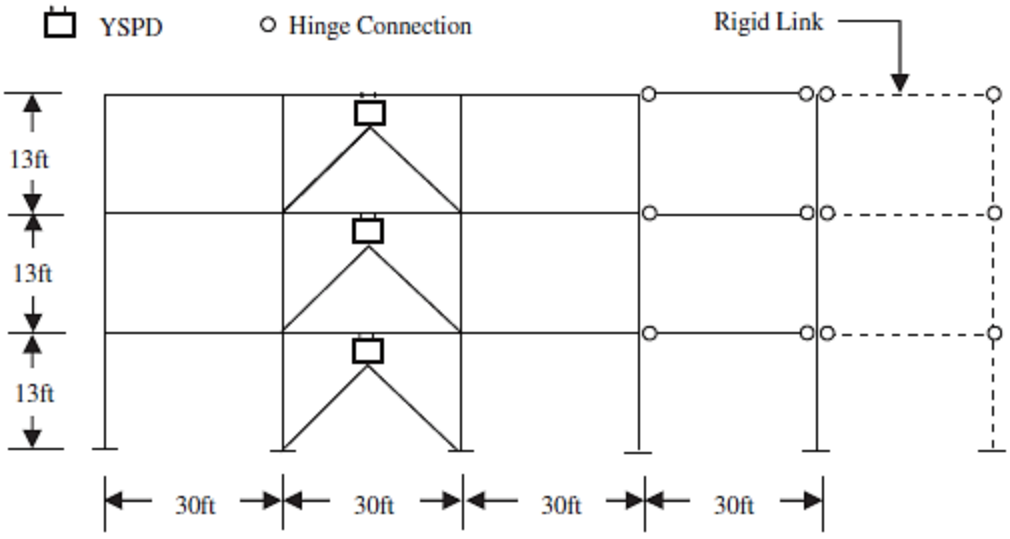

Figure 4.1 North–South lateral load-bearing MRF in SAC Building (LA) equipped with YSPDs (Hossain et al. 2013)

4.2.1. Material modelling

The material modelling is employed in the same way as discussed in Section 3.3.1. For this numerical modelling in ABAQUS, isotropic hardening with bilinear idealization (elastic- plastic) is used for monotonic test. Kinematic hardening is used for the modelling of YSPD in cyclic test. This material modelling reflects properties of the material used by Hossain et al. (2011) for the mathematical modelling.

4.2.2. Element type

All the beams, columns, braces and associated SHS plates are modelled with B31 element whereas the plates are modelled using S4R element. B31 is generalized 3D shear flexible beam element that allows for transverse shear deformation. S4R is shell element generally used for thin plates modelling.

4.2.3. Support Conditions

As the YSPD is installed within moment resisting frame, the upper flange of YSPD is connected to the bottom of beam section with the bolts. This is modelled by using kinematic coupling constraint available in ABAQUS. The constraint signifies coupling the motion of top flange of YSPD with the rigid body motion as defined by the bottom flange of the beam. The bottom flange of YSPD is connected to the V-brace with bolts. The force mechanism works such that the V-braces try to move the bottom flange of YSPD. This is also modelled by coupling the connected node of bottom flange of YSPD with brace end nodes. For the top flange connection, the horizontal direction of motion and the vertical direction both are constrained. For the bottom flange connection, the horizontal direction of motion is only constrained.

The braces are acting as axial members, and they are pin-connected. The connection of brace to column is modelled using MPC Pin constraint. Multi-point constraints (MPC) in ABAQUS allow constraints to be imposed between different degrees of freedom of the model. “MPC Pin” provides a pinned joint between two nodes and makes the displacements equal. However, the rotations of these nodes are independent of each other.

The Yielding Shear Panel Device (YSPD) consists of Square Hollow Section (SHS) and a diaphragm plate is welded inside in the SHS. For the numerical model, the frame with YSPD is modelled as 2-dimensional frame in ABAQUS. Connecters are used to model the weld between the plate and the SHS. The property of these connectors are defined as “weld”, which is available in ABAQUS. The columns are fixed to the base as generally found in moment resisting frames. Also, the beam to column connection is “rigid” type. These connections are modelled appropriately for the related nodes to reflect the realistic scenario.

4.3 Mathematical model of YSPD

Hossain et al. (2011) used the BWBN model for the simulation of the hysteretic response of YSPD to include the pinching characteristics. Table 4-1 shows the value of the parameters as reported by them.

According to the concept of BWBN model (Wen, 1976, Baber and Noori, 1986), the restoring force F produced in the YSPD can be expressed as

[4.1] $F = F_e + F_h$

where, F_e and F_h are the elastic and the hysteretic component of the restoring force respectively.

Table 4-1: BWBN model parameters for the YSPD 100x4x2

YSPD (DxTxt)	k_t (kN/mm)	F_i (kN)	A	β	γ	n	q	ζ_{10}	p	ψ_0	δ_ψ	λ
100x4x2	0.33	26.76	1.0	0.5	0.5	1.213	0.52	0.96	0.018	0.41	0.00001	0.03

D is the Size of YSPD (mm), T is the thickness of SHS plate (mm), t is the thickness of diaphragm plate (mm). k_t is the tangential stiffness of YSPD after tension field formation (kN/mm). A, β, γ, n are hysteretic parameters and q, ζ_{10} , p , ψ_0 , δ_ψ , λ are pinching parameters.

F_y is the yield strength of SHS and diaphragm plates which is 250 MPa for YSPD 100x4x2.

4.4 Validation of FE model with mathematical model

A four cycle loading history of amplitudes 5, 10 and 20 mm is applied for the cyclic loading as shown in Figure 4.2. Generally, the cyclic loading history is applied with increasing variable amplitude. This is to match the scenario of seismic time history which comprises variable displacement amplitudes. Figure 4.3 shows comparisons between the FE simulations and the mathematical model for the cyclic response of YSPDs. Good agreement is achieved from this comparison between the FE results. The FE model shows slightly less pinching for both the cases.

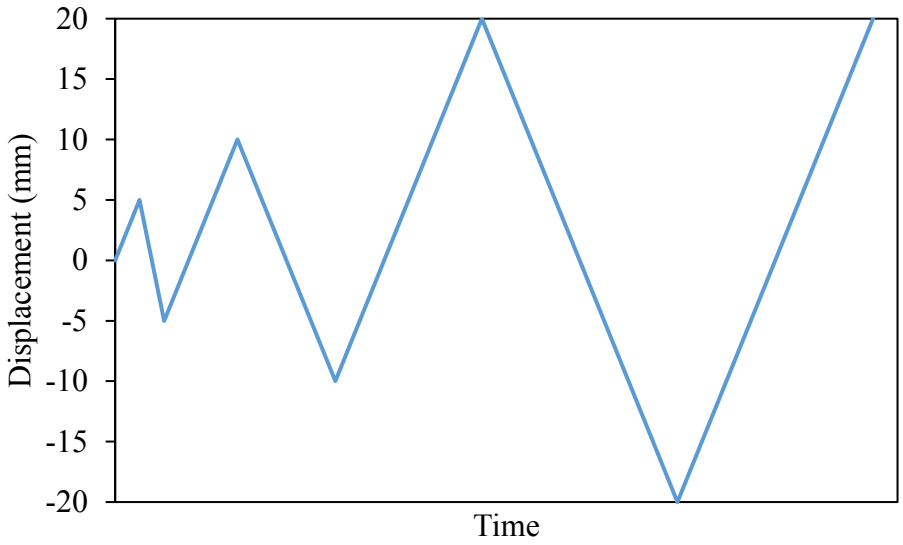

Figure 4.2 Displacement history applied for cyclic loading

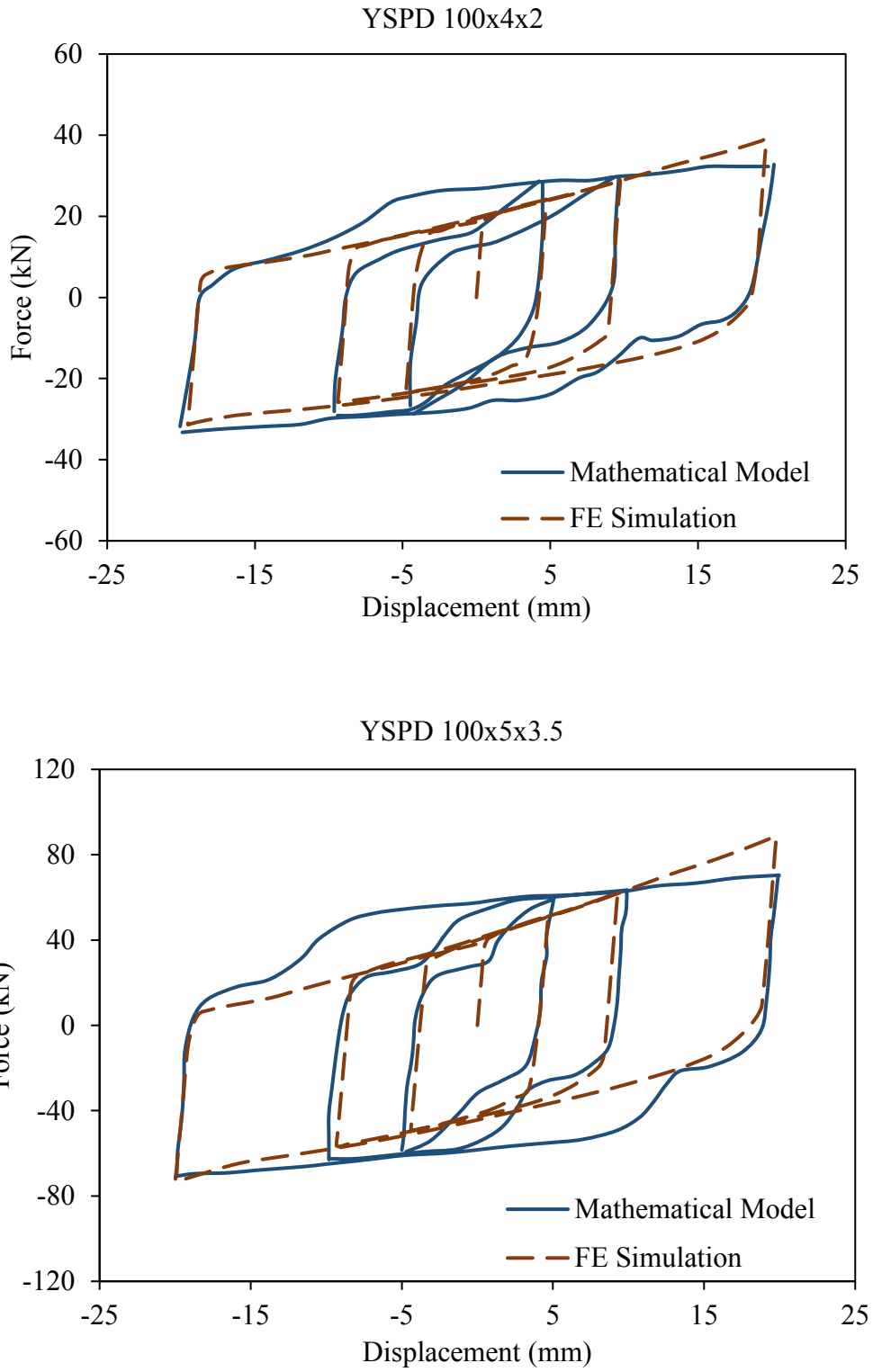

Figure 4.3 Comparisons between the FE simulation and the mathematical model for the cyclic response of YSPDs

Table 4-2 compares the total energy dissipated predicted using FE simulation to the amount of energy absorbed by hysteretic response predicted using the BWBN model. Results show good agreement between the FE simulation and mathematical modelling. Hence, this FE model of the lateral load resisting frame gives a reasonable accuracy of the dissipated energy by YSPDs.

Table 4-2: Comparison of the energy dissipated for different YSPDs under cyclic loading

YSPD Size	Total calculated Energy (kJ) from Mathematical model	Total calculated Energy (kJ) from FE model	Ratio of average energy (FE model/ Mathematical model)
100x4x2	2.761	2.727	0.988
100x5x3.5	6.564	5.613	0.855

For monotonic loading, the FE simulation is also compared with the mathematical modelling for YSPD 100x4x2 and 100x5x2. The force-displacement curves for both the cases are demonstrated in Fig. 4.5. Good agreement is achieved between the two models.

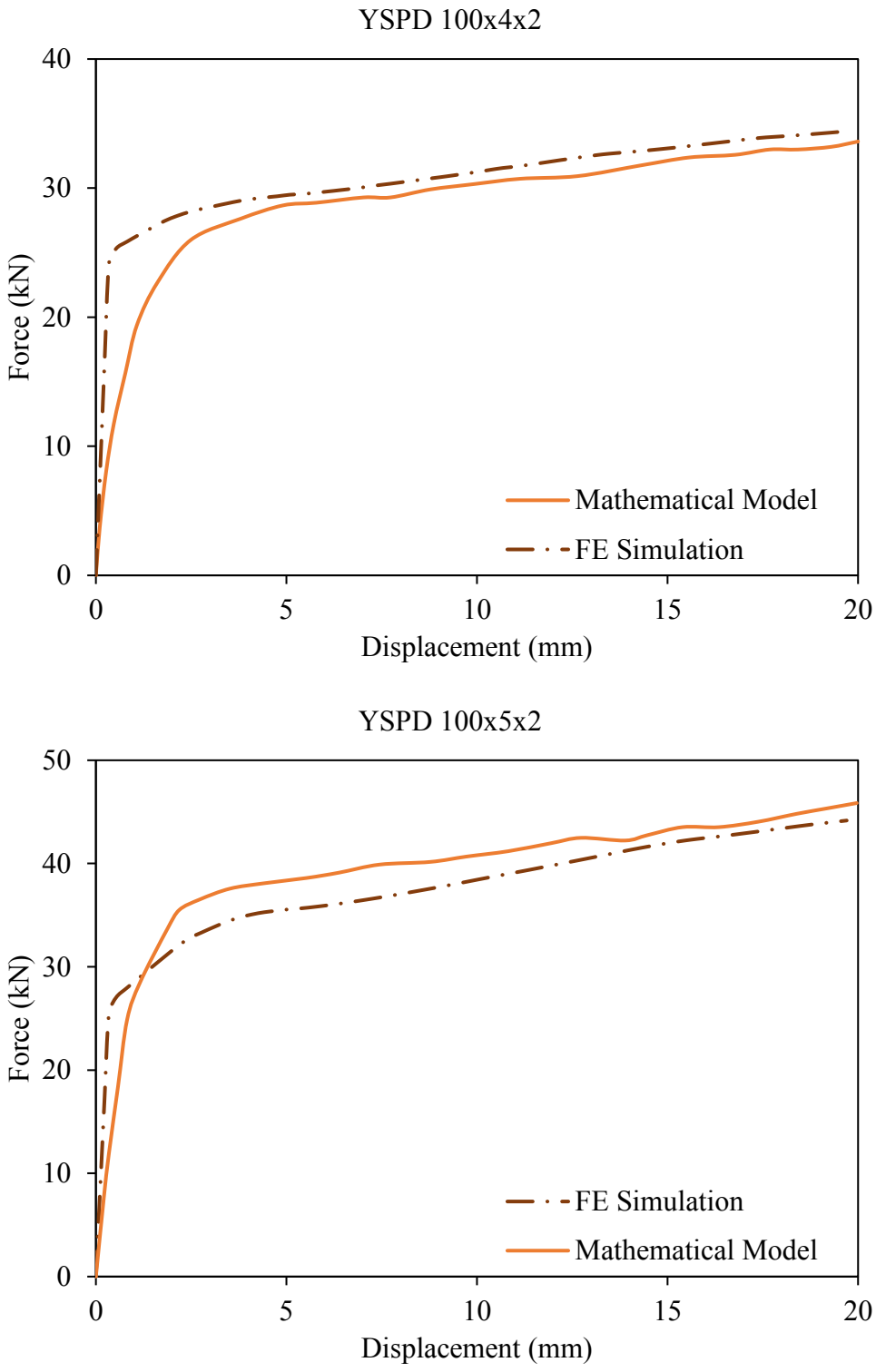

Figure 4.4 Comparisons between the FE simulation and the mathematical model for the monotonic response of YSPDs

This numerical model is also verified with FE simulation of YSPD (isolated from the structure) as described in Chapter 3. Figure 4.6 shows the comparison between finite element simulation and model predictions. Overall, the comparison shows good agreement.

Table 4-3: Comparison of the energy dissipated for different YSPDs under cyclic loading

YSPD Size	Total calculated Energy (kJ) from FE model (isolated YSPD)	Total calculated Energy (kJ) from FE model (YSPD within frame)	Ratio of average energy (FE model/ Mathematical model)
100x4x4	6.362	6.997	1.10

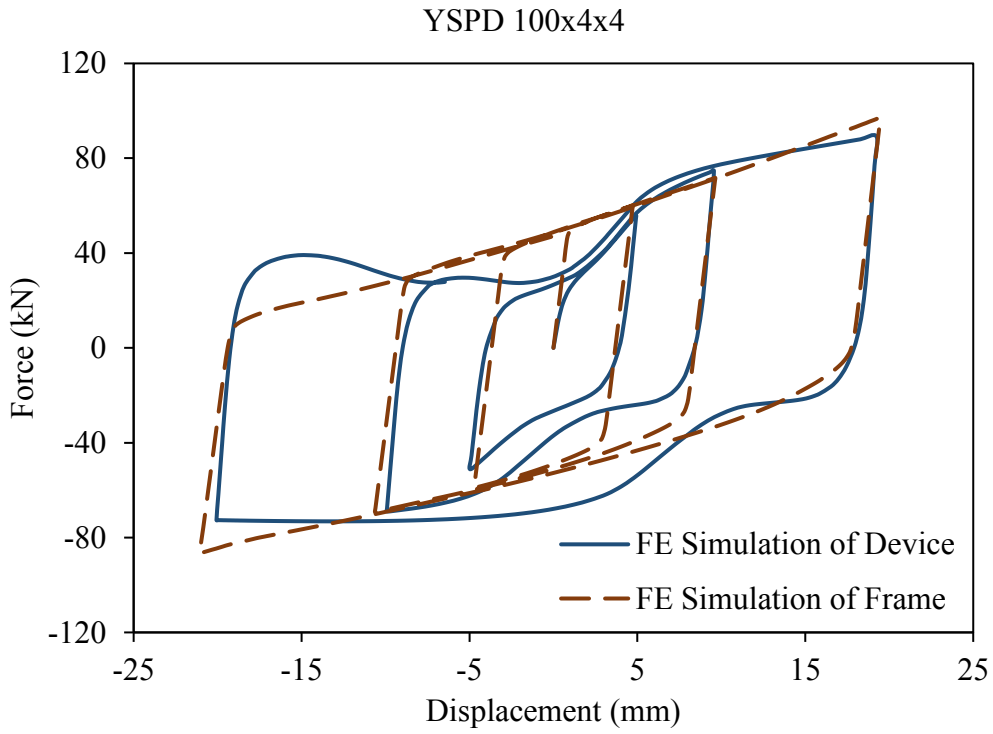

Figure 4.5 Comparisons between the FE simulation of device and the FE simulation of frame

4.5. Seismic performance of YSPD as a device in retrofitting

4.5.1. Building geometry and loading description

To evaluate the seismic performance of yielding shear panel device, a hypothetical 4-story office building is considered The office building is assumed to be located in Vancouver, BC. It has a symmetrical plan with a total area of 1406.25 m^2 (37.5 m x 37.5 m). The site class is considered as C. Two identical MRFs are used symmetrically in N-S and E-W directions to resist lateral forces from earthquake. Thus, each MRF has to resist only 50 percent of the induced seismic load. The building is symmetric and thus, torsion is not generated. Only accidental torsion, as specified in National Building Code of Canada (NBC 2010), is considered in earthquake load calculations. The typical floor plan and elevations used for this study are shown in Figure 4.6 and Figure 4.7. All the frames have equal bay width and story height of 7.5 m and 3.8 m respectively.

The dead load and live load of the floors are considered as 4.2 kPa and 2.4 kPa respectively. The roof dead load is taken as 1.5 kPa. The snow load is calculated as per the provisions in NBCC 2010 and is equal to 1.64 kPa. The load combinations 1D+0.5L+E and 1D+0.25S+E are selected for the floors and the roof, respectively in compliance with NBCC 2010. For this study the moment resisting frames are considered as moderately ductile moment resisting frames and thus, a ductility related force modification factor 'R_d' of 3.5 and an over strength force modification factor 'R_o' of 1.5 are used in the design according to the provisions of NBCC 2010. The nominal yield strength of structural steel is considered to be 350 MPa. The modulus of elasticity (E) of 200,000 MPa and Poisson's ratio (μ) of 0.3 are used for designing all the members.

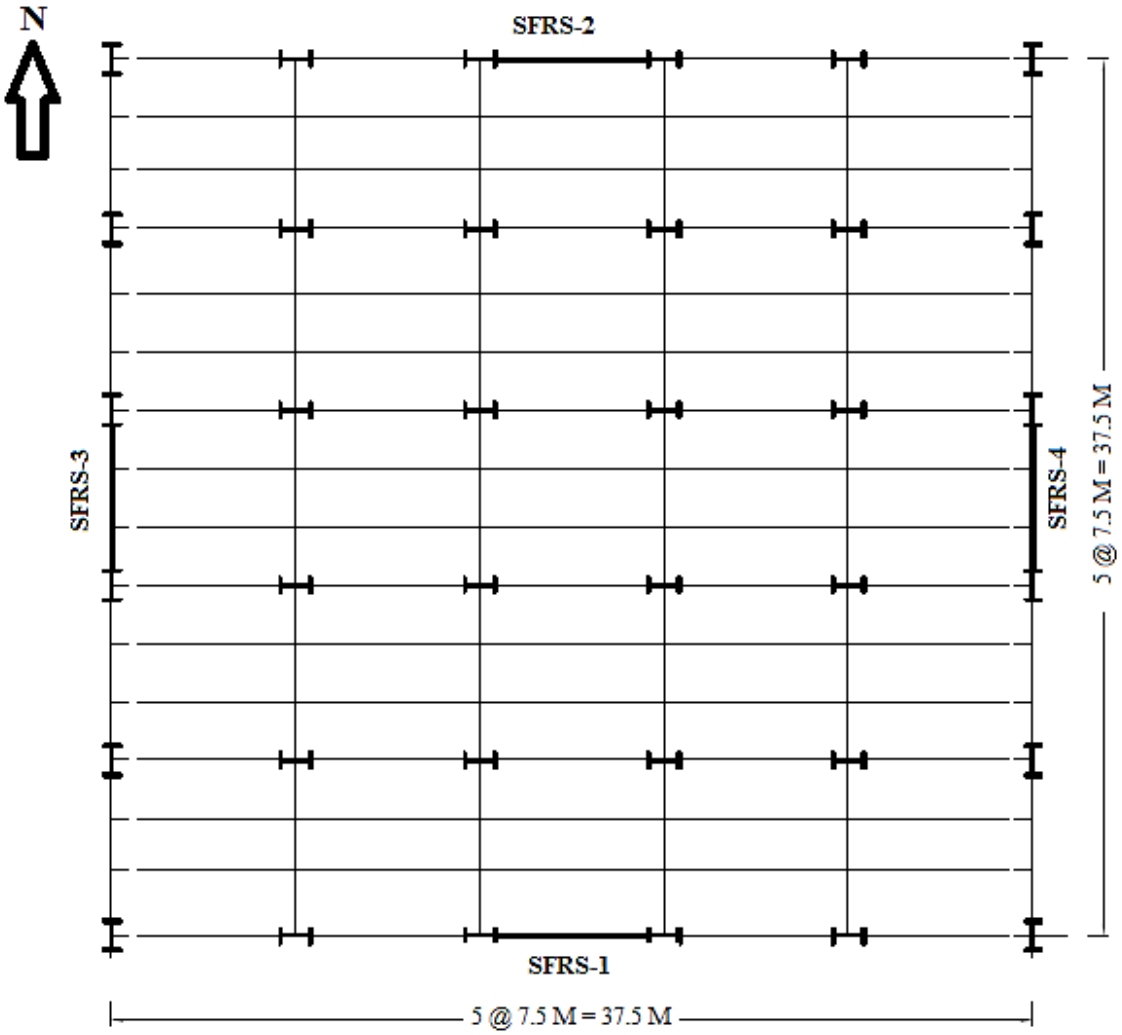

Figure 4.6 Typical floor plan of 4-story office building

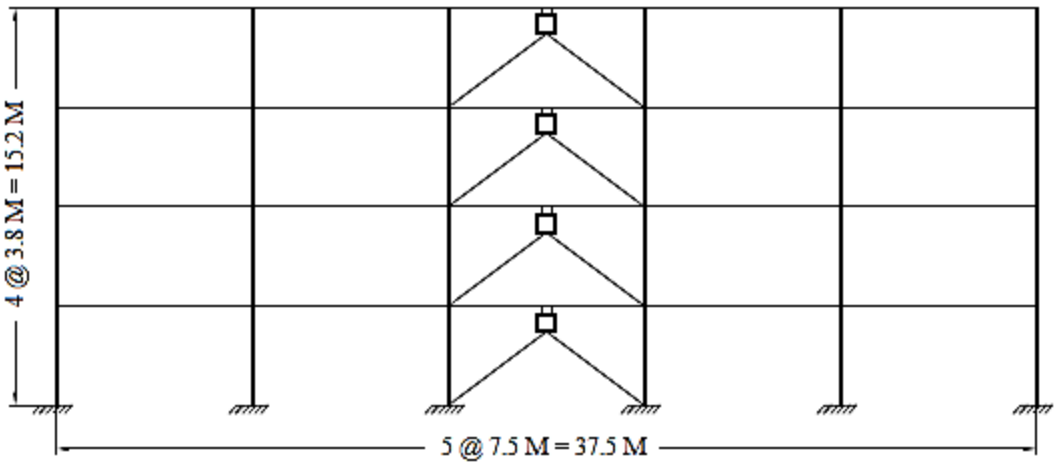

Figure 4.7. Elevation view (along SFRS-1) of 4-story office building

4.5.2. Design of MRF

The equivalent static force procedure as explained in NBCC 2010 is used to calculate the design base shear for the MRF. The fundamental period of the structure is,

$$[4.2] T_a = 0.085 h_n^{3/4}$$

where h_n is the height of the structure in meter. However, NBCC 2010 allows that the maximum period of the structure can be upto 1.5 times of T_a. Further, this design period is checked by the periods obtained from frequency analysis.

The design base shear can be calculated and distributed among the floors using the following equations.

$$[4.3] V_{min} = \frac{S(2)W}{R_d R_o} I_E M_v \leq V = \frac{S(T_a)W}{R_d R_o} I_E M_v \leq V_{max} = \frac{2}{3}\left(\frac{S(0.2) I_E W}{R_d R_o}\right)$$

$$[4.4] F_x = (V - F_t) W_x h_x / \left(\sum_{i=1}^{n} W_i h_i\right)$$

$$[4.5]\ F_t = 0.07 T_a V$$

Where, T_a is the empirical period, $S(T_a)$ is the spectral acceleration, M_v is the factor considering higher modes effects on increasing base shear, I_E is the importance factor, R_d is force reduction factor for ductility, R_o is force reduction factor for over strength, and W is the total seismic weight resisted by the frame.

The time period (T_a) of the building is 1.232 sec and the design base shear for the building is 1234 kN. From the analysis, it has been found that SFRS-2 experiences maximum forces when the seismic force is acting towards East-West direction of the building. Hence, SFRS-2 is designed for its design base shear of 689 kN. The distributed story shears are given in Table 4-4

Table 4-4: Distribution of base shear in moment resisting frame

Story	W (kN)	h_i (m)	Wihi (kN-m)	V-F_t (kN)	Story shear (kN)
4	2685.94	15.2	40826.29	149	196
3	5906.25	11.4	67331.25	247	247
2	5906.25	7.6	44887.5	164	164
1	5906.25	3.8	22443.75	82	82
			Σ = 175488.79		Σ = 689

The design procedure for the moderately ductile MRF can be summarized in the following steps.

1. As the story shears are known from calculation of total base shear, Moment diagram is drawn (at column centerline) for 1E. Also, axial force diagram is drawn for 1E forces.

2. The beams and columns of MRF also carry gravity loads. Thus, moment diagram is drawn for the load combination: DL+0.5LL+0.25SL

3. Beams are expected to develop plastic hinges typically at a short distance from the face of the columns. For this study, the MRF is designed as moderately ductile MRF with Rd =3.5 and Ro =1.5. So, the beam can be Class 1 or Class 2 section as per CAN/CSA S16-09

4. As the beam carries axial force along with the bending, this beam has to be designed as a beam column section. Interaction ratio has to be satisfied while designing the beam.

5. The columns shall resist the gravity loads together with force induced by plastic hinging of the beams. The S16-2009 (Cl. 27.2.3.2) provides the following equation,

   [4.6] $$\sum M_{rc} \geq \sum \left[1.1 R_y M_{pb} + V_h \left(x + \frac{d_c}{2}\right)\right]$$

   The left hand side denotes the sum of the column factored flexural resistances at the intersection of the beam-column centerlines. The right hand side denotes the shear and moment induced to column from the plastic hinging of beams. The distance x is the distance from the center of a beam plastic hinge to the column face. For this study, this distance has been chosen as half of the depth (0.5d) of the beam section.

6. The interaction ratio is also checked for column section as it is carrying both axial load and bending moment. This study deals with the column sections having uniaxial strong axis bending.

The sections of beams and columns of the selected MRF is provided in the following table.

Table 4-5: Designed section details of MRF for the 4-story office building

Story	Beam section	Column section
4	W310X283	W920X725
3	W310X283	W920X725
2	W460X260	W920X970
1	W460X260	W920X970

4.5.3. MRF with yielding shear panel device

Non-linear dynamic analysis has been conducted on MRF in the following sections. Further, the YSPD sections of known tensile yield strength (f_y) are inserted in the MRF to study the performance of the modified system. Maximum shear yield force (F_y) can be calculated from equation [3.8] as the diaphragm plates are compact considering the critical shear stress. Braces hold the YSPD as discussed in chapter 2 and 3. The brace sections are designed to carry forces that is twice of the maximum shear yield force of the respective YSPD devices. The response of the modified frame i.e. MRF with YSPD is also verified when it is subjected to the non-linear dynamic analysis. The following sections illustrates analysis of both the lateral load resisting systems. Table 4-6 provides the details of the YSPDs and the brace sections.

Table 4-6: Designed section details for the MRF with YSPDs

Story	YSPD section	f_y of SHS and plate (kN)	Max. shear yield force of YSPD (kN)	Brace section
4	100x4x2	250	27	HSS 102X102X8
3	100x4x4	250	53.5	HSS 102X102X8
2	120x6x2	300	38.87	HSS 102X102X9.5
1	120x6x4	300	76.3	HSS 102X102X9.5

4.6. Nonlinear Dynamic Analysis of the frame with YSPD

4.6.1. Frequency Analysis

Frequency analysis is performed on the developed FE models to determine the fundamental time periods and mode shapes of the structure. This is done prior to conducting the seismic analysis. The fundamental period as found from the analysis is utilized for the scaling the ground motion records. The scaled ground motion (GM) records are used in seismic analysis of the structure. Raleigh proportional damping coefficients α and β are calculated from frequency analysis results. These coefficients are used in material modelling while conducting seismic analysis. The coefficients α and β can be calculated using equation [4.7]. The Raleigh proportional damping ratio (ξ) is considered to be as 5%. ω_i and ω_j are the circular frequencies corresponding to i^{th} and j^{th} fundamental periods.

$$[4.7] \propto= \xi\frac{2\omega_i\omega_j}{\omega_i+\omega_j} \quad and \quad \beta = \xi\frac{2}{\omega_i+\omega_j}$$

The values of fundamental period (T) from the frequency analysis are also compared with the values as suggested by NBCC 2010 for braced frames (Table 4-7). The empirical formula is given in equation [4.8] and [4.9]

[4.8] $T = 0.085h_n^{3/4}$ for moment resisting frames

[4.9] $T = 0.025h_n$ for braced frames

It is permitted by NBCC to have a building period in the range of T – 1.5T for the moment resisting frames and T - 2T for the braced frames. The results from frequency analysis shows that the code estimation of the period is conservative.

Table 4-7: Comparison between fundamental periods

Building specification	**T from frequency analysis**	**T suggested NBCC 2010**
4 story MRF, height 15.2 m	1.23 sec	0.98 sec
4 story MRF with YSPD, height 15.2 m	0.837 sec	0.76 sec

4.6.2. Ground Motion Records

As per NBCC 2010, the ground motion histories that are utilized while performing the dynamic analysis, should be spectrum compatible. The uniform hazard spectrum (UHS) for each region is provided in NBCC 2010. The design spectrum of Vancouver is used here as the studied office building is located in Vancouver. As per ASCE7-10, when peak maximum responses are considered to investigate seismic response of structure, at least three ground motions must be

utilized; and when the median value of maximum responses is used, a minimum of seven earthquakes are required.

For this study, a total number of seven earthquake records are utilized, of which three are selected from the strong ground motion database of Pacific Earthquake Engineering Research Center (PEER 2010), and the other four records are selected from Engineering Seismology toolbox website (Atkinson et al. 2009). All the required data for four real ground motion and three synthesized records are given in Table 4-8 and Table 4-9.

For a range of 400 years, the magnitudes of most recorded seismic activities in British Columbia are measured between 6 and 7, as reported by Lamontagne et al. (2008). The selected real ground motion records have magnitude in this range. The simulated ground motions are chosen for site class C with the magnitude of 6.5 and 7.5, including both near fault and far fault records. Also, A/V ratio is considered in the selection process. This ratio gives the ratio of peak acceleration (PGA) to the peak velocity (PGV). This ratio should be close to 1 for Vancouver (between 0.8 and 1.2) (Naumoski et al. 2004).

The selected ground motions are scaled based on the partial area method of scaling. According to this method, the area under the acceleration response spectrum curve of the selected ground motion and design response spectrum are compared and then they are made equal by employing a suitable scaling factor. The range of consideration of measuring area under curves is taken as $0.2T_1$ - $1.5T_1$, where T_1 is the fundamental period of the structure. The lower bound $0.2T_1$ is considered to account for the effects of higher modes participation on the seismic response and the upper bound $1.5T_1$ is considered to account for the increase of fundamental period of structure in the plastic range. Figure 4.8 and 4.9 presents the acceleration spectra for selected ground motions and Vancouver design spectra applied on MRF and MRF with YSPD respectively.

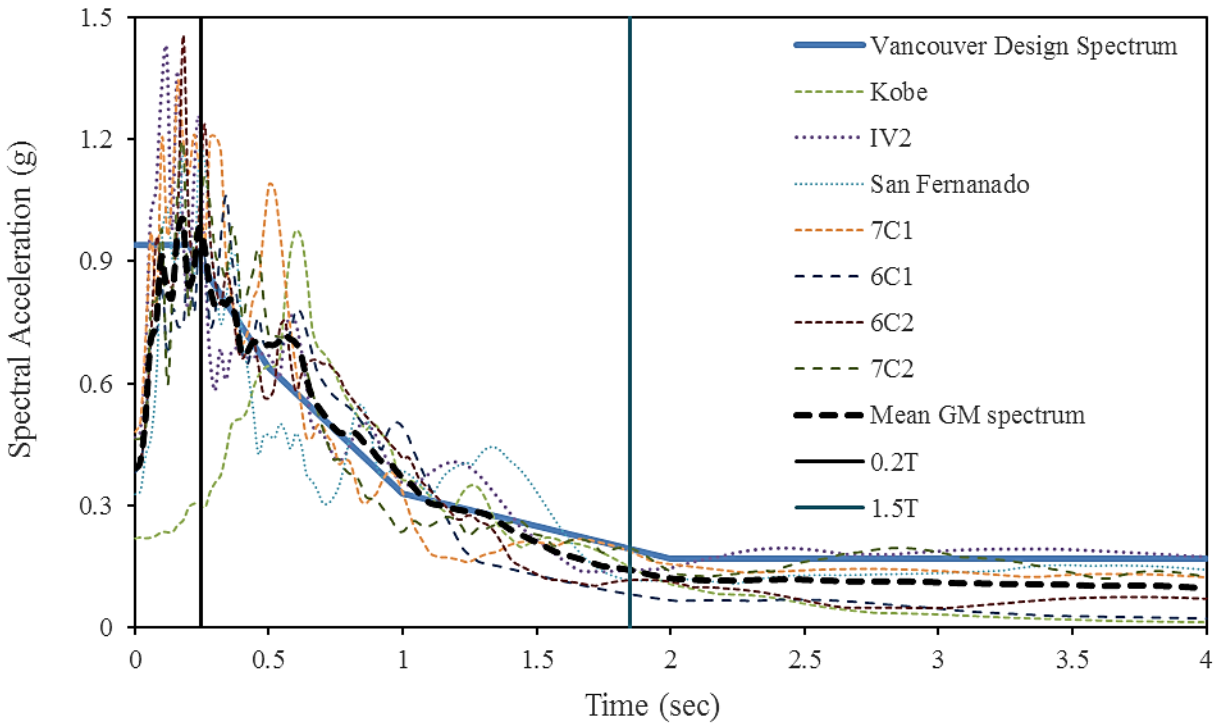

Figure 4.8 Acceleration spectra for selected ground motions applied on MRF

Table 4-8: Real Ground motion records

Event	Magnitude	PGA (g)	PGV (m/s)	A/V	Scaling factor (MRF)	Scaling factor (MRF with YSPD)
San Fernando, 1972	6.6	0.188	0.179	1.05	1.57	1.6
Kobe, 1995	6.6	0.143	0.147	0.973	1.55	1.65
Imperial Valley 2	6.53	0.525	0.502	1.04	1.03	0.99

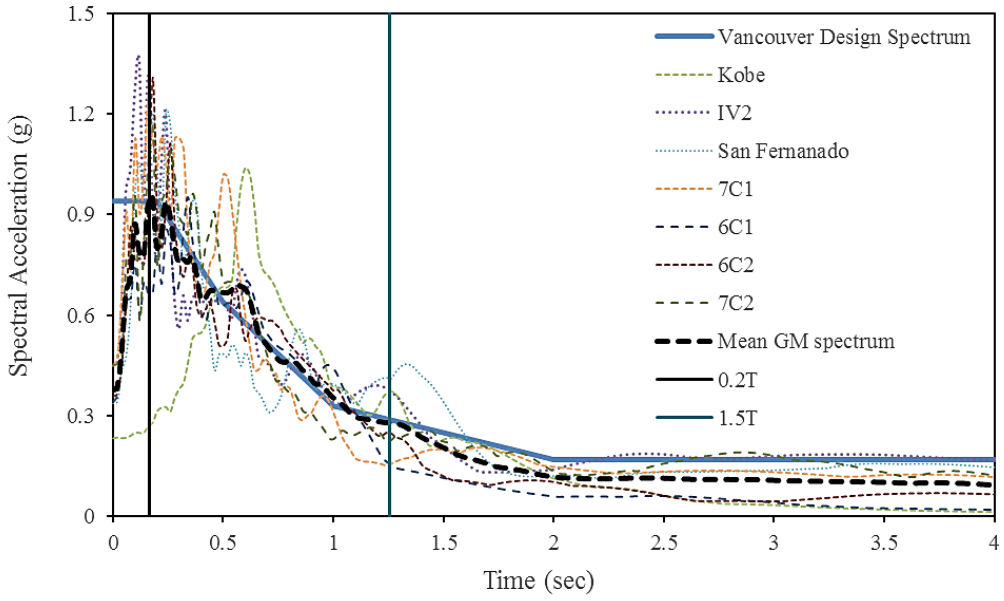

Figure 4.9 Acceleration spectra for selected ground motions applied on MRF with YSPD

Table 4-9: Simulated ground motion records

Event	Magnitude	Distance (kM)	Scaling factor (MRF)	Scaling factor (MRF with YSPD)
6C1	6.5	8.4	0.77	0.69
6C2	6.5	13.2	1.47	1.32
7C1	7.5	15.2	0.91	0.85
7C2	7.5	45.7	1.83	1.79

4.7. Seismic Analysis Results

4.7.1. Inter-story drift

The added stiffness and damping to the structure both decrease the peak displacement and inter-story drift. Figure 4.10 shows the comparison between the bare MRF and MRF with YSPD for San Fernando earthquake. Table 4-10 shows the numerical values of inter-story drifts for the same earthquake. A minimum reduction of 15.94 percent drift has been observed when the YSPDs are installed within MRF. Same observations are recorded for the other earthquakes which are shown in figure 4.11.

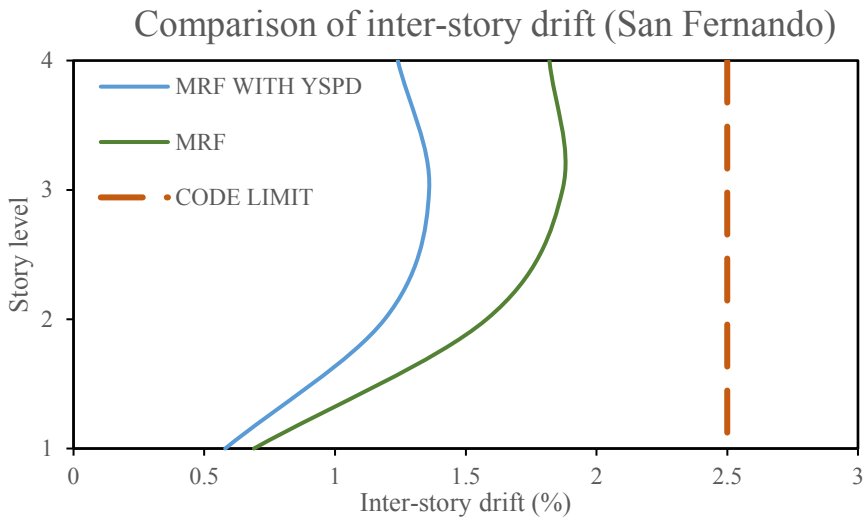

Figure 4.10 Comparison of inter-story drift for San Fernando earthquake

Table 4-10: Inter-story drift values in different SFRS for San Fernando earthquake

Story	Inter-story drifts in % (MRF)	Inter-story drifts in % (MRF with YSPD)	Difference (%)
4	1.82	1.24	31.87
3	1.87	1.36	27.27
2	1.58	1.19	24.68
1	0.7	0.58	15.94

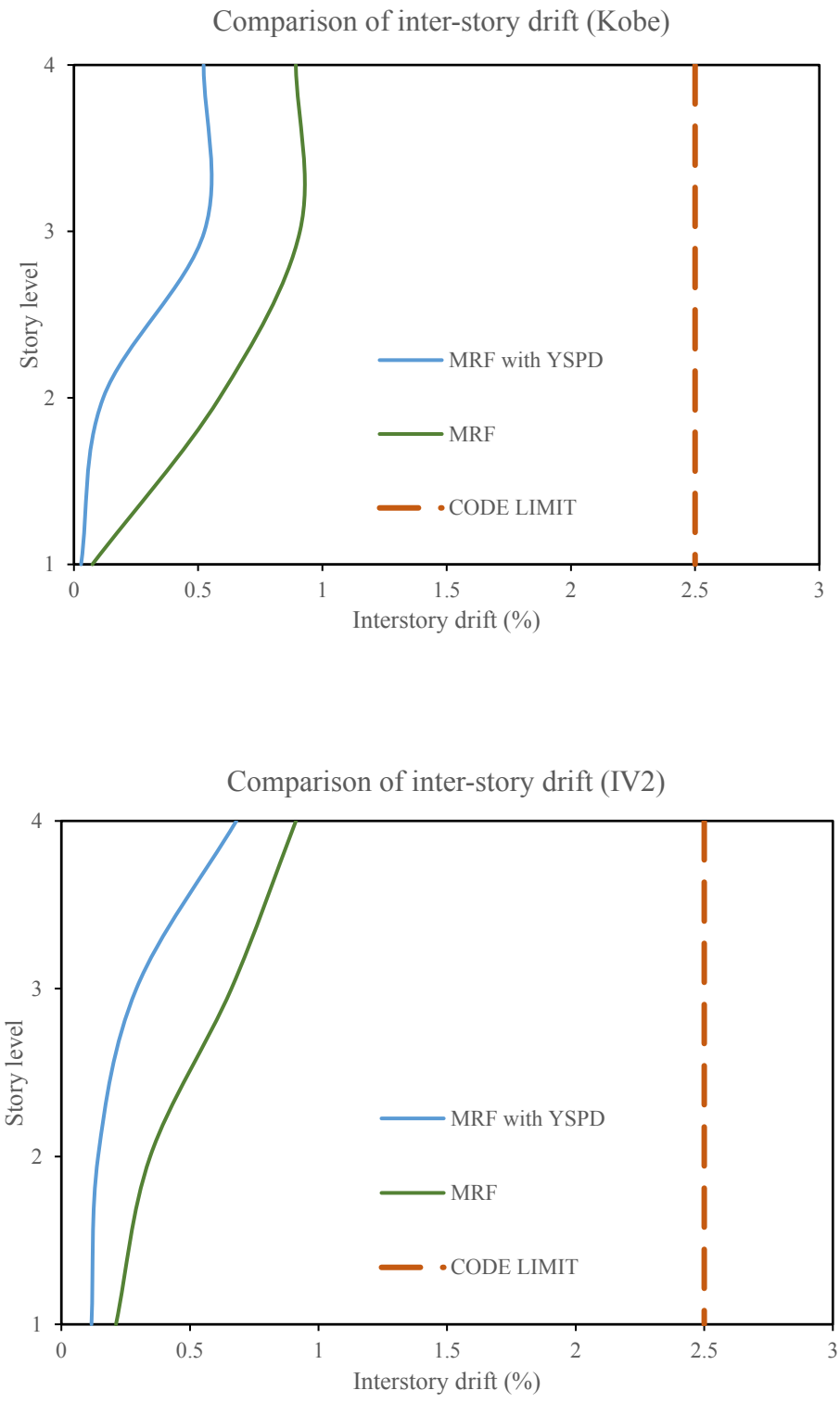

Figure 4.11 Comparison of inter-story drift under seismic action

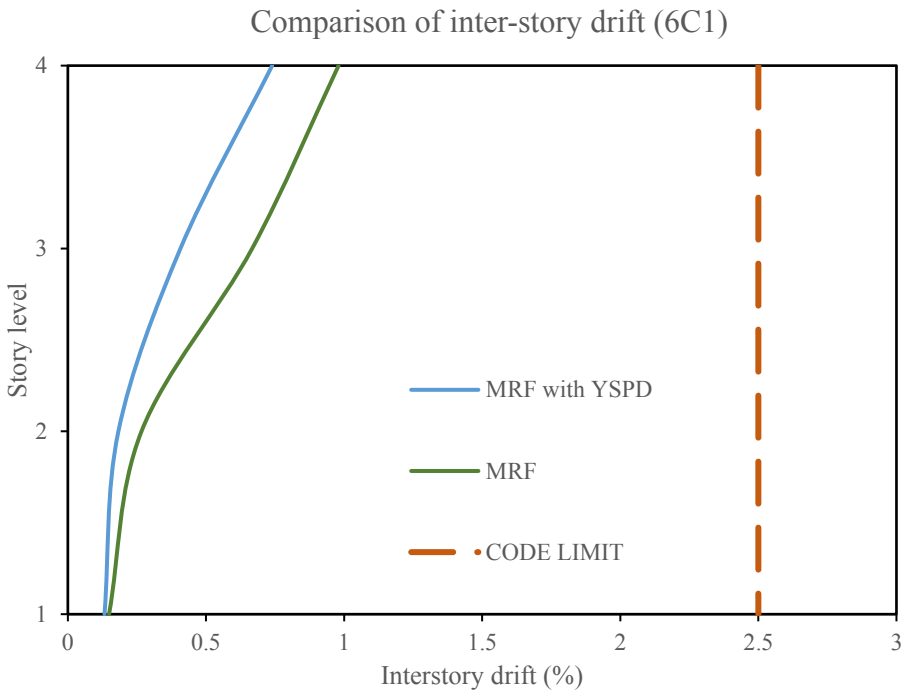

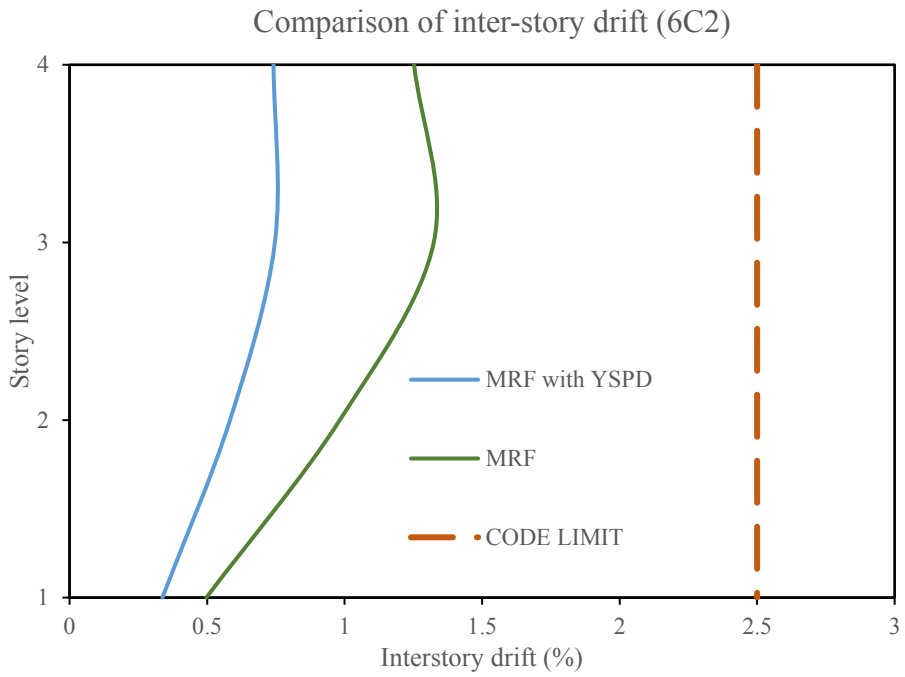

Figure 4.11 (Contd.) Comparison of inter-story drift under seismic action

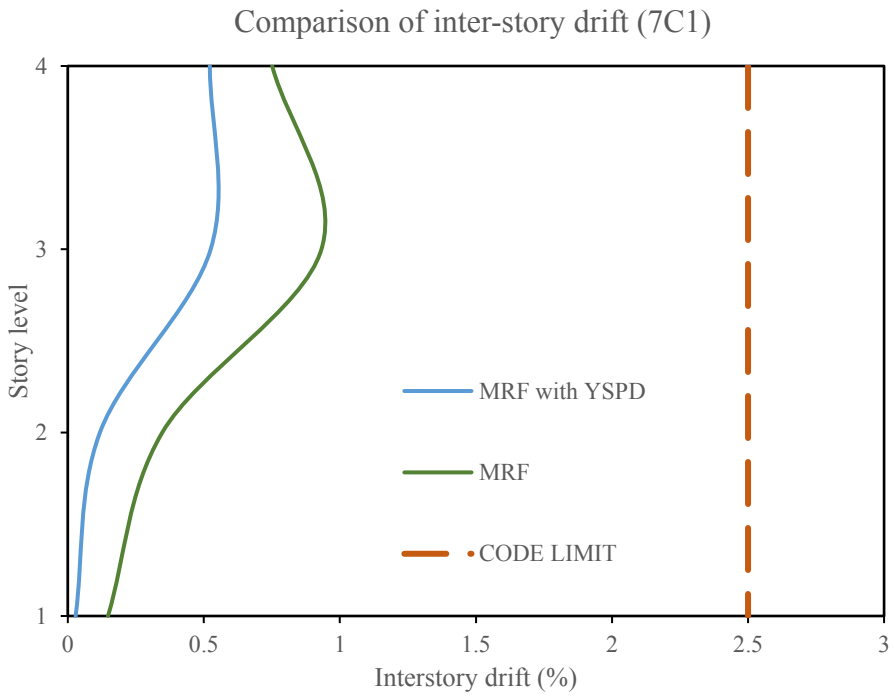

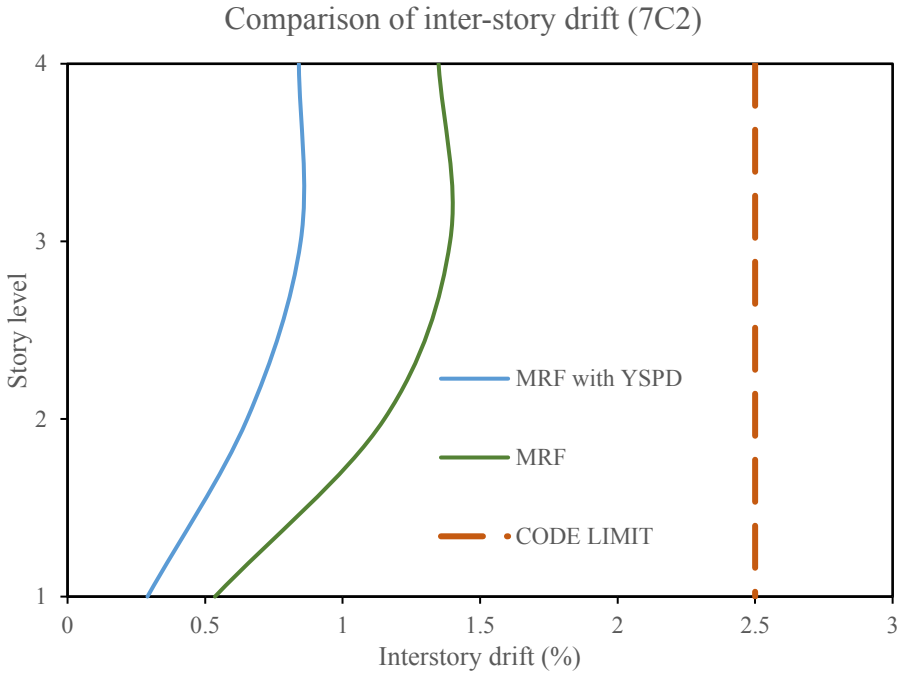

Figure 4.11 (Contd.) Comparison of inter-story drift under seismic action

4.7.2. Base shear

The yielding shear panels installed within the moment resisting frame also result in reduction of the base shear. The inclusion of YSPD in the frame increases the damping, and it results in decreased shear force in the structure. In contrary, the device and brace assembly add stiffness to the structure which results in increased shear force (FEMA 451). The selection of the device and brace sections can influence the combined effect. This section presents the comparison of the peak base shear values in the bare moment resisting frame and the moment resisting frame retrofitted with YSPD. Table 4-11 shows the comparison and calculates the reduction of base shear in retrofitting.

Table 4-11: Comparison in peak base shear values in different SFRS

Earthquake name	Peak Base shear		Reduction (%) of peak base shear in retrofitting
	MRF	MRF with YSPD	
San Fernando, 1972	6136	5700	7.1
Kobe, 1995	4679	4126	11.8
Imperial Valley 2	4648	3799	18.2
6C1	3801	2999	21.1
6C2	5579	4293	23.1
7C1	5566	3626	34.9
7C2	5843	3912	33.0

4.8. Summary

The chapter describes the seismic performance of yielding shear panel device when it is used within a lateral load resisting frame. A moment resisting frame (MRF) is designed to act as a LLRF in an office building located in Vancouver. Non-dynamic analysis has been conducted on the MRF. Further, the MRFs are retrofitted with YSPDs have shown reduced drift and reduced base shear for all seven ground motion records, when used in retrofitting. So, this encouraging performance of YSPD leads to the seismic design of a frame with YSPD, which is discussed in the next chapter. The device within a MRF can be designed to achieve a target level of performance such as damping or displacement.

CHAPTER 5: DIRECT DISPLACEMENT BASED SESIMIC DESIGN OF YIELDING SHEAR PANEL DEVICE

5.1. Introduction

The behavior of YSPD (isolated from the parent structure) has been studied in chapter 3 and the performance of the device under seismic action has been shown in chapter 4 when YSPD is used for retrofitting purpose. This chapter presents the seismic design of yielding shear panel device by direct displacement based design method. A lateral load resisting frame with YSPD is designed for a 2-story office building located in Vancouver as a new construction. The design is checked further by conducting nonlinear dynamic analysis. The results from analysis are being used to evaluate the efficiency of YSPD as a device in new construction.

5.2. Design procedure

5.2.1. Force based design method

Forced-based design method is the basis of the most of the modern seismic provisions as given in the codes. This approach requires seismic demand. Then, a seismic force reduction factor is used for reduction of the elastic force demand to design force level. This factor is used to consider the effect of structural ductility and structural overstrength (Uang, 1991). At the end, the inter-story drifts are checked and compared with the specified code limit.

Hence, the force-based design method relies on a force reduction factor. Hence, this method is unable to address the inelastic nature of the structure during an earthquake. Only the displacement from the analysis is verified to satisfy the serviceability criteria (Habibi, 2013).

5.2.2. Displacement based design method

In order to overcome the deficiency of the force method, displacement-based seismic design methods have been proposed such as FEMA-273 coefficient method and ATC-40 capacity-spectrum method. These two methods consider the inelastic nature of a structure during the seismic excitation and also doesn't rely on any force reduction factor. These methods can only be employed to the seismic evaluation and rehabilitation of existing buildings. Moreover, these methods calculate the target displacement from empirical formulae and may be inaccurate, especially for the buildings having shorter time period (Habibi, 2013).

5.2.3. Direct displacement based design method

Lin et al. (2003) proposed direct displacement based seismic design method to overcome the short-comings of conventional displacement based design method. This design approach utilizes substitute structure concept. In design, the method directly addresses the inelastic behavior of the primary frame. The modelling of the inelastic system is done as an equivalent linear system as shown in Fig. 5.1. In figure 5.1, K_h refers to an equivalent stiffness. It can be noted that the substitute structure has the same ultimate force (V_u) and displacement (Δ_u) as the inelastic primary structure.

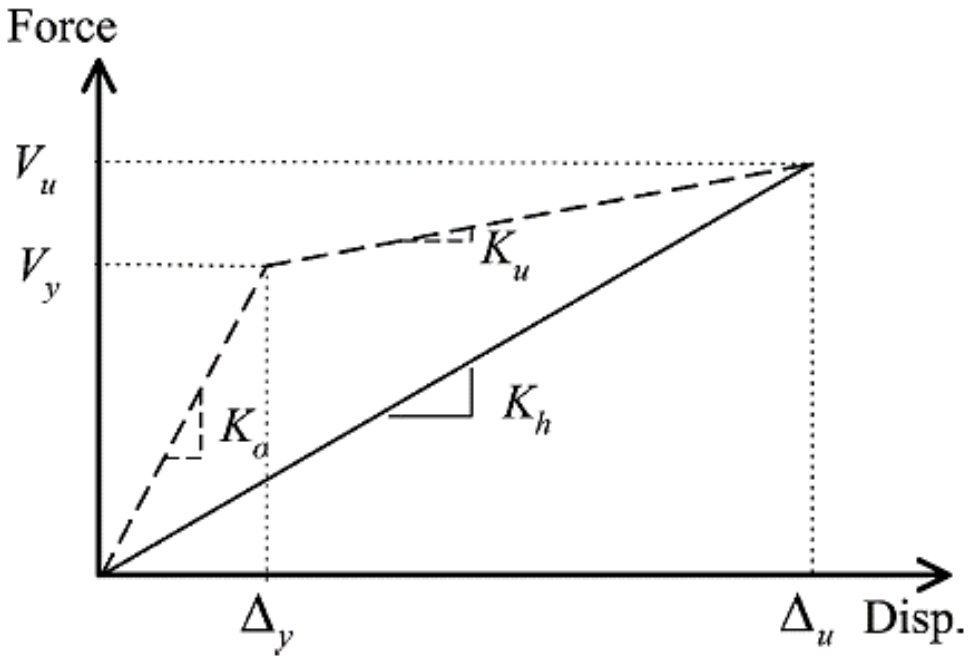

Figure 5.1 Substitute structure concept (Lin et al. 2003)

The step-by-step procedure of the displacement-based design method as presented by Lin et al. (2003) for structures with added energy dissipation devices is as follows:

Step 1: The target roof displacement (Δ_u) and yield roof displacement (Δ_y) for the designed building are assumed. Therefore, the initial ductility can be calculated as $\mu = \Delta_u / \Delta_y$. The value of target roof displacement (i.e. ultimate displacement, Δu) depends on the design limit state.

Step 2: The type of energy dissipation device is selected and an estimate of the effective viscous damping ratio (ξ_{EDS}) is done. For this study, the metallic yielding device YSPD is selected as energy dissipation device. The practical applicable range of ξ_{EDS} is within the range of 10– 20%. The equivalent damping ratio provided by the primary frame is denoted by ξ_h and can be calculated from equation [5.1].

[5.1] $\xi_h = \frac{1}{\pi}\left[1 - \left(\frac{1-\propto}{\mu} + \propto\right)\right]$

Step 3: The total equivalent damping ratio is calculated as per equation [5.2]. It refers to the substitute structure combined with energy dissipation systems. ξ_I refers to the inherent damping ratio which is estimated as 2% for steel buildings.

[5.2] $\xi_{eq} = \xi_I + \xi_h + \xi_{EDS}$

Step 4: The target roof displacement and the mass of the building (MDOF) are converted to the equivalent target displacement $(\Delta_u)_{eq}$ and the equivalent mass M_{eq} of a SDOF substitute structure using equations [5.3] and [5.4] respectively, where N is the number of stories in the building, m_i is the mass of i-th story and h_i is the height from the base to the i-th story

[5.3] $(\Delta_u)_{eq} = (\Delta_u) \times \frac{2N+1}{3N}$

[5.4] $M_{eq} = \left(\sum_{i=1}^{N} m_i h_i\right) \Big/ h_N$

Step 5: The equivalent time period T_{eq} can be determined using the elastic response spectrum for a given location. The equivalent stiffness K_{eq} of a SDOF substitute structure can be found out from the following equation

[5.5] $K_{eq} = \left(\frac{2\pi}{T_{eq}}\right)^2$

Step 6: The ultimate force capacity (V_u) and the design force (V_d) are calculated. The design force (i.e., yield force, V_y) can be computed based on the bilinear force-displacement model (Fig. 5.1) and can be obtained by the equation [5.7]

[5.6] $V_u = K_{eq} \times (\Delta_u)_{eq}$

[5.7] $V_d = V_y = \frac{V_u}{1+\propto (\mu - 1)}$

Step 7: The structure can now be designed based on V_d and Δ_y. Next, the design force, V_d can be distributed over the height of the entire building according to Eq. [5.8] in which w_x is the mass of *x*-th story. The beams and columns can be designed such that the building produces a roof displacement of Δ_y as assumed in Step 1 when subjected to the laterally distributed force.

The strong-column-and-weak-beam design criteria is followed in the design. The equation [5.9] is adopted (γ is a constant) for the study and the sizes of the structural members can be found accordingly.

[5.8] $F_x = V_d \frac{w_x h_x}{\sum_{i=1}^{N} w_i h_i}$

[5.9] $\sum M_c = \gamma \sum M_b$

Step 8: The effective stiffness of metallic yielding EDDs (K_{EDS}) can be determined using the following equations. K_{EDS} and ξ_{EDS} are demonstrated in Fig. 5.2.

[5.10] $\xi_{EDS} = \frac{1}{4\pi} \frac{W_{hysteretic}}{W_s} = \left(\frac{2}{\pi}\right) \frac{\sum_j F_{y,j} u_{o,j} \left(1 - \propto_j\right) \left(1 - \frac{1}{\mu_j}\right)}{\sum_i F_i u_i}$

[5.11] $K_{EDS,j} = \dfrac{F_{y,j}\left[1 + \alpha_j\left(\mu_j - 1\right)\right]}{u_{o,j}}$

where, $F_{y,j}$ α_j and μ_j are yield force, strain hardening ratio and ductility ratio of the metallic yielding devices respectively; $u_{o,j}$ is the relative axial displacement between the ends of device j; F_i is the laterally distributed force at floor level i; u_i is the horizontal displacement at floor level i under the laterally distributed force.

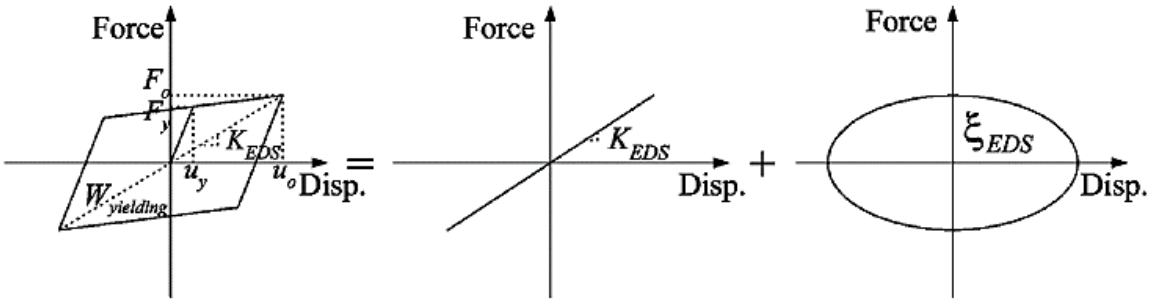

Figure 5.2 Modelling of Metallic yielding type EDD (Lin et al. 2003)

Step 9: Step 7 – Step 8 are repeated until the convergence of the iteration procedure is achieved. Then, the end moment against the yield moment of each member is checked. The damped structure may not have the real yield point although it deflects Δ_y at the roof under the action of laterally distributed force. For the case where yield point is not met for the structure, an iteration procedure according to Eq. [5.12] is suggested. M and M_y represent the end moment and the yield moment of the member, respectively. The final results can be achieved when M_y/M ratio is close to 1.0

[5.12] $\Delta_{y+1} = \Delta_y \dfrac{M_y}{M}$

5.3. Design of SFRF with YSPD

5.3.1. Building geometry and loading description

To illustrate the applicability of direct displacement based seismic design method for lateral load resisting frame with YSPD, a 2-story office buildings is designed according to the direct displacement based design method explained above. The office building is assumed to be located in Vancouver. It has a symmetrical plan with a total area of 506.25 Sq.m (22.5 m x 22.5 m). The site class is considered as C. Two identical SFRFs are used symmetrically in N-S and E-W directions to resist lateral forces from earthquake. The building is symmetric and thus, torsion is not generated. The typical floor plan and elevations used for this study are shown in Figure 5.3 and Figure 5.4. All the frames have equal bay width and story height of 7.5 m and 3.8 m respectively. The dead load and live load of the floors are considered as 3.5 kPa and 2.4 kPa respectively. The roof dead load is taken as 3.0 kPa. The snow load is calculated as per the provisions in NBCC 2010 and is equal to 1.64 kPa. The load combinations 1D+0.5L+E and 1D+0.25S+E are considered for floors and the roof respectively in compliance with NBCC 2010. The nominal yield strength of structural steel is considered to be 350 MPa. The modulus of elasticity (E) of 200,000 MPa and Poisson's ratio (μ) of 0.3 are used for designing all the members.

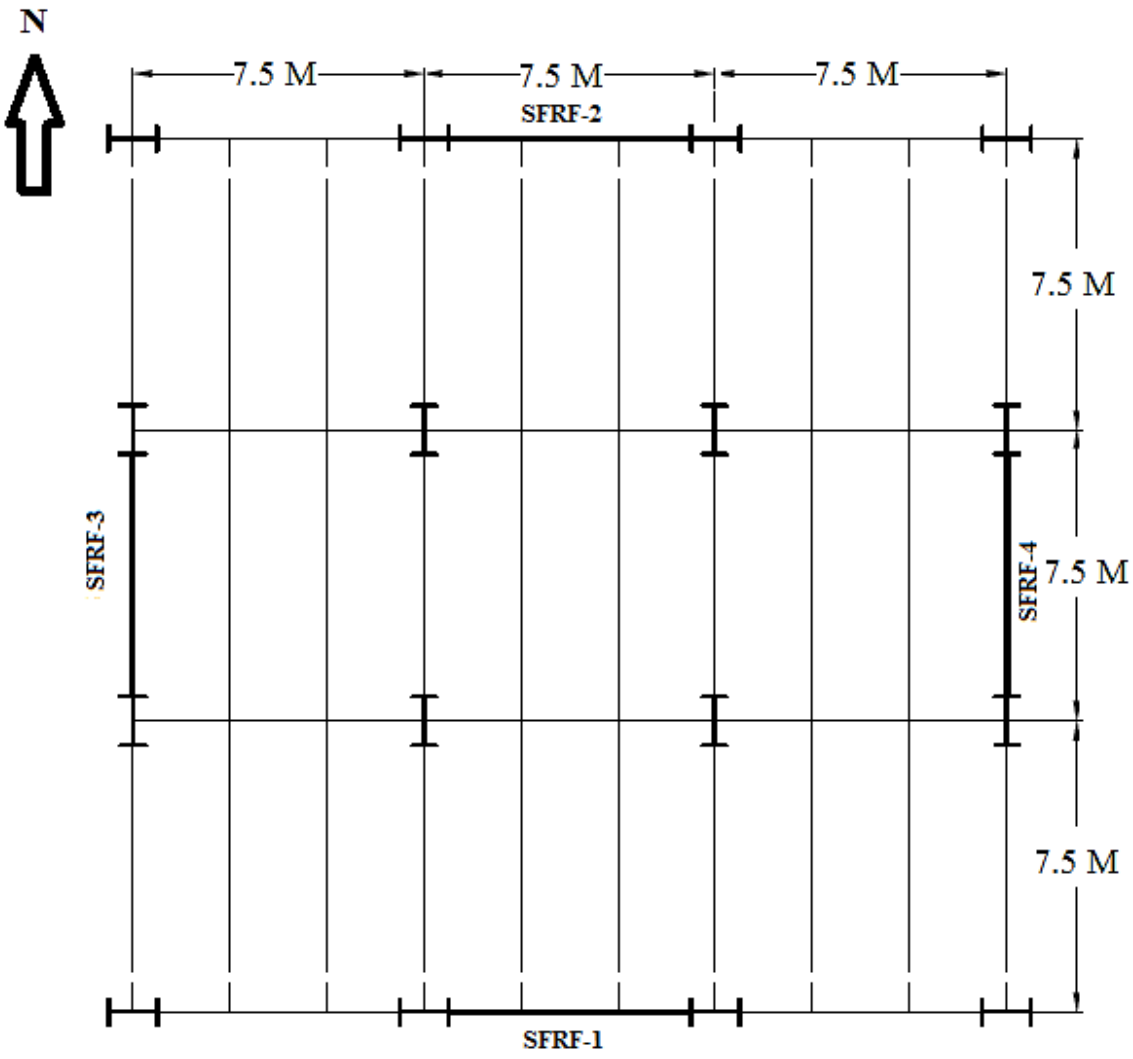

Figure 5.3 Typical floor plan of 2-story office building

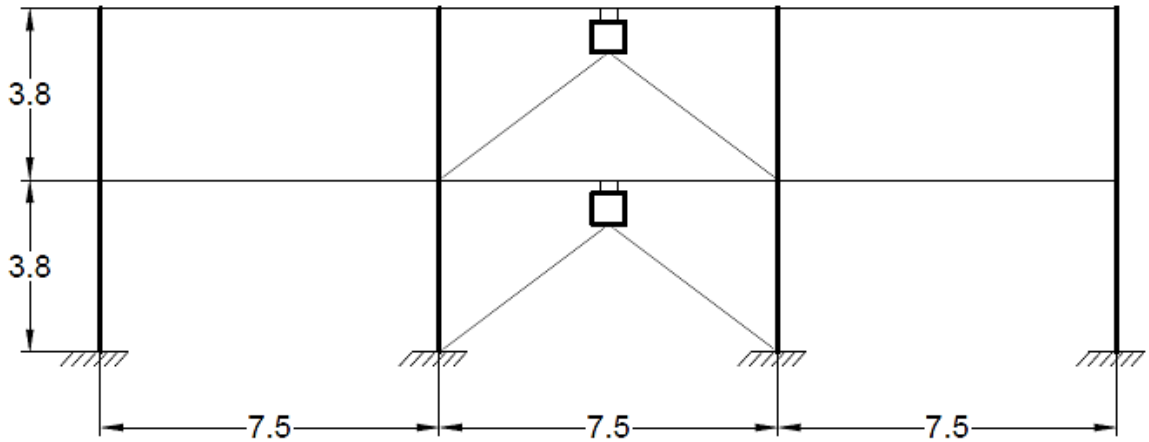

Figure 5.4. Elevation view of 2-story office building

5.3.2. Design Calculation

Step 1:

A drift ratio of 1.5 percent is chosen and thus, the ultimate displacement is calculated as Δ_u = 1.5% of 7.6 m = 114 mm. A yield displacement of 76 mm is assumed and thus, the initial ductility ratio, μ is equal to 1.5.

Step 2:

YSPD is used for passive energy dissipation in the system and a damping ratio of 10 % is adopted for this study, i.e. ξ_{EDS} = 10%

Step 3:

An inherent damping ratio of 0.02 and a strain hardening ratio of 0.01 are assumed here. Then, from equation [5.1], ξ_h = 0.105

The total equivalent damping ratio from equation [5.2], $\xi_{eq} = \xi_1 + \xi_h + \xi_{EDS}$ = 0.225

Step 4:

The equivalent target displacement $(\Delta u)_{eq}$ and equivalent mass, M_{eq} can be calculated from equation [5.3] and [5.4]. Both these parameters are obtained for SDOF substitute structure.

$(\Delta u)_{eq}$ = 95 mm = 0.095 m and M_{eq} = 266 kN-s^2/m

Step 5:

For this step, elastic response spectrum is made for Vancouver with PGA = 0.46g. The response spectrum provides a convenient means to summarize the peak response of all possible linear SDOF systems to a particular component of ground motion (Chopra A., Dynamics of structures). Five different ground motions are selected from PEER database and each ground motion is normalized (scaled up or down) so that all ground motions have the same peak ground acceleration as 0.46g. Three different damping i.e. 10, 20 and 30 percent are considered. Time domain solution using Newmark's method in MATLAB program is utilized to get the maximum displacement response for a particular time period, T_n of the structure.

Considering five different seismic records, five different maximum responses are found out for a particular time period. Mean of these five values produces the mean displacement. The mean displacement response spectrum is drawn by connecting these mean displacement values for different time periods. Similarly, connecting all the mean plus-one-standard-deviation values gives the mean-plus-one-standard-deviation displacement response spectrum (Chopra A., Dynamics of structures). For this study, a range of time period i.e. 0.2 sec – 2.0 sec is considered and the obtained

elastic displacement response spectrum, mean-plus-one-standard-deviation displacement values, is shown in the Fig. 5.5.

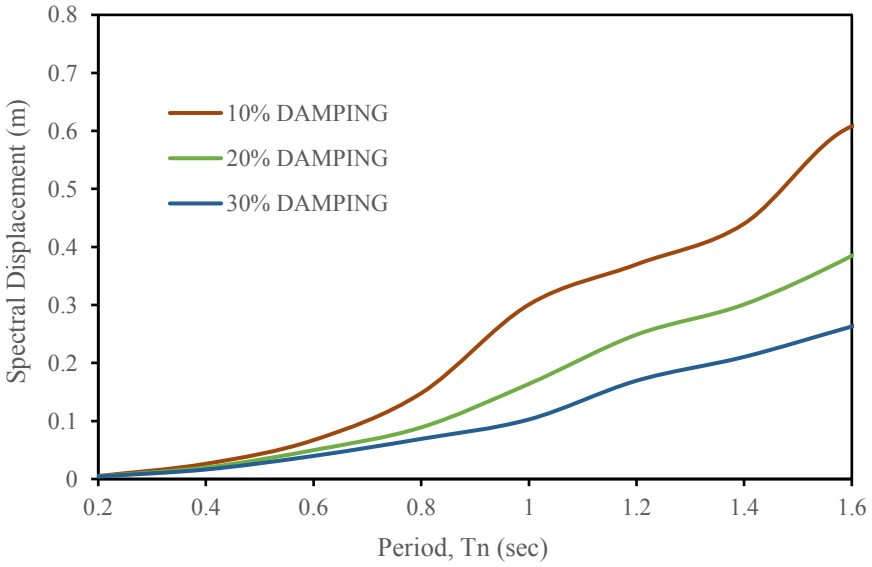

Figure 5.5 Elastic displacement response spectrum for Vancouver

From the chart, for spectral displacement of 0.095 m i.e.$(\Delta_u)_{eq}$ and ξ_{eq} = 22.5%, equivalent time period T_{eq} for the SDOF substitute structure is found as 0.83 sec. The total equivalent stiffness at maximum response displacement is found from equation [5.5] as 7560 kN/m.

Step 6:

The ultimate force capacity V_u and the design force can be obtained from equation [5.6] and [5.7] respectively. The values are: V_u = 718 kN and V_d = 714 kN

Step 7:

Using equation [5.8], the lateral forces F_x distributed to the 2nd story and roof are 242 kN and 472 kN respectively. The weak-beam- strong-column design criteria is utilized and for this study, γ is

taken as 1.2 to fit in the equation [5.9]. The beam and column sections can be found out using the trial process to have a target roof displacement of Δ_y i.e. 76 mm. The beam and column sections are provided in Table 5-1. The 2nd story displacement is found to be 35 mm.

Table 5-1: Beam and column sections of 2-story frame without YSPD

Story	**Beam section**	**Column section**
Roof	W310x118	W310x143
2nd	W610x140	W310x143

Step 8:

Now, from equations [5.10] and [5.11] all the required properties related to the passive energy dissipater, i.e. YSPD in this study can be calculated. The yield force (F_y) of each energy dissipater is found to be 108 kN. The effective stiffness (K_{EDS}) of each energy dissipater is calculated 2490 kN/m and 2026 kN/m for roof and 2nd floor respectively. α_j and μ_j are strain hardening ratio and ductility ratio of the metallic yielding devices respectively and their values are assumed as 0.01 and 6 for this study.

Step 9:

Using this effective stiffness, the beam and column sections are re-determined by iteration procedure until the building produces a roof displacement of 76 mm. With this modified sections, the end moment of each member is checked. The value of Δ_y is modified as per the equation [5.12] and the iteration process is carried out until My/M reaches close to 1.

The finally selected sections of beam, column, and YSPD devices are provided in Table 5-2. Only one bay in each SFRS is designed with YSPD. Hence, each floor has 2 devices in N-S direction.

Table 5-2: Beam, column and YSPD final sections of 2-story building

Story	Beam section	Column section	YSPD section	Brace section
Roof	W360x101	W310x129	120x6x4	HSS102x102x9.5
2nd	W360x162	W310x129	120x6x4	HSS102x102x9.5

The final design values are listed in table 5-3.

Table 5-3: Final design values of different parameters

Design parameters	**Final values in design**
Roof yield displacement (Δ_y)	93 mm
Ductility of the building (μ)	1.22
Equivalent damping ratio (ξ_{eq})	0.178
Equivalent time period (T_{eq})	0.816 sec
Ultimate force capacity (V_u)	750 kN
Design force capacity (V_d)	748 kN

The effective stiffness (K_{EDS}) of each energy dissipater is re-calculated as 2460 kN/m for both roof and 2nd floor. Now, the yield force in shear of a YSPD section (F_y) can be calculated from equation [3.7] and [3.8]. Recalling the equation,

$$K_d = K_{SHS} + K_{dia} = \frac{2ET^3}{D^2} + Gt$$

$F_y = K_d \, x \, u_y$

Now, assuming yield strength of YSPD section as 430 MPa, YSPD 120x6x4 section has a yield force of 109 kN. Hence, the YSPD section 120x6x4 is selected as passive energy dissipater. The braces can be designed to carry a force of $2F_y$, where F_y is the yield force of the YSPD section (Hossain et al. 2013). The brace sections are also listed in table 5-2.

5.4. Finite Element modelling of a 2-Story frame equipped with YSPD

FE modelling for a 2-story lateral load resisting frame equipped with yielding shear panel device (YSPD) has been done as stated in section 4.2. All the beams, columns, braces and SHS sections are modelled with B31 element whereas the plates are modelled using S4R element. B31 is generalized 3D shear flexible beam element that allows for transverse shear deformation. S4R is shell element generally used for thin plates modelling. The modelling and analysis details are already described in Section 4.2.

5.5. Nonlinear Dynamic Analysis of the frame with YSPD

5.5.1. Frequency Analysis

Frequency analysis is performed on the FE models to determine the fundamental time periods and mode shapes of the structure. The details of frequency analysis are already discussed in Section 4.7.1. The values of fundamental period (T) from the frequency analysis are also compared with the values as suggested by NBCC 2010 for braced frames (Table 5-4). The empirical formula is given in equation [5.14]

[5.14] $T = 0.025h_n$

It is permitted by NBCC to have a building period in the range of T - 2T for the braced frames. The results from frequency analysis shows that the code estimation of the period is conservative.

Table 5-4: Comparison between fundamental periods

Building specification	**T from frequency analysis**	**T suggested NBCC 2010**
2 story, height 7.6 M	0.45 sec	0.38 sec

5.5.2. Ground motion records

The uniform hazard spectrum (UHS) for each region is provided in NBCC 2010. The design spectrum of Vancouver is used here as the studied office building is located in Vancouver. The details of the scaling of ground motions is discussed in section 4.6.2. For this study, a total number of seven earthquake records are utilized, of which four are selected from the strong ground motion database of Pacific Earthquake Engineering Research Center (PEER 2010), and the other three records are selected from Engineering Seismology toolbox website (Atkinson et al. 2009). All the required data for ground motion records are given in Table 5-5 and Table 5-6.

Table 5-5: Real Ground motion records

Event	Magnitude	PGA (g)	PGV (m/s)	A/V	Scaling factor
San Fernando, 1972	6.6	0.188	0.179	1.05	1.65
Imperial Valley 1	6.53	0.3118	0.300	1.03	1.90
Imperial Valley 2	6.53	0.525	0.502	1.04	0.98
Northridge	6.69	0.51	0.483	1.055	1.43

Table 5-6: Simulated ground motion records

Event	Magnitude	Distance (km)	Scaling factor
6C1	6.5	8.4	0.74
6C2	6.5	13.2	1.38
7C2	7.5	45.7	1.65

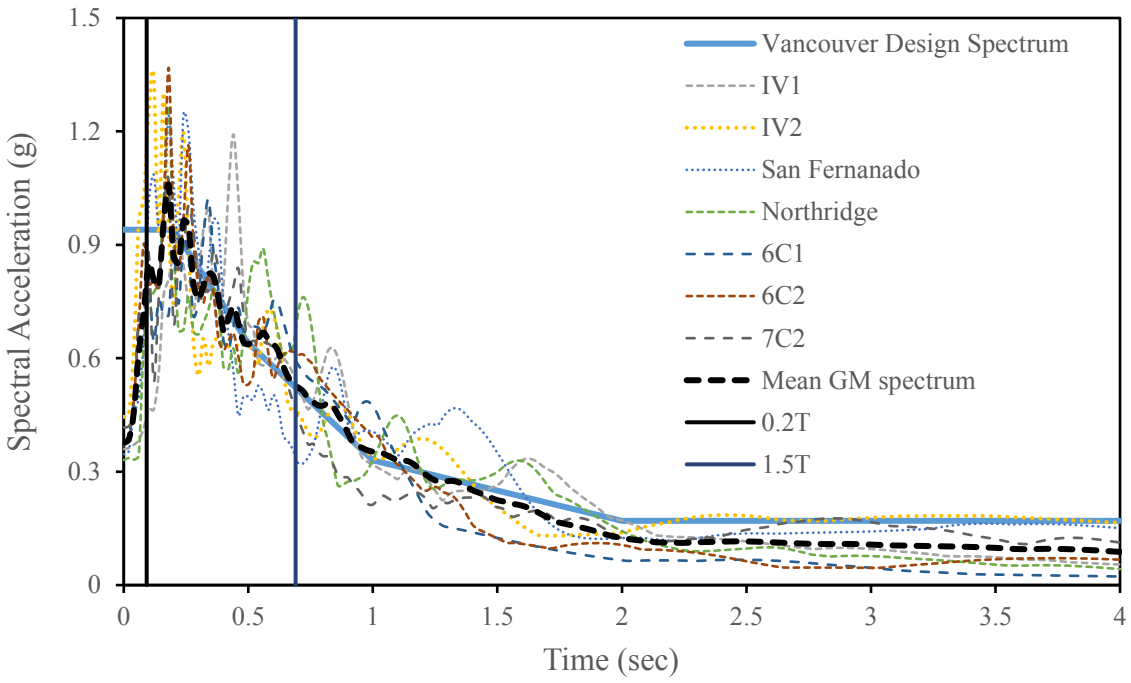

Figure 5.6 Acceleration spectra for selected ground motions and Vancouver design spectra

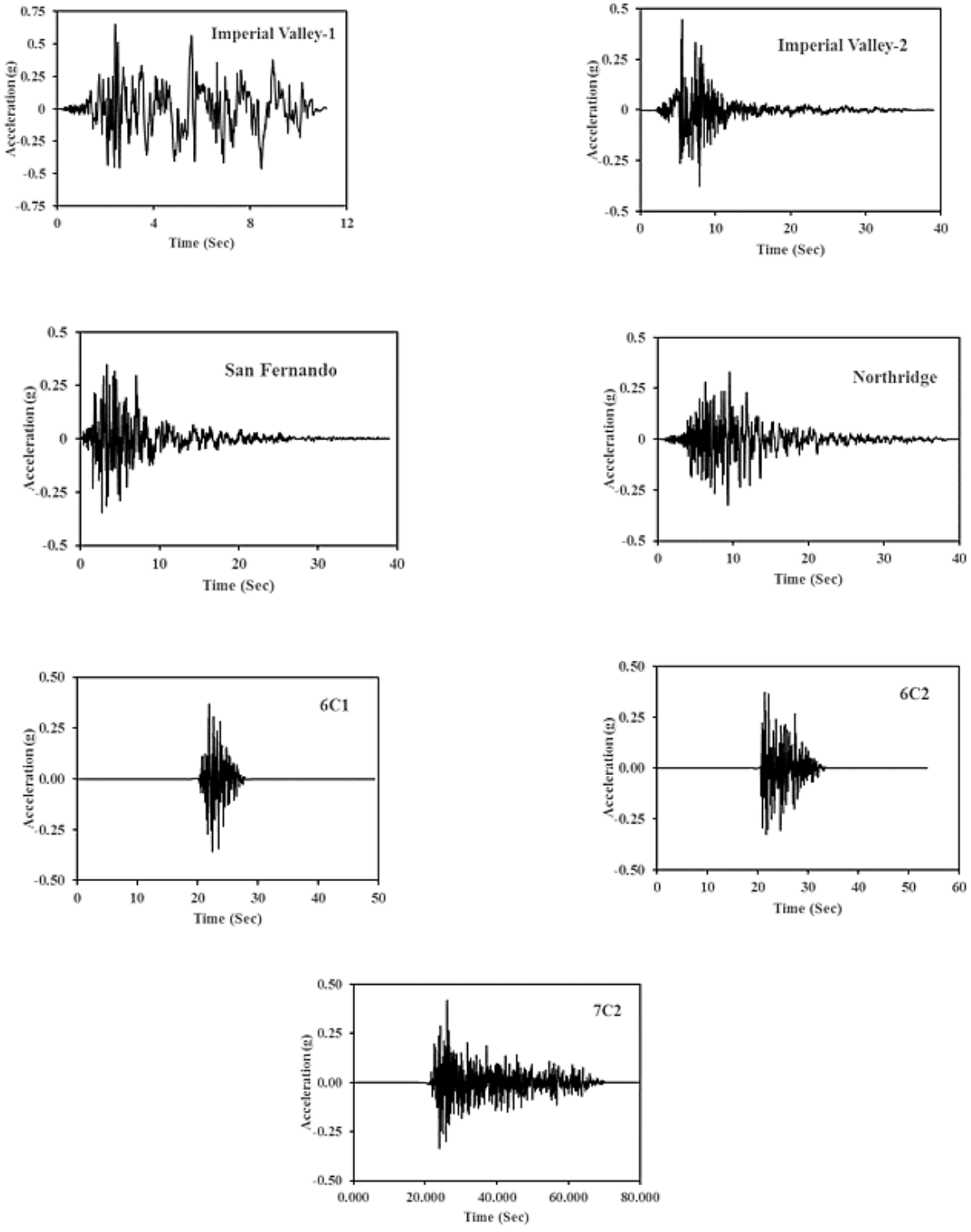

Figure 5.7. Scaled earthquake records for the 2-story office building

5.6. Seismic response of YSPD

Nonlinear Dynamic Analysis is performed on the 2-story building using the ground motions as described in Section 5.5.2. The ultimate displacement is checked and compared with the target ultimate displacement considered in direct displacement based design of the frame. The peak values of responses obtained for each earthquake are considered. An average of the peak responses of 7 earthquake records is also calculated to present the seismic behavior of the system. ASCE7-10 permits considering the average of the maximum responses, only if at least seven earthquake records are utilized for time history analysis.

5.6.1. Ultimate displacement

In the seismic design, the ultimate displacement is considered as 1.5 percent of the total building height and thus, Δ_u is equal to 114 mm. In order to assess the performance of the displacement based design method, maximum relative displacement of the roof is recorded for each ground motion. Also, the average of the 7 maximum responses is compared. The results show that Δ_u is maximum for Imperial Valley-1 earthquake. The average Δ_u for the building is 95 mm, which is less than 114 mm. Hence, the designed frame performed well in the earthquake and maximum displacement is close to the designed value. Table 5-7 shows the maximum roof displacement values of the structure under seismic analysis.

Table 5-7: Maximum roof displacement values from seismic analysis

Earthquake	Maximum roof displacement (mm)
San Fernando, 1972	111
Imperial Valley 1	168
Imperial Valley 2	92
Northridge	108
6C1	76
6C2	93
7C2	43
Average	95

5.6.2. Yielding Pattern

To study the yielding pattern of the 2-story building, the results obtained for the Imperial Valley are utilized. This earthquake was chosen because it has caused the maximum displacement to the structure among all the seven earthquake records.

The first yielding is observed at the all the YSPDs, specifically at the diaphragm plates. As expected, the devices yield at a low level of displacement and continues to dissipate energy in its post-yielding regime. Subsequently, the floor beams yield satisfying the weak-beam-strong-column philosophy of the design. The yielding is also observed in column after the beam yielding. No yielding has been detected in the brace members as expected.

5.6.3. Base shear

The final design value of the base shear for the building is 748 kN. The resulted base shear from the seismic analysis can be found out and can be compared with the designed base shear value. Table 5-8 shows the base shear values of the structure under seismic analysis. This is well agreed with the designed value i.e. 748 kN. As the direct displacement based design method doesn't rely on any reduction factor, the difference between these two values is less and hence, it proves the efficiency of this design method.

Table 5-8: Maximum base shear values from seismic analysis

Earthquake	Maximum base shear (kN)
San Fernando, 1972	962
Imperial Valley 1	1154
Imperial Valley 2	721
Northridge	869
6C1	675
6C2	783
7C2	461
Average	803

5.7. Summary

In this chapter, the seismic design for a frame with yielding shear panel device has been carried out. Direct displacement method of seismic design is suggested for the design purpose. It clearly shows that beam and column sections are reduced on employment of YSPD as passive energy dissipater. Then, non-linear dynamic analysis is carried out subjecting the frame by a set of ground motion records. The seismic response has been demonstrated in terms of ultimate displacement and base shear. The results prove that the frame has performed according to the design, under the seismic action. Also, the yielding sequence of the frame is studied. It shows that the YSPDs yield at low stress and continues to dissipate energy. Overall, the lateral load resisting frame with YSPD works satisfactorily. Hence, this device can be an efficient passive energy dissipater.

CHAPTER 6: ESTIMATION OF FUNDAMENTAL FREQUENCY FOR FRAME EQUIPPED WITH YSPD

6.1. Introduction

The previous chapters concentrated on the numerical model development of YSPD and seismic performance of the frame equipped with YSPD. The numerical model of the YSPD (isolated from the parent structure) was also studied under monotonic and cyclic loading. Stable load-displacement hysteresis proved the effectiveness of YSPD as an energy dissipation device. The yielding was observed at the shear panel first and then the beam yielded. The braces act as a support to the device.

When the YSPD is installed into a parent frame, both the device and its supporting elements such as an inverted-V brace become part of the lateral load-resisting system. Thus, the dynamic properties changes for the whole frame. For example, the natural periods of the complete system, are changed. The response of the complete system during an event of earthquake is dependent on the structural properties. In this chapter, an analytical procedure is developed to determine the fundamental period of a moment resisting frame equipped with a YSPD. The proposed procedure is applied to estimate period of different configurations of frame equipped with YSPD. The periods from the analytical method are compared against the periods obtained from the frequency analysis.

6.2. Mechanics of the device-brace-structure assembly

A single-story steel frame with an YSPD supported by an inverted V-brace is shown in Fig 6.1. The connection is "rigid" between beam and column. Also, the columns are fixed at base. Thus, the parent frame has a certain degree of lateral load resistance. This lateral stiffness is denoted by k_s, which is story stiffness. The inverted-V brace is pin-ended at the ends. These braces provide additional stiffness both in tension and compression. The acting lateral force on the frame produces a relative displacement between the top and bottom of the YSPD.

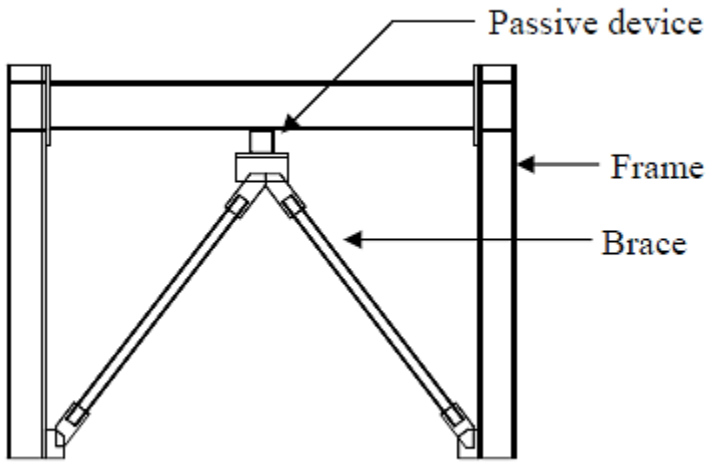

Figure 6.1 Brace-device-structure assembly

Figure 6.2 shows a stiffness analogy presented by Chan (2008) for the brace-device-structure assembly. The stiffness of the YSPD k_d is represented by a spring connected in a series with brace k_b. Story stiffness is k_s which is bare frame lateral stiffness. The acting seismic force is P(t).

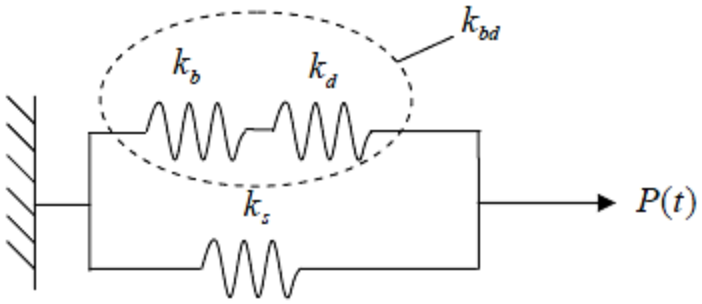

Figure 6.2 Brace-device-structure stiffness analogy (Chan, 2008)

The resultant stiffness of the YSPD and brace, is k_{bd} and it can be calculated from the following equation of connecting two springs in series:

$$[6.1] k_{bd} = \frac{1}{\frac{1}{k_b} + \frac{1}{k_d}} = \frac{k_b k_d}{k_b + k_d}$$

From the above equation, it is clear that the stiffness of the brace-device assembly (k_{bd}) is significantly reduced when YSPD is inserted. For example, with an YSPD having four times stiffness than the brace stiffness, the resultant device-brace assembly stiffness is only 80% of the brace stiffness.

The total stiffness of the frame (k) can be calculated by simply adding the frame stiffness and device-brace stiffness. Hence,

$$[6.2] k = k_s + k_{bd}$$

The Force-displacement response of the brace-device-structure assembly is illustrated in Fig. 6.3. It can be observed that the stiffness of the whole structure changes two times. The first yielding in the figure corresponds to the yielding of the YSPD, and the second refers to the yielding of the

main frame. The second stiffness is related to the elastic stiffness of the complete system by a ratio α. This ratio is dependent upon the device's post-yield stiffness, the brace stiffness, and the frame stiffness (Chan, 2008).

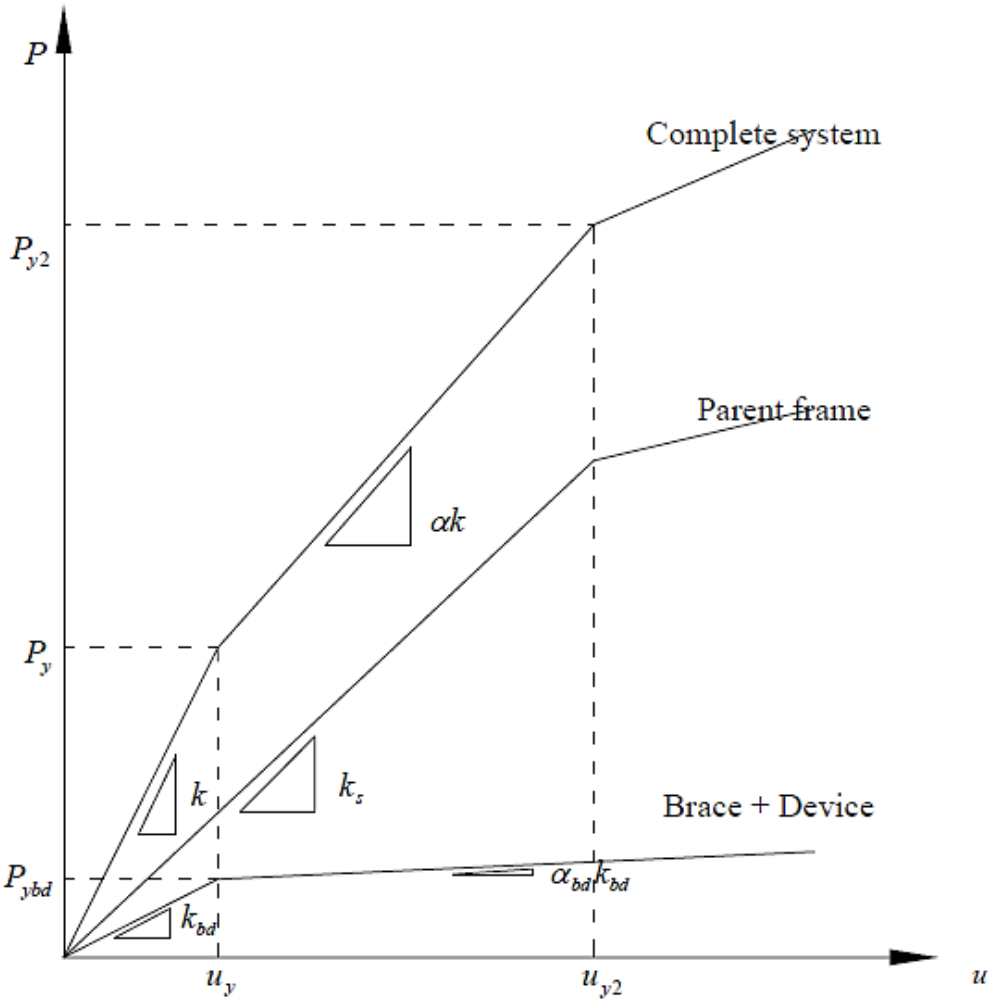

Figure 6.3 Resilience behavior of brace-device-structure assembly (Chan, 2008)

For low-yield shear panels, the behavior of the device may be considered as elastic-perfectly plastic i.e. $\alpha_{bd} = 0$ (Nakashima et al. 1996, De Matteis et al. 2002, Chan 2008). This statement is

further justified by the experiment carried out by Chan (2008) where it has been found that, for YSPD specimen100x4x2, the post-yield stiffness of the YSPD is eleven percent only to elastic stiffness. Hence, α is dependent on the story stiffness and the elastic stiffness of the brace-device assembly.

$$[6.3] \propto = \frac{k_s}{k_s + k_{bd}}$$

6.3. Estimation of fundamental frequency for MRF with YSPD

The knowledge of lateral stiffness is an important parameter in calculating lateral displacements of a frame subjected to lateral loads, such as seismic excitation. This is done for static analysis. For dynamic analysis, modal frequencies and shapes also have to be determined. This also requires determination of lateral stiffness. Modern computing methods are well known to facilitate development of complex numerical models of the buildings. Yet, simple analytical models are used by the researchers to calculate these parameters to have the knowledge about building response to lateral loads.

The concept of shear building (Schultz, 1992) is often used by the researchers to study the response of frames subjected to lateral loads. The shear building is a simple cantilever in which all mass of a story is assumed to be concentrated at a point and the stiffness of each story is represented by a spring with the same stiffness. Thus, the shear building is referred as lumped parameter model (Fig. 6.4). The joint rotations are assumed to be equal to zero, as the girders are infinitely rigid in comparison to the columns.

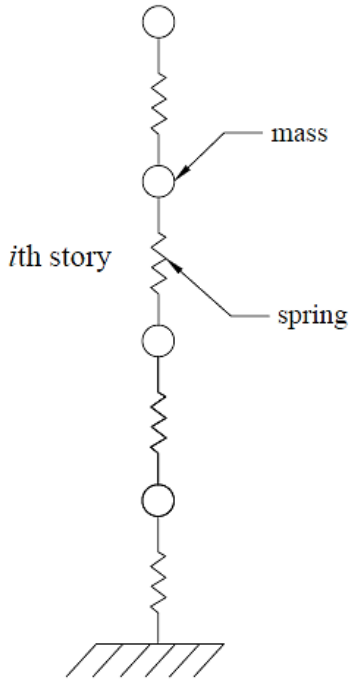

Figure 6.4 Lumped-Parameter Model (Schultz, 1992)

The lateral stiffness of each story is calculated by combining all columns into a single elastic spring. The spring connects the lateral degrees of freedom at the adjacent stories. Thus, the resulting mass and stiffness matrices are, respectively, diagonal (nonzero coefficients in principal diagonal only) and tridiagonal (nonzero coefficients in principal diagonal and adjacent minor diagonals only) (Schultz, 1992).

In reality, the assumption of zero joint rotations leads to erroneous values in computing dynamic properties of a structure. The work of many researchers (Rubinstein et al., 1961; Goldberg, 1972 etc.) clearly demonstrates that the stiffness of stories are needed to be modified to reflect girder flexibility in a realistic manner. Thus, the traditional shear building can be modified to a mathematical model for approximating the response of laterally loaded elastic frames.

6.3.1. Lateral stiffness of MRF

The lateral stiffness K_s of a story is generally defined as the ratio of story shear to story drift. The story drift is further defined as the difference in the lateral displacements of floors bounding a story. Vertical distribution of lateral loads influences these story drifts. Hence, the lateral stiffness of a story is not a constant property. However, the variation of lateral stiffness of a given story for different load cases are small and can be neglected and one single value of stiffness can be used for calculation. This applies to the regular linear load distribution, means that loads act in the same direction on all floors and the lateral loads vary from floor to floor in a controlled manner (Schultz et al., 1992).

There are numerous studies on the determination of lateral stiffness in Moment Resisting Frames. The methods proposed by Muto (1974) defines the total lateral stiffness, *k* for a column at ground story.

$$[6.4] k = \frac{12EI_c}{h^3}\beta$$

$$\beta = \frac{0.5 + \lambda}{2 + \lambda}\ ; \qquad \lambda = \frac{\frac{I_{b1}}{l_1} + \frac{I_{b2}}{l_2}}{I_c/_h}$$

Hosseini and Imagh-e-Naiini (1999) illustrates the lateral stiffness of MRFs in terms of an equivalent simple system. The system consists of sub-modules for one-bay frames. This method is similar to a shear building type structure, including the advantage of the flexural properties for the beams. This method doesn't need to calculate the lateral displacement of the frame with solving a system of linear equations. Figure 6.5 is a simple frame module, having the lateral stiffness of

[6.5] $k_{fm} = \frac{12k_c}{h^2} \frac{k_c(k_d + k_u) + 6k_d k_u}{k_c^2 + 2k_c(k_d + k_u) + 3k_d k_u}$

$where, \quad k_c = \frac{EI_c}{h} \quad k_d = \frac{EI_{gd}}{L} \quad k_u = \frac{EI_{gu}}{h}$

Here h, L, I_c, I_{gd} and I_{gu} are the dimensions and the cross-sectional properties of the frame module as shown in Figure 6.5. E is the modulus of elasticity of the frame material.

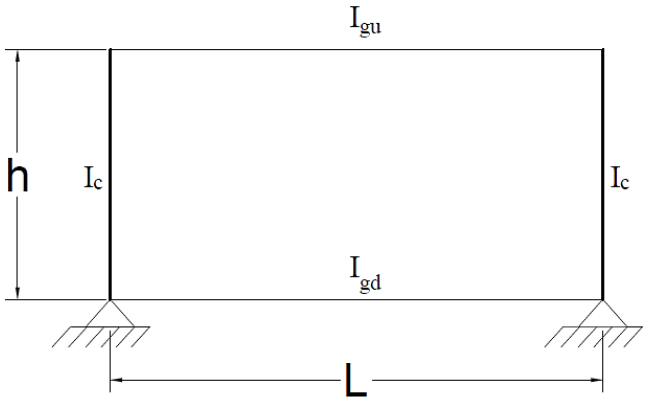

Figure 6.5 Simplified system for regular moment frames (Hosseini and Imagh-e-Naiini, 1999)

6.3.2. Lateral stiffness of YSPD

For elastic deformation, the shear stress can be computed in the diaphragm plate as

[6.6] $\tau = G\gamma = {}^{G}/_{d}$

Hence, in pure shear, the elastic stiffness of diaphragm plate can be written as

[6.7] $k_{dia} = \tau dt = Gt$

Now, for the SHS section in YSPD, the bolted flanges are under the action of flexure generated by the in-plane compression of the diaphragm plate and the vertical flanges of SHS. Bolted flanges experience bending about an axis perpendicular to the loading direction due to the force F_1. Hossain et al. (2011) calculated the value of F_1 making an assumption of a zero rotation along the line passing through the center of nearby bolts.

$$[6.8]\ F_1 = \frac{3EI_1}{d_1^3} = \frac{DT^3E}{4(a+r)^3}$$

where $I_1 = DT^3/12$, and r is the radius of the bolt hole.

The acting force F_2 responsible for this deformation is assumed to have a triangular distribution due to the large in-plane rigidity of the diaphragm plate. This force may be obtained by taking strips in the flange.

$$[6.9] F_2 = 2\left(\frac{\frac{6EI_2}{d_2^3}}{2}\right) = \frac{6EI_2}{d_2^3} = \frac{dT^3E}{2d_2^3}$$

$$d_2 = \frac{d_0}{2} + \frac{a^2\tan\theta + b^2\tan\theta - \pi r^2}{d}$$

$I_2 = (DT^3/12)$

Fig. 6.6 shows the details of assumed deformations with acting forces F_1 and F_2

Force required to produce this common deformation is the reduction force Fr, which can be calculated as

$$[6.10] F_r = \frac{3E\ (a+r)T^3}{8d_2^3}$$

The compression of the diaphragm plate and the vertical flanges in an YSPD is analogous to the deformation of an I-Section as shown in Fig. 6.8 The force required to make a unit deformation i.e. strain = 1/d at the end of the flange

$$[6.11] F_3 = DT\ x\ \frac{E}{d} + \frac{dt}{2}\ x\ \frac{E}{d}$$

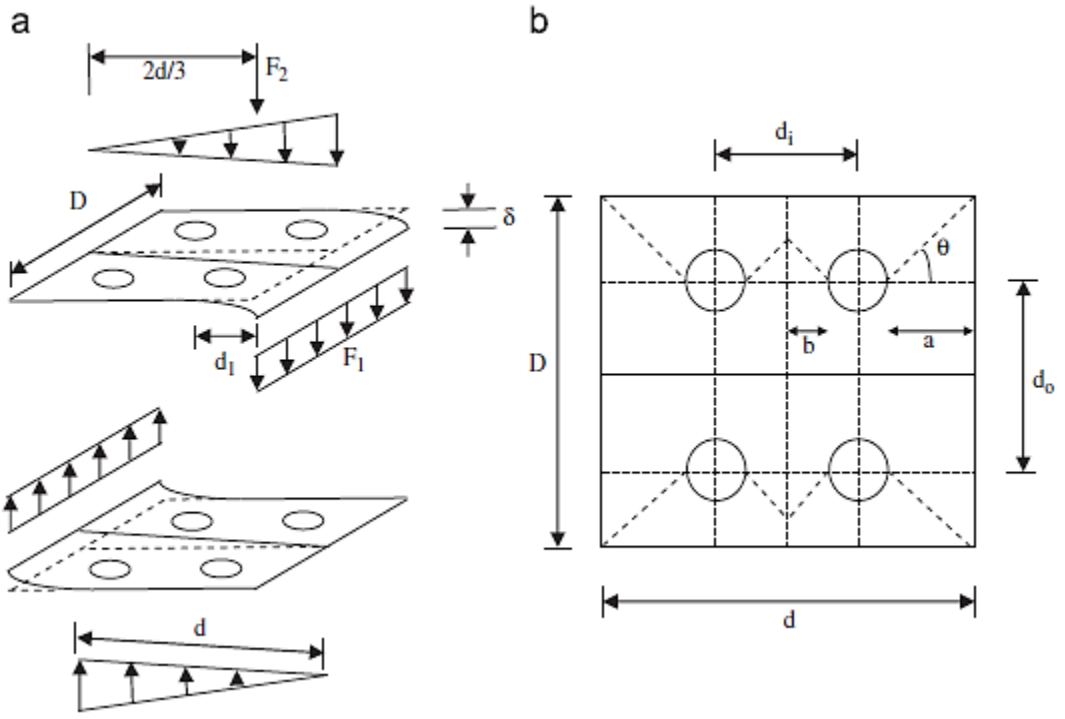

Figure 6.6 (a) Deformation of bolted flanges. (b) Dimensions of bolted flange (Hossain et al. 2011)

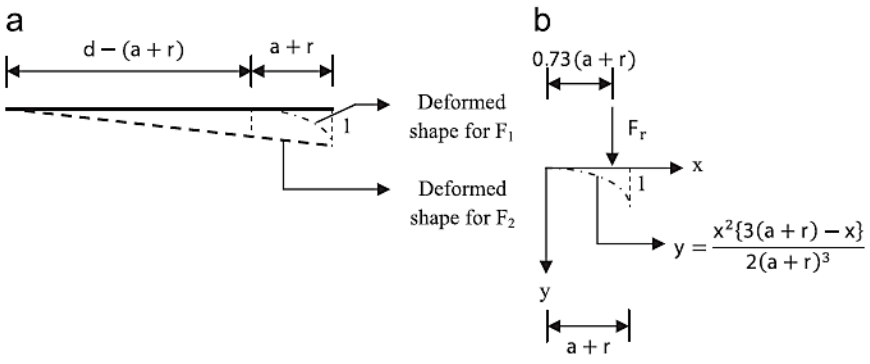

Figure 6.7 (a) Deformed shapes due to force F_1 and F_2 of SHS flange (b) Equation of the deformed shape for the force F_1 and reduction force F_r (Hossain et al. 2011)

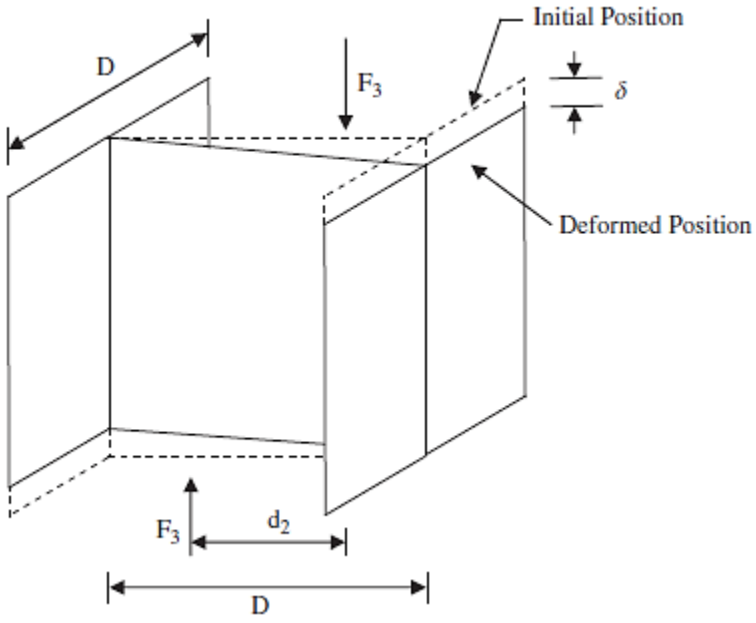

Figure 6.8 Compressive deformation of diaphragm plate and vertical flanges (Hossain et al. 2011)

The total stiffness can be calculated as

$$[6.12] k_{SHS} = F_1 + \frac{F_2}{3} - \frac{F_r(2d_r - d)}{d} + \frac{F_3(2d_3 - d)}{d}$$

$$d_3 = \frac{DTE + dtE/3}{F_3}$$

$$[6.13] \frac{1}{k_{YSPD}} = \frac{1}{k_d} = \frac{1}{k_{dia}} + \frac{1}{\emptyset k_{SHS}}$$

The value of ϕ can be determined using the initial stiffness of YSPDs obtained from experimental investigation and is equal to 0.03

6.3.3. Combined Stiffness

As described in Section 6.2, the total stiffness of the frame (k) can be calculated by adding the bare MRF stiffness (k_s) and device-brace stiffness (k_{bd}). Recalling equation [6.2], [6.1] and [6.13]

$$k = k_s + k_{bd}$$

$$k_{bd} = \frac{1}{\frac{1}{k_b} + \frac{1}{k_d}} = \frac{k_b k_d}{k_b + k_d}$$

$$\frac{1}{k_d} = \frac{1}{k_{dia}} + \frac{1}{\emptyset k_{SHS}}$$

Now, the stiffness of braces for each story can be defined as

$$[6.14] k_b = \frac{2AE}{L} cos^2 \propto$$

where, α is the brace angle in respect to the horizontal axis of the frame.

6.4. Building specifications

For estimating fundamental periods of MRF with YSPD, a total of eight buildings are considered. They consist of two sets of buildings with different symmetrical floor plans equipped with MRF with YSPD. The first set has a bay width of 5.4 m. The second set has a bay width of 3.8 m. For each set of floor plan, 1-story, 2-story, 3- story and 4-story buildings are considered.

The buildings are chosen to be hypothetical office buildings located in Vancouver, Canada. The plan area is 729 m^2 and they are founded on site class C (NBCC 2010). Each building consists of two identical MRF with YSPDs to resist lateral forces in each direction as shown in Figure 6.9. Thus, each SFRS is intended to resist only one half of the design seismic load. The story height of the buildings are chosen to be 3.8 m. Dead load is considered as 3.5 kPa for each floor and 3 kPa for roof. Live loads for each floor is taken as 2.4 kPa. Snow load is calculated as 1.64 kPa. Steel is having a yield strength of 350 MPa and Young's Modulus of 200,000 MPa.

According to the provisions of NBCC 2010 load combination 'D + 0.5L + E' (where, D = dead load, L = live load and E = earthquake load) is considered for floors and for the roof, the load combination 'D + 0.25S + E' (where S = snow load) is considered. The MRF is designed as per capacity design approach described in CSA 16. The YSPDs are installed in the frame for improving the seismic performance of the frame (Hossain et al. 2013). The brace sections are designed to carry a force that is two times of the maximum yield force carried by a YSPD section (Hossain et al., 2013). A ductility related force modification factor R_d of 3.5 and an over-strength force modification factor R_o of 1.5 are used in the design. Table 6.1 - 6.8 provide the dimensions and section details for the chosen SFRS.

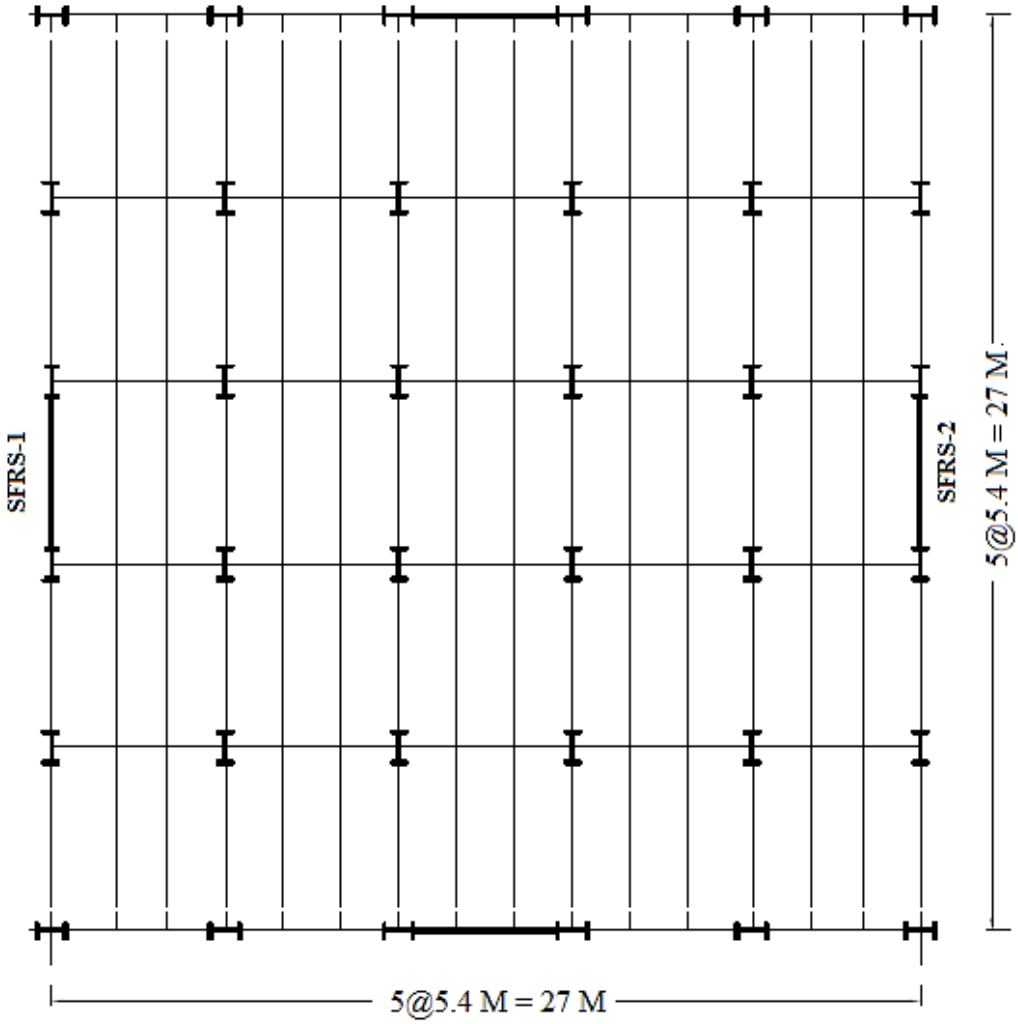

Figure 6.9 Floor plan of the building with SFRS (MRF with YSPD)

Table 6.1 Section details of 4-story MRF with YSPD for Set-1 (Bay width: 5400 mm)

Story	Beam Section	Column Section	Brace Section	YSPD section (D x T x t)
4	W310x283	W690x289	HSS 102x102x8	100x4x4
3	W310x283	W690x289	HSS 102x102x8	100x4x4
2	W460x315	W690x457	HSS 102x102x8	100x4x4
1	W460x315	W690x457	HSS 102x102x8	100x4x4

Table 6.2 Section details of 3-story MRF with YSPD for Set-1 (Bay width: 5400 mm)

Story	Beam Section	Column Section	Brace Section	YSPD section (D x T x t)
3	W310x283	W690x289	HSS 102x102x8	100x4x4
2	W460x315	W690x289	HSS 102x102x8	100x4x4
1	W460x315	W690x289	HSS 102x102x8	100x4x4

Table 6.3 Section details of 2-story MRF with YSPD for Set-1 (Bay width: 5400 mm)

Story	Beam Section	Column Section	Brace Section	YSPD section (D x T x t)
2	W460x315	W690x289	HSS 102x102x8	100x4x4
1	W460x315	W690x289	HSS 102x102x8	100x4x4

Table 6.4 Section details of 1-story MRF with YSPD for Set-1 (Bay width: 5400 mm)

Story	Beam Section	Column Section	Brace Section	YSPD section (D x T x t)
1	W460x315	W690x289	HSS 102x102x8	100x4x4

Table 6.5 Section details of 4-story MRF with YSPD for Set-2 (Bay width:3800 mm)

Story	Beam Section	Column Section	Brace Section	YSPD section (D x T x t)
4	W310x283	W690x289	HSS 102x102x8	100x4x4
3	W310x283	W690x289	HSS 102x102x8	100x4x4
2	W460x315	W690x457	HSS 102x102x8	100x4x4
1	W460x315	W690x457	HSS 102x102x8	100x4x4

Table 6.6 Section details of 3-story MRF with YSPD for Set-2 (Bay width: 3800 mm)

Story	Beam Section	Column Section	Brace Section	YSPD section (D x T x t)
3	W310x283	W690x289	HSS 102x102x3.2	100x4x2
2	W460x315	W690x289	HSS 102x102x8	100x4x4
1	W460x315	W690x289	HSS 102x102x8	100x4x4

Table 6.7 Section details of 2-story MRF with YSPD for Set-2 (Bay width: 3800 mm)

Story	Beam Section	Column Section	Brace Section	YSPD section (D x T x t)
2	W310x283	W690x289	HSS 102x102x8	100x4x3
1	W460x315	W690x289	HSS 102x102x8	100x4x3

Table 6.8 Section details of 1-story MRF with YSPD for Set-2 (Bay width: 3800 mm)

Story	Beam Section	Column Section	Brace Section	YSPD section (D x T x t)
1	W310x283	W690x289	HSS 102x102x8	100x4x2

6.5. Analytical model of calculating Fundamental frequency:

Figure 6.10 (a) shows a simplified system of 2-story frame. It consists of two masses connected by linear springs. Though the mass is distributed throughout the building, it can be idealized as concentrated at the floor levels. This assumption is generally appropriate for multistory buildings because most of the building mass is indeed at the floor levels (Chopra, 2012)

At any instant of time the forces acting on the two masses are as shown in their free-body diagrams in Fig. 6.10 (b). k_1 is the stiffness of the ground story and k_2 is the stiffness of the second story. k_1 and k_2 can be calculated using the method described in Section 6.3.3. Fundamental frequency of the structure can be calculated by the following equations as described below. Similar equations are developed for all the 8 different structures studied in this chapter.

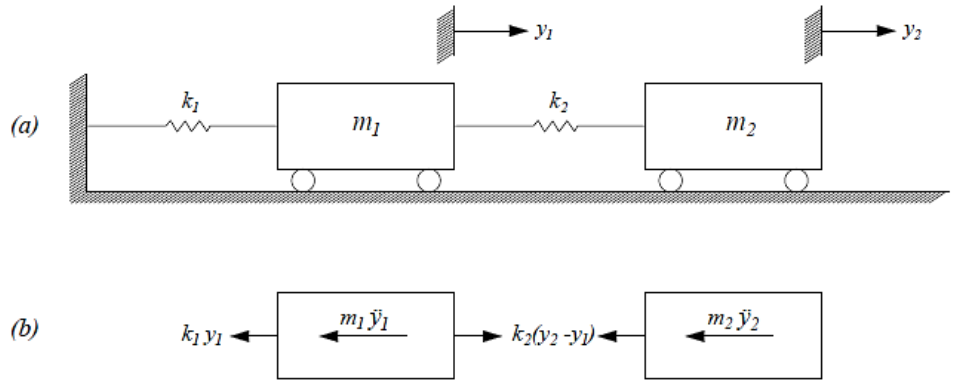

Figure 6.10 (a) 2-Story MRF simplification (b) Free body diagram of forces

The mass matrix and stiffness matrix of the system can be written as

$$[m] = \begin{bmatrix} m_1 & 0 \\ 0 & m_2 \end{bmatrix}$$

$$[k] = \begin{bmatrix} k_1 + k_2 & -k_2 \\ -k_2 & k_2 \end{bmatrix}$$

The equations of motion are:

$$[6.15] m_1 \ddot{y}_1 + k_1 y_1 - k_2(y_2 - y_1) = 0$$

$$[6.16] m_2 \ddot{y}_2 + k_2(y_2 - y_1) = 0$$

The eigenvalue equation for the system is:

$$\begin{vmatrix} k_1 + k_2 - m_1\omega^2 & -k_2 \\ -k_2 & k_2 - m_2\omega^2 \end{vmatrix} = 0$$

From the above equation, ω can be solved and finally, time period of the system can be obtained from the following equation.

$$[6.17] T = \frac{2\pi}{\omega}$$

6.6. Numerical Model

Numerical models are developed for all the 8 buildings studied. Similar procedure is followed to develop the numerical models, as described in Chapter 4. Shell elements (S4R) are used to simulate the diaphragm plate of YSPD. All the other frame members are modelled using the beam element (B31). The lumped masses are considered to the column nodes at their corresponding levels. The supports of all columns are considered fixed at the base. The yield strength of steel is 350 MPa. The mass of the components are also taken into account by adding the density of the steel to the material model.

6.7. Results and comparison

The sample calculation for 2-story MRF with YSPD (Set 1) from analytical model is shown in the Table 6.9. All the section details for the system are given in Table 6.3.

Table 6.9 Mass and stiffness values for 2-story MRF with YSPD (Set 2: Bay width 3800 mm)

Story	Mass (t)	k_s (kN/mm)	k_b (kN/mm)	k_d (kN/mm)	k_{bd} (kN/mm)	$k = k_s + k_{bd}$ (kN/mm)	T (seconds)
2	141.6	76058.4	135642	23730	20196.68	96255.08	0.36
1	200	117564.74	135642	23730	20196.68	137761.42	

The numerical model for the system is shown in Figure 6.11 which shows the original and deflected shape of the frame. Frequency analysis is performed and the fundamental frequency is found to be 0.37 sec.

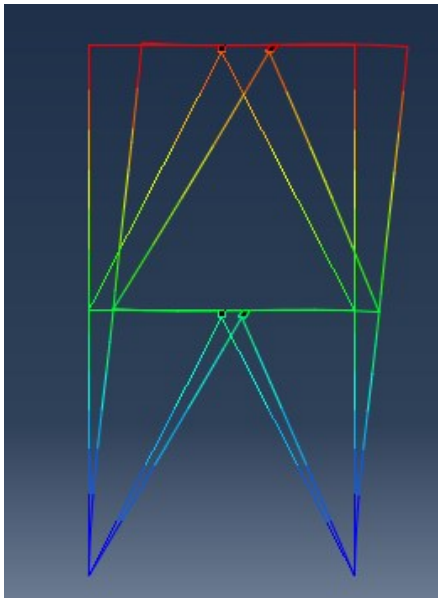

Figure 6.11 Original and deflected shape of the MRF with YSPD

The results from the analytical models and numerical are compared in Table 6.10.

Table 6.10 Comparisons of Fundamental Periods of MRF with YSPD

Case No.	No. of stories	Frame width (m)	Fundamental period, T (seconds)	
			Analytical Model	Numerical Model
1	1	3.8	0.22	0.20
2	1	5.4	0.2	0.23
3	2	3.8	0.37	0.36
4	2	5.4	0.39	0.39
5	3	3.8	0.52	0.55
6	3	5.4	0.55	0.56
7	4	3.8	0.66	0.72
8	4	5.4	0.78	0.74

6.8. Summary

An analytical model to estimate the fundamental period of a frame equipped with YSPD is proposed in this chapter. The proposed method is used to estimate the fundamental periods of a number of MRFs with YSPD comprising of varying dimensions and height. Detailed finite element models of these frames are developed and their fundamental periods are found out from frequency analysis using ABAQUS. The fundamental periods obtained from both the cases are compared and the comparisons show a good agreement. This leads to an excellent initial estimation of the time period for the frame equipped with YSPD.

CHAPTER 7: SUMMARY AND CONCLUSION

7.1. Summary

Research activities have shown that energy dissipating devices installed within structures can effectively reduce damages to main structural components. These devices absorb a significant portion of the seismic energy by working as a 'structural fuse'. Passive control devices demonstrate relatively superior performance over their active control devices. Yielding shear panel device (YSPD) is a metal yielding passive control device that is designed to exploit the inelastic shear deformation capability of a steel diaphragm plate during seismic excitation.

Appropriate numerical model incorporating the physical characteristics of the device has been explained in Chapter 3. A bilinear material model is considered for mild steel whilst shell elements are used to incorporate geometric nonlinearity. Appropriate boundary conditions are adopted to develop a numerical model for YSPD. Spring elements with appropriate stiffness have been used for simulating the effect of the bolted connection. The numerical model has been done in ABAQUS and validated with available test results of YSPD. The validated numerical model is then used to carry out detailed parametric study on the behavior of YSPD. Diaphragm plate thickness, SHS plate thickness, SHS section width are the parameters considered for this study. Large sections of YSPD are also simulated and checked for the parametric studies.

YSPDs are installed in lateral load resisting frames to dissipate energy in the case of seismic event. In chapter 4, a frame equipped with YSPD has been numerically modelled in ABAQUS and validated with the mathematical model of the device. The load-displacement response of YSPD in a frame is also checked with the load-displacement response of an isolated YSPD modelled numerically in Chapter 3. With the validated model, seismic analysis is conducted on a 4-story

moment resisting frame retrofitted with YSPD. Inter-story drift and base shear of both the lateral load resisting system, i.e. bare MRF and MRF with YSPD has been discussed.

In chapter 5, seismic design of a 2-story building having YSPD as a passive energy dissipation device is done by the direct displacement method. The design process is an iterative process and it utilizes a concept of substitute SDOF structure. An ultimate roof displacement is assumed in the design and the frame is designed to have that ultimate displacement under seismic event. To determine the seismic performance of the device, non-linear time history analysis has been carried out. A set of seven ground motions including real and simulated records compatible with design spectrum of Vancouver has been selected for seismic analysis.

When the YSPD is installed in a frame, the device and the inverted-V brace become part of the lateral load-resisting system. The fundamental periods of the complete system, are changed from the time period of the parent frame. In Chapter 6, an attempt has been made to determine the fundamental period of a frame equipped with a YSPD. Analytical model has been developed for different frame configurations. Frequency analysis for the same configurations has been carried out and the periods from frequency analysis were compared with the periods from analytical solutions.

7.2. Conclusion

The numerical model developed for the YSPD (isolated from the device) can reasonably predict the force-displacement behavior. Costly and time-demanding experiments can be avoided for this reason. The parametric studies show that a stiff SHS section and a slender diaphragm plate make the most efficient YSPD for energy dissipation.

The finite element model of the whole frame is an effective way to check the response of YSPD under seismic excitation. Appropriate boundary conditions to reflect proper connection details can help in developing an effective FE model. The yielding shear panel device, when used as a device within a moment resisting frame in retrofitting, results in reducing the inter-story drift and base shear.

Direct displacement-based seismic design method (Lin et al., 2013) has been proved as an effective solution for designing a lateral load resisting system equipped with passive energy dissipater. An energy dissipater is characterized by effective stiffness and damping ratio. The design method utilizes the formula of deriving both the parameters. Also, the beam and column sections can be modified to more economical sections after installing YSPD as the device carries sufficient amount of energy during an earthquake. The seismic analysis results show that the target ultimate displacement can be achieved and thus, the design can have the appropriate estimation of the material ductility. The YSPD devices yield a low stress level and continues to dissipate energy from the system so that the main structural components are subjected to less damage. YSPD proves to be an effective damage control device which exploits metal yielding in seismic excitation.

Finally, the developed analytical model gives a reasonable estimate of the fundamental period related to the frame with YSPD. This model can be effective to get an initial estimation about the time period before performing seismic analysis of the frame.

7.3. Recommendations for future work

The yielding shear panel device is an excellent passive energy dissipation device. The following works are recommended for the further development of YSPD.

A full scale experimental investigation is recommended. As Chan (2009) carried out experimental work only for the device isolated from the parent frame. The full scale test can be done after designing the member and YSPD according to direct displacement based design method. Damage pattern along with the force displacement response of the device and frame may be studied. Also, bolted connection can be replaced with welded connection.

The contribution of SHS in the force-displacement response has been reported as minimum (Chan et al. 2008, Hossain et al. 2013). Same conclusion is drawn in this study. The minimum requirement of strength of SHS section may be studied. This would pave a way for the built-up sections instead of regular square hollow sections.

Also, the use of parallel slender plates in diaphragm plate instead of using a single compact plate may be explored.

REFERENCES

ABAQUS Inc. 2014. ABAQUS Standard User's Manual, version 6.14.

Aguirre M., Earthquake-resistant structure: structural frame damper system-an approach to design. Proceedings of the Institution of Civil Engineers. Structures and buildings, 1997. 122(2): p. 165-172.

ANSI/AISC. 2005. Seismic Provisions for Structural Steel Buildings. American Institute of Steel Construction Inc, Chicago, Illinois.

Atkinson, Gail, Karen Assatourians, And Bernie Dunn. 2009. Engineering Seismology Toolbox. http://www.seismotoolbox.ca/GMDatabases.html.

Aiken, I. D., Nims, D. K., Whittaker, A. S. & Kelly, J. M., Testing of Passive Energy Dissipation Systems. Earthquake Spectra (1993), 9.

Alinia, M. M., Gheitasi, A. & Erfani, S., Plastic shear buckling of unstiffened stocky plates. Journal of Constructional Steel Research (2009), 65, Page 1631-1643

Baber, T. & Noori, M., Modelling general hysteresis behavior and random vibration application. Journal of Vibration, Acoustics (1986), Stress and Reliability in Design, 108**,** 411-420.

Black, C. J., Makris, N. & Aiken, I. D., Component testing, seismic evaluation and characterization of buckling-restrained braces. Journal of Structural Engineering (2004) -ASCE, 130**,** 880-894.

Brown, P., Aiken, I. & Jafarzadeh, F., Seismic Retrofit of the Wallace F. Bennett Federal Building. Modern steel construction, (2001) 41**,** 29-39.

CAN/CSA S16-09. Limit states design of steel structures, Canadian Standard Association, Rexdale (Ontario).

Chan, R. W. K. Metallic yielding devices for passive dissipation of seismic energy, 2008, PhD thesis, University of Queensland.

Chan, R. W. K., Albermani, F. & Williams, M. S., Evaluation of yielding shear panel device for passive energy dissipation. Journal of Constructional Steel Research (2009), 65, 260-268.

Chen, C., Recent Advances of Seismic Design of Steel Buildings in Taiwan (2002). International Training Programs for Seismic Design of Building Structures.

Chen, C. C. & Lu, L. W. Development and experimental investigation of a ductile CBF system. Proceedings of the 4th National Conference on Earthquake Engineering, 1990. Palm Springs, California.

Chopra, A. (1995) Dynamics of structures, Prentice Hall Englewood Cliffs, New Jersey.

Clark, P. W., Aiken, I. D., Tajirian, F., Kasai, K., Ko, E. & Kimura, I. (1999) Design procedures for buildings incorporating hysteretic damping devices. Proc. Int. Post-SmiRT Conf. Seminar on Seismic Isolation, Passive Energy Dissipation and Active Control of Vibrations of Structures. Cheju, South Korea.

De Matteis, G., Formisano, A., Panico, S. & Mazzolani, F. M., Numerical and experimental analysis of pure aluminum shear panels with welded stiffeners. Computers & Structures (2008), 86, 545-555.

European Convention for Constructional Steelwork, E., Ultimate limit state calculation of sway frames with rigid joints. Technical Committee 8(1984) - Structural Stability Technical Working Group 8.2 - System.

FEMA (2000a) 355-C: State of the Art Report on Systems Performance of Steel Moment Frames Subject to Earthquake Ground Shaking. Federal Emergency Management Agency, Washington, DC.

FEMA (2000b) 356: Prestandard and Commentary for the Seismic Rehabilitation of Buildings. Federal Emergency Management Agency, Washington, DC.

Goldberg, J. E., "Approximate elastic analysis." Proc, Int. Conf. on Planning and Design of Tall Buildings (1972), ASCE, New York, N.Y., Vol. II, 169-183.

Habibi, A., R.W.K. Chan, And F. Albermani, Energy-based design method for seismic retrofitting with passive energy dissipation systems. Engineering Structures (2013), 46(0): p. 77-86.

Habibi, A., New energy-based design method for seismic retrofitting with passive energy dissipation devices, 2013, PhD thesis, University of Queensland.

Hossain, R., Theoretical Evaluation of Yielding Shear Panel Device for Passive Energy Dissipation, 2013, PhD thesis, University of Queensland.

Hossain, R., M. Ashraf, And F. Albermani, Numerical modelling of yielding shear panel device for passive energy dissipation. Thin-Walled Structures (2011). 49(8): p. 1032-1044.

Hossain, R., Ashraf M., And Padgett J. Risk-based seismic performance assessment of Yielding Shear Panel Device, Engineering Structures 56 (2013) 1570–1579

Hosseini M., Imagh-E-Naiini M.R. A Quick Method for Estimating the Lateral Stiffness of Building Systems, The Structural Design of Tall Buildings, Struct. Design Tall Build. **8**, 247–260 (1999)

Hwang, JS. Applications of seismic passive control in Taiwan, Proceedings of the Joint NCREE/JRC (European Community), International Collaboration on Earthquake Disaster Mitigation Research, Taipei, Taiwan, 2003.

Kelly JM, Skinner RI, and Heine AJ, Mechanisms of energy absorption in special devices for use in earthquake–resistant structures, Bull. N.Z. Nat. Soc. For Earthquake Eng., Vol. 5, No. 3, 1972.

Lamontagne, M., Halchuk, S., Cassidy, J. F., and Rogers, G. C. Significant Canadian Earthquakes of the Period 1600–2006. 2008. Seismological Research Letters 79 (2): 211-223.

Lin, Y.Y., et al., Direct displacement-based design for building with passive energy dissipation systems. Engineering Structures (2003), 25(1): p. 25-37.

Lubell AS, Prion HGL, Ventura CE and Rezai M, Unstiffened steel plate shear wall performance under cyclic loading, J. Struct. Engrg, ASCE, Vol. 126, No. 4, April 2000.

MARTINEZ-ROMERO, E. (1993) Experiences on the use of supplemental energy dissipaters on building structures. Earthquake Spectra, 9**,** 581-624.

MARTINEZ-ROMERO, E. (1995) Supplementary energy dissipaters for maximum earthquake protection of tall building structures. The Structural design of Tall Buildings, 4**,** 91-101.

MATLAB online reference, The MathWorks, 2007 (http://www.mathworks.com).

Muto, K. (1974). Aseismic design analysis of buildings. Maruzen Co., Ltd., Tokyo, Japan.

Naumoski, N., Saatcioglu, M., and Amiri-Hormozaki, K. 2004. Effects of Scaling of Earthquake Excitations on the Dynamic Response of Reinforced Concrete Frame Buildings. 13th World Conference on Earthquake Engineering 2917, No. 15.

Nakashima M, Iwai S, Iwata M, Takeuchi T, Konomi S, Akazawa T and Saburi K, Energy dissipation behaviours of shear panels made of low yield steel, Earthquake Engineering and Structural Dynamics, Vol. 23, 1299-1313, 1994.

Nakashima M, Strain-hardening behaviour of shear panels made of low-yield steel, I: Test, Journal of Structural Engineering, December 1995.

Nakashima M, Strain-hardening behaviour of shear panels made of low-yield steel, II: Model, Journal of Structural Engineering, December 1995.

Nath M., Bhowmick A.K., Finite Element Modelling and Analysis of Yielding Steel Shear Panel Device for passive energy dissipation, CSCE Annual Conference (2016), London Ontario.

Ohtori, Y. & Spencer Jr, B. Benchmark control problems for seismically excited nonlinear buildings. Journal of Engineering Mechanics, (2004,) 130**,** 366.

PEER. 2010. Next Generation Attenuation of Ground Motions Project (NGA) Database. Pacific Earthquake Engineering Research Center, Berkeley, California. http://ngawest2.berkeley.edu/.

Perry CL, Fierro EA, Sedarat H, and Scholl RE, Seismic upgrade in San Francisco using energy dissipation devices, Earthquake Spectra, 9(3): 559-79, 1993

Priestley, M. and G. Calvi, Concepts and procedures for direct displacement-based design and assessment. Seismic Design Methodologies for the Next Generation of Codes, 1997: p. 171-182.

Rubinstein, M. F., and Hurty, W. C. (1961). "Effect of joint rotation on dynamics of structures." J. Engrg. Mech. Div., ASCE, 87(6), 135-157.

Schmidt, A E, Approximating Lateral Stiffness of Stories in Elastic Frames. Journal of Structural Engineering, Vol. 118, No. 1, January, 1992.

Schmidt, K., Dorka, U. E., Taucer, F. & Magnonette, G. Seismic retrofit of a steel frame and an RC frame with HYDE systems. Institute for the Protection and the Security of the Citizen European Laboratory for Structural Assessment (2004), European Commission Joint Research Centre.

Soo Kim, T. & Kuwamura, H. Finite element modeling of bolted connections in thin walled stainless steel plates under static shear. Thin-Walled Structures (2007), 45, 407-421.

Soong, T. & Dargush, G. Passive energy dissipation systems in structural engineering (1997).

Soong, T. T. & Spencer, B. F. (2002) Supplemental energy dissipation: state-of-the-art and state-of-the practice. Engineering Structures, 24**,** 243-259.

Tenacolunga, A. Mathematical modelling of the ADAS energy dissipation device. Engineering Structures (1997), 19, 811-821.

Timler PA and Kulak GL. Experimental study of steel plate shear walls, Structural Engineering Report No. 114, Department of Civil Engineering, University of Alberta, Edmonton, Alberta, Canada, 1983.

Tsai, K. C., Chen, H. W., Hong, C. P. & Su, Y. F. Design of Steel Triangular Plate Energy Absorbers for Seismic-Resistant Construction. Earthquake Spectra (1993), 9, 505-528.

Tsai, K. C. & Hong, C. P. Steel triangular plate energy absorber for earthquake-resistant buildings. Constructional Steel Design: World Developments (1992). Elsevier Applied Science.

Uang, C.-M. and V.V. Bertero, Use of energy as a design criterion in earthquake-resistant design. Vol. 88. 1988: Earthquake Engineering Research Center, University of California.

Walter Yang, C. S., Desroches, R. & Leon, R. T. Design and analysis of braced frames with shape memory alloy and energy-absorbing hybrid devices. Engineering Structures (2010), 32, 498-507.

Wen, Y. Method for random vibration of hysteretic systems. Journal of the Engineering Mechanics Division (1976), 102, 249-263.

Whittaker, A. S., Bertero, V. V., Thompson, C. L. & Alonso, L. J. Seismic testing of steel plate energy dissipation devices. Earthquake Spectra (1991), 7, 563-604.

Williams, M. & Albermani, F. Monotonic and Cyclic Tests on Shear Diaphragm Dissipaters for Steel Frames. Civil Engineering Bulletin No. 23 (2003), Department of Civil Engineering, University of Queensland, Australia.

Xia, C. & Hanson, R. D. Influence of ADAS Element Parameters on Building Seismic Response. Journal of Structural Engineering-ASCE (1992), 118, 1903-1918.

Wada A, Huang YH, Iwata M, Passive damping technology for buildings in Japan, Proceeding of Progress in Structural Engineering Materials, 2:335-350, 2000. 72.

Yeh, C. H., Lu, L. Y., Chung, L. L. & Huang, C. S. Test of a Full-Scale Steel Frame with TADAS, Earthquake Engineering and Engineering Seismology (2001).

Yung, W.T., Low cycle fatigue study of yielding shear panel device (YSPD) for passive energy dissipation. 2010 (University of Queensland).